

General Disclaimer

One or more of the Following Statements may affect this Document

- This document has been reproduced from the best copy furnished by the organizational source. It is being released in the interest of making available as much information as possible.
- This document may contain data, which exceeds the sheet parameters. It was furnished in this condition by the organizational source and is the best copy available.
- This document may contain tone-on-tone or color graphs, charts and/or pictures, which have been reproduced in black and white.
- This document is paginated as submitted by the original source.
- Portions of this document are not fully legible due to the historical nature of some of the material. However, it is the best reproduction available from the original submission.

FINAL REPORT

Skylab Experiment S073:

Gegenschein/Zodiacal Light

(NASA-CR-150186) SKYLAB EXPERIMENT S073: N77-17989
GEGENSCHNEIN/ZODIACAL LIGHT Final Report,
Oct. 1973 - Jan. 1976 (State Univ. of New
York) 155 p HC A08/ME A01 CSCI 03E Unclas
G3/92 15610



Skylab Experiment S073: Gegenschein/Zodiacal Light
Final Contract Report, NAS8-30251

Table of Contents

	page
Preface	i
Summary	ii
Acknowledgements	iii
Background Information	1
Instrument Description and Experiment Operations	3
Mission Operations - Planned and Accomplished	8
Complementary Observations from the Ground and from Pioneers 10 and 11	10
The Observations and their Reduction	
1. Photometer	11
2. Data Acquisition Camera	15
Calibration	18
Initial Results	23
Publications Related to the Experiment	26

Appendices

1. Summary of Observations
2. Status of the Photometer Data
3. Pointing Direction Computations
4. Miscellaneous Difficulties or Anomalies
5. Analysis of Selected Photometer Data on Contamination, excerpt from Final Report, NASA contract NAS8-31902: Preliminary Study of Contaminant Particulates around Skylab, SUNYA, May 1976.

Attachments

1. Reprint, The Skylab Ten Color Photoelectric Polarimeter, J. L. Weinberg, J. G. Sparrow, and R. C. Hahn, Space Science Instrumentation, 1, 407-418, 1975.
2. S073 Preliminary Experiment Report, Skylab Mission SL-4, 5 July 1974.

Final Report, NASA Contract NAS8-30251
Skylab Experiment S073

Preface

After nearly 10 years' investment in time and cost by NASA, and more than 7 years by us, the subject contract was terminated on January 31, 1976 due to the closeout level of funding provided to this experiment for FY 1976 - just as we received the last batch of valid experiment data. This report summarizes experiment activities under contract NAS8-30251 to State University of New York at Albany (October 1973 - January 1976) and under its predecessor contract NAS8-24865, at Dudley Observatory (January 1969 - October 1973). Data analysis will continue beyond July 1976 with support by a NASA grant.

FINAL REPORT*

Skylab Experiment S073: Gegenschein/Zodiacal Light

National Aeronautics and Space Administration
Contract NAS8-30251
to the State University of New York at Albany

J. L. Weinberg

J. L. Weinberg
Principal Investigator

Space Astronomy Laboratory
State University of New York at Albany
Executive Park East
Albany, New York 12203

August 1976

*This is a final contract report, not a final experiment report.

Summary

Skylab experiment S073 was designed to measure the surface brightness and polarization associated with zodiacal light, background starlight, and spacecraft corona during each of the Skylab missions using a 10-color photoelectric polarimeter. The polarimeter and a 16 mm camera were mounted in parallel on a scanning platform at the end of an extension mechanism which could be deployed up to a distance of 5.5 m beyond the spacecraft through scientific airlocks (SAL's) in either the solar or antisolar directions. Unfortunately, the solar SAL could not be used because a permanent heat shield was deployed out the solar SAL following the loss of the spacecraft meteoroid shield during launch. Therefore observations were restricted to the antisolar hemisphere.

Fixed-position and sky-scanning observations were obtained during Skylab missions SL-2 and SL-3 at 10 wavelengths between 4000Å and 8200Å. Although valid telemetry data were not received until October 1975, initial results from the fixed-position data are presented on the spacecraft corona and on the polarized brightness of the zodiacal light.

To provide information on the spacecraft corona in near real time, the photometer was fixed in position at approximately 95 degrees from the sun, and 10-color observations were made on SL-2 mission day 19 starting with the spacecraft in the Earth's shadow and ending in daylight. The reverse sequence was performed later in the same orbit, i.e., day to night. Total instrument reproducibility and the method of differencing day/night or night/day brightnesses were found to give a minimum detectable brightness change of from 1 to 3 $S_{10}(V)^*$. We found no evidence on SL-2 mission day 19 for integrated light from contaminant particulates down to this column brightness threshold for detection. The same analysis will be performed on similar observations obtained at other times during the missions.

Included among the fixed position regions that were observed are the north celestial pole, south ecliptic pole, two regions near the north galactic pole, and 90 degrees from the sun in the ecliptic. The polarized brightness (Stokes parameter Q) of the zodiacal light was found to have the color of the sun at each of these positions. Since previous observers had found the total brightness (Stokes parameter I) to have the color of the sun from the near ultraviolet out to 2.4 μm , the degree of polarization of the zodiacal light is independent of wavelength from 4000Å to 8200Å.

With valid telemetry data now available, it will be possible to derive results for the scanning programs and to complete the analysis of fixed position data, including simultaneous multicolor observations of the north celestial pole from Skylab and from Mt. Haleakala, Hawaii on 12 June 1973.

* Equivalent number of 10th magnitude solar (G2V) stars per square degree at mean solar distance.

Acknowledgements

This research was initiated in 1969 at Dudley Observatory where it was supported by NASA contract NAS8-24865. Since October 1973 the research has been carried out at the State University of New York at Albany with the support of NASA contract NAS8-30251. Design of the photometer and of the automatic programmer were conceived by J. L. Weinberg and H. M. Mann while at Dudley Observatory. Design of the remaining hardware, including the universal extension mechanism/mounting facility, was performed by Martin-Marietta, Denver, together with the engineering and construction and most of the testing.

At NASA Headquarters we thank M. Dubin of the experiment Sponsoring Office and W. Schneider, J. Lundholm, T. Hanes, and others of the Skylab Program Office for their support and encouragement dating back to early 1969. It would not have been possible to implement this experiment successfully without the efforts of scores of people at the Marshall Space Flight Center and the Johnson Space Center and without the tireless efforts of the SL-2 and SL-3 flight and backup crews. Finally, we thank each member of the zodiacal light group at Dudley Observatory (1969-1973) and at State University of New York at Albany (1973-1976): without their dedicated effort, this experiment would not have made it through the hardware and operations phases.

Background Information

Skylab experiment S073, "Gegenschein/Zodiacal Light", originated with E. P. Ney and collaborators at the University of Minnesota, where work continued until delayed by the KSC/Apollo fire. The Minnesota group was unable to continue the experiment when it was included in the AAP experiment list in early 1969, and J. L. Weinberg was asked to become Principal Investigator. A new instrument, a 10-color photoelectric photometer (polarimeter) similar to that used by Weinberg in ground-based studies between 1961 and 1968, was developed to take advantage of the revised schedule and increased vehicle capability and of the subsequent availability of scientific airlocks, to obtain detailed photometric data on the zodiacal light and background starlight, and to provide quantitative information in near real time on the spacecraft corona. The photometer was designed to measure light levels ranging from zodiacal light in the antisolar hemisphere to forward scattering of sunlight from contaminant particulates surrounding the Saturn workshop. All-sky multicolor observations of brightness and polarization had not previously been made from above the earth's atmosphere. The design, construction, testing and calibration were performed in collaboration with Martin-Marietta, Denver and NASA/MSFC. In October 1973 the zodiacal light group at Dudley Observatory, including most of the S073 team, left Dudley Observatory to form the Space Astronomy Laboratory in affiliation with the Department of Astronomy and Space Science of the State University of New York at Albany (SUNYA).

The photometer was designed to perform various fixed-position or sky-scanning programs which could be scheduled during satellite day or night. In order to extend the region of sky observable without incurring reflections from the Apollo Telescope Mount and Saturn workshop, the photometer was to be extended out either the solar or antisolar scientific airlock at

the end of a boom of length either 1.0 m or 5.5 m. The boom was designed for use by experiments S073, T027 (Contamination Measurement), and S149 (Micrometeoroid Particle Collection).

The original planⁱ called for repeated observations from the solar and antisolar scientific airlocks during each of the Skylab missions and coordinated observations with Pioneers 10 and 11 and with colleagues at field sites in Hawaii, Japan, India, France, and the Canary Islands. Loss of the solar scientific airlock to experimenter useⁱⁱ restricted observations to the antisolar hemisphere. Some of the scientific potential of S073 was lost when the solar scientific airlock could not be used and because observations were not scheduled before SL-2 mission day 18 (i.e., near full moon instead of near new moon). Additional potential was lost when the extension mechanism/mounting facility failed early in SL-3 with the photometer attached, making it impossible to retract the facility; both the facility and photometer were jettisoned. In spite of these difficulties, multicolor observations of brightness and polarization were obtained of portions of the antisolar hemisphere.

ⁱ see, for example:

J. L. Weinberg, AAP Flight Experiment S073 (Gegenschein/Zodiacal Light) and Automatic Programming, Feb 1970, rev. May 1970.

Experiment Implementation Plan (EIP), Experiment S073, June 17, 1971.

J. L. Weinberg, A Coordinated Program of Satellite and Ground-Based Observations of the Zodiacal Light, presented at XIVth General Assembly, IAU, 1970; Trans. IAU XIVB, 166, 1971.

Observatory Report, Dudley Observatory and Department of Astronomy and Space Science, SUNYA, Bull. AAS 4, 13-21, 1972.

ⁱⁱ Our backup instrument canister was modified and carried aloft by the SL-2 crew to deploy a parasol out the solar scientific airlock to reduce the high workshop temperature due to loss of the meteoroid shield during launch.

Instrument Description

The Skylab photoelectric photometer was designed to fulfill the overlapping requirements of experiments S073 and T027; namely, to measure light levels ranging from zodiacal light in the antisolar hemisphere to forward scattering of sunlight from contaminant particulates surrounding the Saturn workshop. It was also required to measure the direction and amount of polarization over a range of wavelengths from 4000Å to 8200Å.

The photometer head and extension mechanism are shown in Figure 1. The photometer head consists of a photoelectric photometer (polarimeter), a 16mm Maurer camera, and sunshields. These were positioned on an alt-azimuth mounting and could be extended by an astronaut up to a distance of 5.5 m from the spacecraft to insure that the instrument did not see any part of the spacecraft when the photometer was pointed 90 degrees away from the sun.

The camera system was included to provide information on anomalous results obtained with the photometer and to provide backup information on position using bright stars. A photograph was taken every 11.25 degrees in elevationⁱ and every 45 degrees in azimuth or, for fixed programs, at each filter change of the photometer. Kodak film type 2485 was used with exposures of 2.375 seconds. The camera field of view is approximately 15 degrees; it is defined by the camera sunshield.

The photometer (Figure 2) is similar to that used by us for ground-based studies and consists of a sunshield, a telescope cap, so-called Fabry optics with a 6.35 cm primary objective, two six-position wheels con-

ⁱZero elevation is the direction of the extension mechanism (approximately toward the Sun or anti-Sun) and the azimuth plane is perpendicular to the direction of zero elevation.

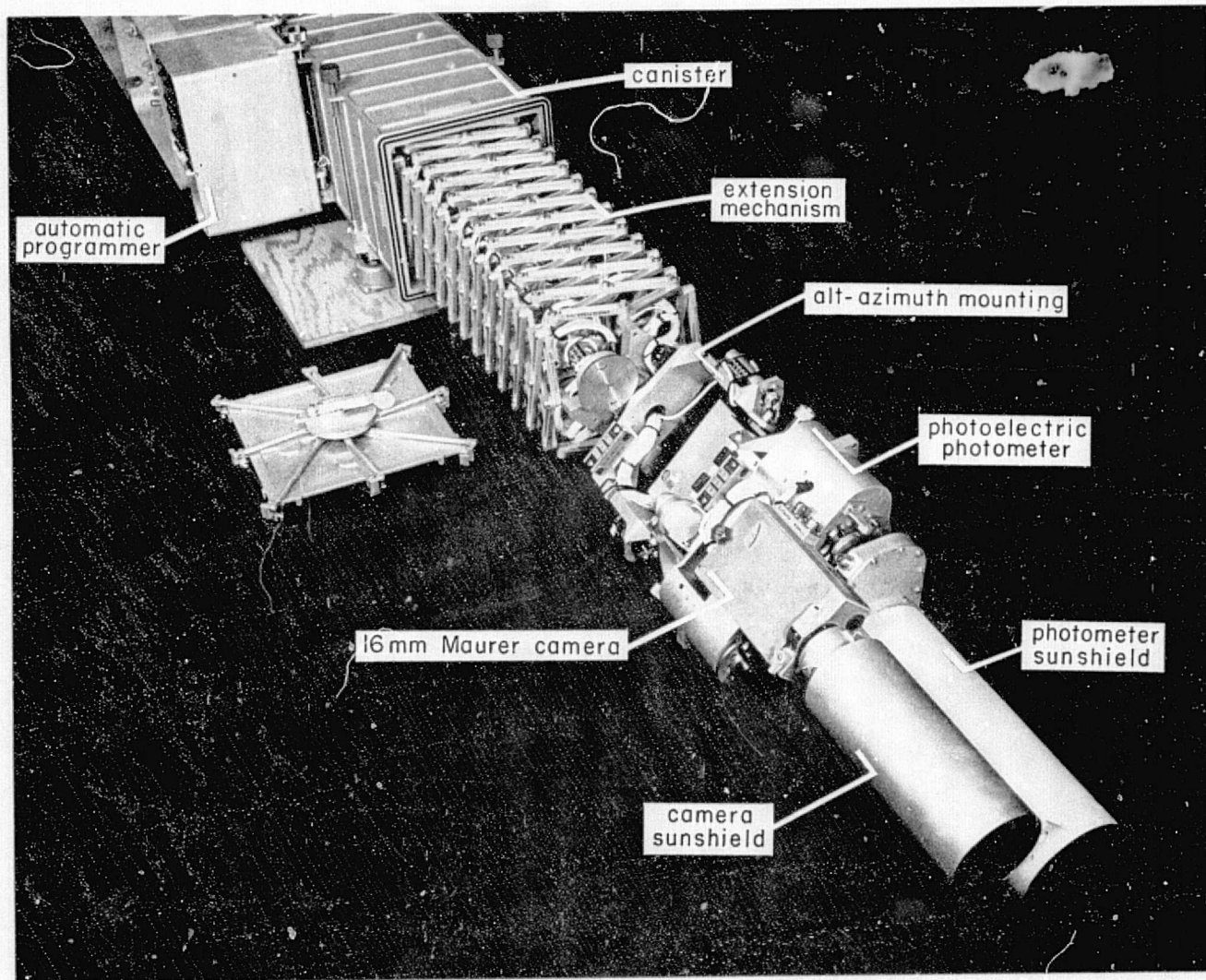


Figure 1. The Skylab S073 photometer/camera system attached to the universal extension mechanism/mounting facility. The canister and attached panels also contain power supplies and automatic and manual control equipment.

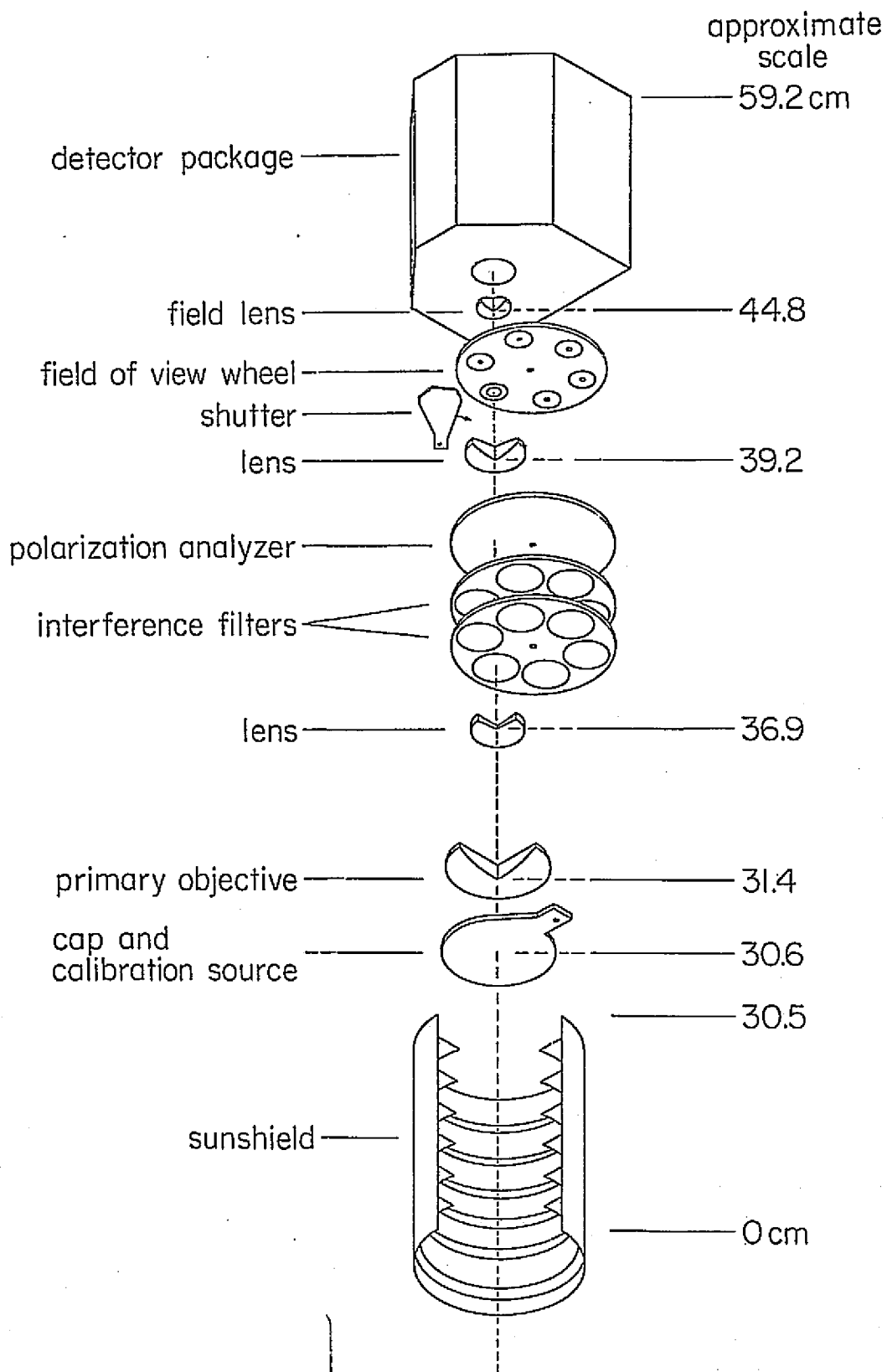


Figure 2. Exploded, oblique view of the photometer head

taining interference filters, a rotating polaroid (HN 32), a field-of-view wheel, a shutter, and a detector package. The control equipment is located on the canister shown in Figure 1.

The size of the Fabry photometer was limited by the aperture of the scientific airlock. The filter bandwidths and transmissions were chosen in conjunction with the photomultiplier spectral response, the 5.84 cm clear objective diameter, and the maximum field of view (6 degrees) to assure an adequate signal/noise ratio at the low light levels expected in the antisolar hemisphere and to provide comparable output at all wavelengths for radiation of solar color.

Color discrimination was provided by two six-position filter wheels; each wheel contained 5 interference filters and an open position. The filter wavelengths were chosen from among those used by usⁱ in ground observations. The filter characteristics are given below.

Interference filter characteristics

Color, nominal (Å)	Central wavelength ^a (Å)	Bandwidth at $\frac{1}{2}$ peak transmission ^a (Å)
4000	4001	110.0
4760	4748	47.5
5080	5068	49.7
5300	5294	61.0
5577	5562	17.0
6080	6063	83.0
6300	6286	20.0
6435	6427	108.2
7100	7093	135.0
8200	8160	220.0

^aAt center of filter, -32°C.

ⁱJ. L. Weinberg, Ann. d'Astrophys. 27, 718-737, 1964.

J. L. Weinberg and H. M. Mann, in The Zodiacal Light and the Interplanetary Medium, (J. L. Weinberg, ed.), 3-8, NASA SP-150, 1967.

The photometer was designed around an EMR 541E photomultiplier (selected S20 response), with a high voltage supply and output voltage differential amplifier having three gain settings (10^5 , 10^6 , and 10^7). These gain settings, coupled with a range of aperture/neutral density filter combinations (see below), gave an instrument sensitivity dynamic range of more than 10^7 . The 6° diameter field of view was chosen for use when observing the zodiacal light in the antisolar hemisphere; this required only a short baffle system with the 6.35 cm diameter objective. However, for planned observations of the zodiacal light to within 15° of the sun, a longer sunshield was included, this fitting within the short baffle and masking the objective down to 1.09cm.

Aperture/Neutral Density Filter Combinations

octal indication	field of view (FOV)	factor difference	
0	6 deg	1	
1	3	4	(i.e., 4 times less light gets through than with FOV 0)
2	3 + ND 2	400	
3	3 + ND 3	4000	
4	1	36	
5	1 + ND 4	360000	

The order of decreasing FOV is thus 0, 1, 4, 2, 3, 5.

An HN 32 polaroid disk rotating at approximately 2 RPS enabled the polarization of the incoming light to be determined from the amplitude and phase of the 4 Hz detector signal. A Pm^{147} -activated phosphor source mounted on the cap could be swung into the optical path (Figure 2) for instrument monitoring while shutter closure enabled the photomultiplier dark current to be measured. For protection, the shutter was activated automatically whenever the intensity reached approximately 10 volts; "full

scale" was nominally 5 volts.

Since one mode of operation of the instrument was designed to map large areas of sky by stepping in elevation and scanning in azimuth, the scan rate set limits on the integration time available to improve the signal/noise ratio. A scan rate of 4 degrees/second was chosen in order to obtain a one color hemispheric map during a single orbital night. The system noise was governed principally by the low photon numbers with some contribution from spikes presumably arising from charged particle induced Cerenkov radiation in the photomultiplier front glass surface, particularly in or near the South Atlantic anomaly. Some reduction in the effect of the latter would have been possible if photon counting electronics could have been used. The time constant of the differential amplifier (~ 2 msec) was compatible with the photomultiplier output sample rate (320/sec). A polaroid synchronous pulse was generated once per revolution and was recorded on another 320 sample/second telemetry channel.

Because of the range of ambient temperatures in which the photometer was expected to operate, a thermoelectric heater/cooler was coupled to the photomultiplier photocathode. This was designed to maintain the photocathode temperature at approximately -10°C during operation in space. Sensors monitored this temperature and the temperature near the filters and the Pm^{147} source.

To achieve experiment objectives, it was necessary to use a large number of complex, two-dimensional scanning routines to assure that the selected regions of sky would be observed in the right way at the right times. An automatic programmer was designed and built for this purpose. The programmer permitted the photometer system to be operated manually or in any of seven automatic modes:

- 0 calibration
- 1 fixed-position
- 2 vertical circle (scan in elevation at fixed azimuth)
- 3 almucantar (scan in azimuth at fixed elevation)
- 4 limited-area sky-mapping (almucantars separated 2.8 deg in elev)
- 5 all-sky mapping (almucantars separated 5.6 deg in elev)
- 6 stowage position return.

Modes 0 and 1 were used for fixed-position observations: of the cap source (mode 0) or of the sky (mode 1). One sequence of 10 filters took 2 minutes. Modes 2 through 5 were used for mapping selected regions at the 4 deg/sec scanning rate of the photometer. A program could be operated any number of times from 1 to 64 and, through the use of an orbital period counter, could be performed automatically during parts of consecutive orbits. The elevation and azimuth range could be selected by the astronaut to provide scans over all, or any portion of, the sky. The programmer also permitted the camera system to be operated manually or automatically.

Fixed-position targets included the Gegenschein and the north and south ecliptic, celestial, and galactic poles. A prime contamination program involved fixed-position observations at 90 - 95 degrees from the sun, starting in the Earth's shadow and continuing to a position in sunlight. A change in brightness and, especially, in polarization as the spacecraft leaves the Earth's shadow is a direct and immediate measure of the spacecraft corona. This program was to be performed early in each mission to provide information on contamination in near real time. Other planned programs included scanning in the ecliptic, scanning the region around the sun and anti-sun, making all-sky maps, scanning through the Earth's atmosphere when the Earth occults the sun, etc.

The instrument was designed to carry out an observing program unattended, after a series of input parameters had been set on the control panels by one of the astronauts. A description of the observing programs carried out during missions SL-2 and SL-3 is given in the next section.

Mission Operations - Planned and Accomplished

50 to 60 percent of the scientific potential of S073 was lost when the solar scientific airlock (SAL) could not be used and because observations were not scheduled before SL-2 mission day 18. Additional opportunities were lost through improper or late scheduling on the ground, incorrect operation of the instrument by the crew, and failure of the mounting drive system at the beginning of the second mission.

Table 1 shows the planned observing programs for SL-2 and SL-3: SL-2, based on ASAL operations only and on a late start, and SL-3, based on limited operations and data from SL-2. Table 2 gives a calendar of S073 observations accomplished during SL-2 and SL-3; the observations are summarized further in Appendix 1.

As noted earlier and in the attached reprint, fixed-position and sky-scanning observations were made during mission SL-2 and, to a lesser extent, during SL-3. Figure 3 depicts sky regions/colors observed in mission SL-2 (mid-June 1973), during which the Gergenschein (elevation 0° , center of circle) was in the Milky Way and the moon was nearly full. Roman numerals indicate the locations of the fixed-position observations: north celestial pole, south ecliptic pole, 90° from the sun near the ecliptic, and north galactic pole. During SL-2 the instrument was operated on 13 separate but not independent occasions, giving a total of only $15\frac{1}{2}$ hours of observing time. In addition:

1. No observations were made in the Z-IV mode which was intended to replace some lost opportunities due to the loss of the solar SAL;
2. No observations were obtained before MD 18, in violation of the MRD which specifically stated that early observation was mandatory:

Table 1. Planned observing programs for SL-2 and SL-3.

<u>Priority</u>	<u>SL-2 (Note 5)</u>	<u>SL-3</u>		
1	1e(N)	1a	Note 1 For SL-2 perform only from within the earth's shadow.	
2	0a	0a		
3	1a	2a		
4	2a (Note 1)	Z-LV (Note 3)		
5	2c	Z-LV (Note 4)		
6	5a	1b		
7	3a (Note 2)	4a		
8	3d	5a		Note 2 Two sequences, and start just before midnight.
9	1d(N)	3a		
10	1b	1e(N)		
11	4a	2c		
12	1d(S)	1d(N)		
13	0a	1d(s)		Note 3 Mode 1 program. This program accomplishes some of the intent of the originally planned Solar SAL performance.
14	1a	3d		
15	2a (Note 1)	1c		
16	2c	1e(S)		
17	1e(S)	1b		
18	1e(N)	2a		
19	3a (Note 2)	3c		
20	4a	1a		
21	3c	0a		
22	1b	1e(N)	Note 4 As above, but using scanning mode.	
23	1c	1e(SL)		
24		3a	Note 5 This plan was generated after it became known that the Solar SAL was unavailable and that <u>no</u> experiment time would be made available before MD 14...at the earliest.	
25		4a		
26		1b		
27		3c		
28		2a		
29		1e(N)		
30		1e(S)		
31		3a		
32		1a		

Skylab Experiment S073 - coordination with Hawaii field site - SL-3

Legend

- perform only during Hawaii window
- Hawaii coordination desirable
- △ perform near equinox and in Hawaii window

<u>Program</u>						
1. Contamination	1a	1a	1a	1c	3d	
2. Gegenschein	1b	1b	1b	3c	3c	4a 4a
3. Ecliptic Pole (N) (S)	1d					
	1d					
4. Celestial Pole (N) (S)	1e	1e	1e			
	1e	1e	1e			
5. Ecliptic Scan	2a	2a	2a			
6. Scan 1 to Ecliptic	3a	3a	3a			
7. All-Sky Map	5a					
8. System Monitor	0a	0a				
9. Vertical Circle	2c					
10. Other Mode 1 programs:	i. Other fixed-position targets (e.g., galactic poles (N,S), libration points, orbit pole points, etc.).					
	ii. Z-LV for part of one orbit. This program must be coordinated with Hawaii.					
11. Other scanning programs:	i. Z-LV. Same as 10.ii. above but a scanning mode is used.					

NOTES

1. Other programs such as those of 10 and 11 should be designated 1o or 2o or 3o.
2. Hawaii window is defined as all times when the moon is below the horizon and the sun is 18 or more degrees below the horizon. SL-3 ground-support is not possible on MD's 15 through 19 and 45 through 49.

Table 1, continued

Table 2. Observations with the Photometer

Mission	Mission day	1973 date	Mode	Program ^a
SL-2	19	June 12	4	sky map (7 colors, 5300-8200)
	19		1	I north celestial pole
	19		1	II south ecliptic pole
	19		1	III contamination, 2 parts: night/day, day/night
	22	15	4	sky map (9 colors, 4000-7100)
	22		1	IV north galactic pole
	22	15	2	V elevation scans
	22	15	4 ^b	sky map (4000, 4760)
	23	16	4 ^b	sky map (7 colors, 5080-7100)
	23	16	3	azimuth scans (5 colors, 4000-5577)
	23	16	3 ^b	azimuth scans
	24	17	3 ^b	azimuth scans
	SL-3	5	August 1	4 ^b
6		4 ^b		sky map (4760)
7		3	1	Gegenschein (5 colors, 4000-5577)
7		3	1	contamination, night/day
7		3	1	night/day scan, gravity-oriented
7		3	1	Gegenschein
7		3	2 ^b	elevation scans
8		4	2 ^b	elevation scans

^a 10-color observations, unless otherwise indicated.

^b Program started one day and ended the following day.

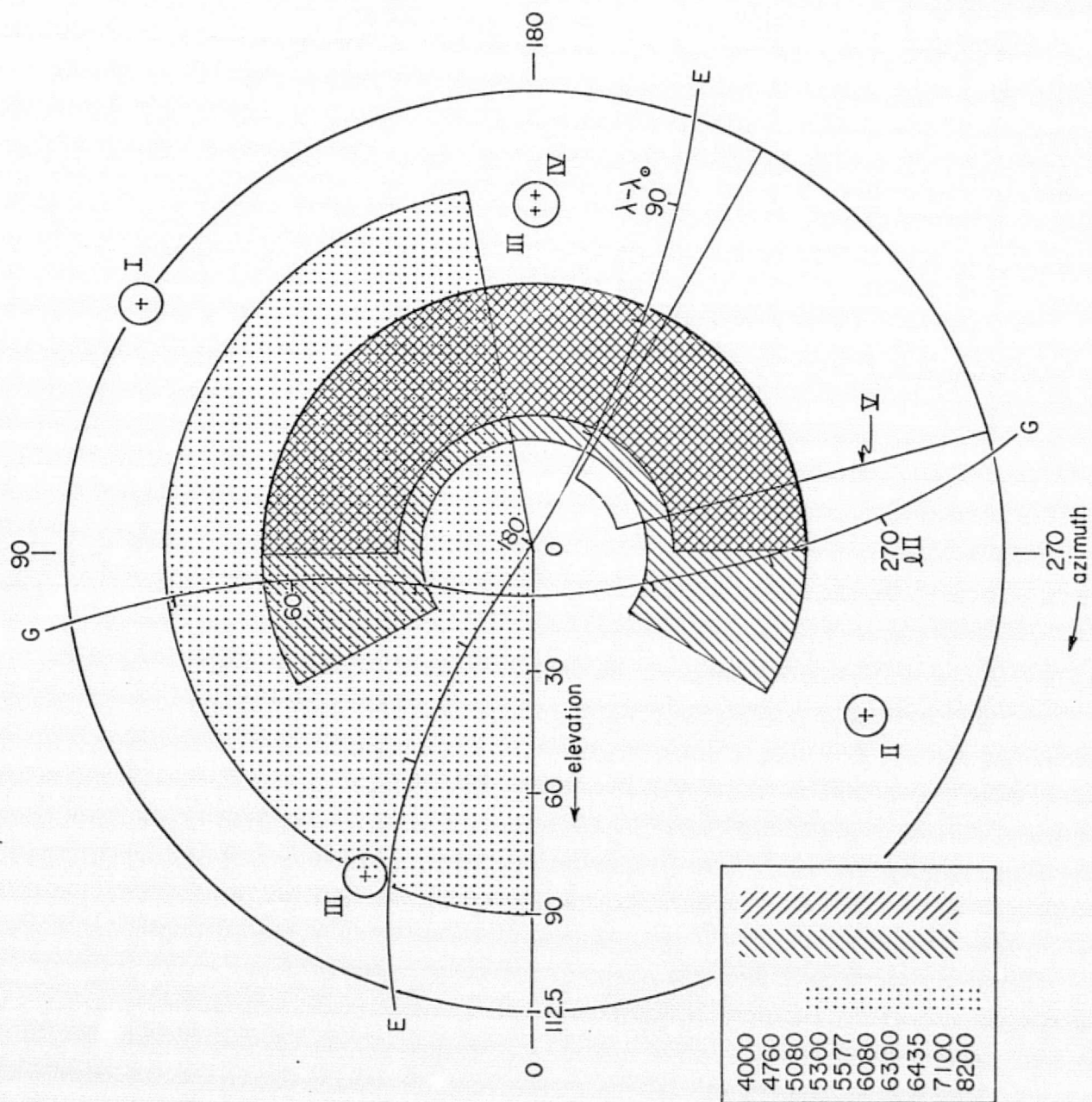


Figure 3. Regions of the antisolar hemisphere for which useful data were obtained during SL-2 (see, also, Table 2). G and E show the positions of the galactic equator and ecliptic, respectively. l^{II} refers to system II galactic longitude in degrees and $\lambda - \lambda_0$ refers to the ecliptic longitude of the observed point with respect to the Sun, in degrees. The inset shows the filters used with the sky-mapping programs.

3. No observations were obtained in the period new moon + 1 week and it was not even recognized that S073 observations were effected by the position and phase of the moon.

Commencement of observations in SL-3 was delayed again by spacecraft problems and by the performance of limited malfunction procedures on the photometer dictated by the shaft drive anomaly detected late in SL-2 (ref. Appendix 4). During SL-3 (early August 1973) the Gegenschein was out of the Milky Way and the moon was between new and first quarter. Thus, it was possible during SL-3 to perform a wide range of programs, including mapping the entire antisolar hemisphere in each of the 10 wavelengths. Unfortunately, a crew error resulted in our obtaining these observations at only 2 of the 10 wavelengths, and one of these (4000A) only covered half of the antisolar hemisphere due to higher priority use of the on-board recorder. After performing several other selected programs, the extension mechanism/mounting facility failed and we were unable to repeat the sky mapping program at the other wavelengths. Observations obtained during SL-3 prior to jettison are summarized in Appendix 1.

The confusion and lack of organization and planning and the repeated violation of S073 requirements and of the requirements of other SAL experiments has been documented elsewhere. We only note here that those observations that were obtained were obtained with great difficulty.

Complementary Observations from the Ground and from Pioneers 10 and 11

Complementary and simultaneous observations were planned, utilizing Skylab (multicolor visible-near infrared polarimeter), Pioneers 10 and 11 (two-color (blue, red) polarimeter), and instrumentation in Hawaii (multicolor visible-near infrared polarimeter). The nightsky continuum cannot be observed from the ground when the moon is above the horizon, and June 12 (AM), 1973 was the last opportunity during SL-2 to observe from our field site atop Mt. Haleakala, Hawaii. It was also the first opportunity for S073 to observe the sky from Skylab during a crew day while it was still night in Hawaii. Fortunately, the weather at Haleakala cooperated, and simultaneous observations of the north celestial pole were made from Skylab and from Haleakala at the following colors:

<u>wavelength</u>	<u>observations</u>	
	<u>Skylab</u>	<u>Haleakala</u>
4000 Å	x	
4760	x	
5080	x	x
5300	x	x
5577	x	x
6080	x	x
6300	x	x
6435	x	
7100	x	x
8200	x	

Supporting observations of the north celestial pole were also obtained from Haleakala on June 10 and 11. The ground data have been partly reduced; the Skylab data have just now been made available. Other complementary and simultaneous observations:

June 7 - a partial sky map from Pioneer 10 at a sun-spacecraft distance of 4.26 AU;

June 12 - a partial sky map from Pioneer 11 which was simultaneous with celestial pole observations from Skylab and from Haleakala;

June 14 - the first full sky map from Pioneer 11 (at a sun-spacecraft distance of 1.39 AU); simultaneous with program 4a observations from Skylab.

This represents the first time that coordinated observations (ground - S/C and S/C - S/C (near-earth, deep space)) have ever been performed in studies of the light of the night sky.

The Observations and their Reduction

1. Photometer.

The primary measurements of the photometer are detector output voltage versus time (i.e., polaroid position) and position on the sky. Since the sky brightness is partially polarized, the rotating polaroid modulates the polarized component (and polarizes the unpolarized component), resulting in a sinusoidal variation in the photometer detector output. The amplitude and phase of this modulation are proportional to the brightness of the polarized component and the azimuth of vibration, respectively. The level above dark current is proportional to the total brightness. Thus, it is possible to determine the principal Stokes parameters (I, Q, U) and, therefore, to derive the degree of polarization of the measured radiation. Figure 4 shows a computer plot of post-mission data, detector output versus time; although these data have a larger-than-typical polarization (the data are contaminated by earthshine), they show the form of the data.

The photometer output data are being analyzed by digital synchronous detection and by a least squares fit to an expression of the form

$$\text{PMT output} = A + Bt + C \sin(\omega t + D),$$

where the frequency ω is determined from the repetition rate of the polaroid synchronous pulses. The "B" term must be introduced since the

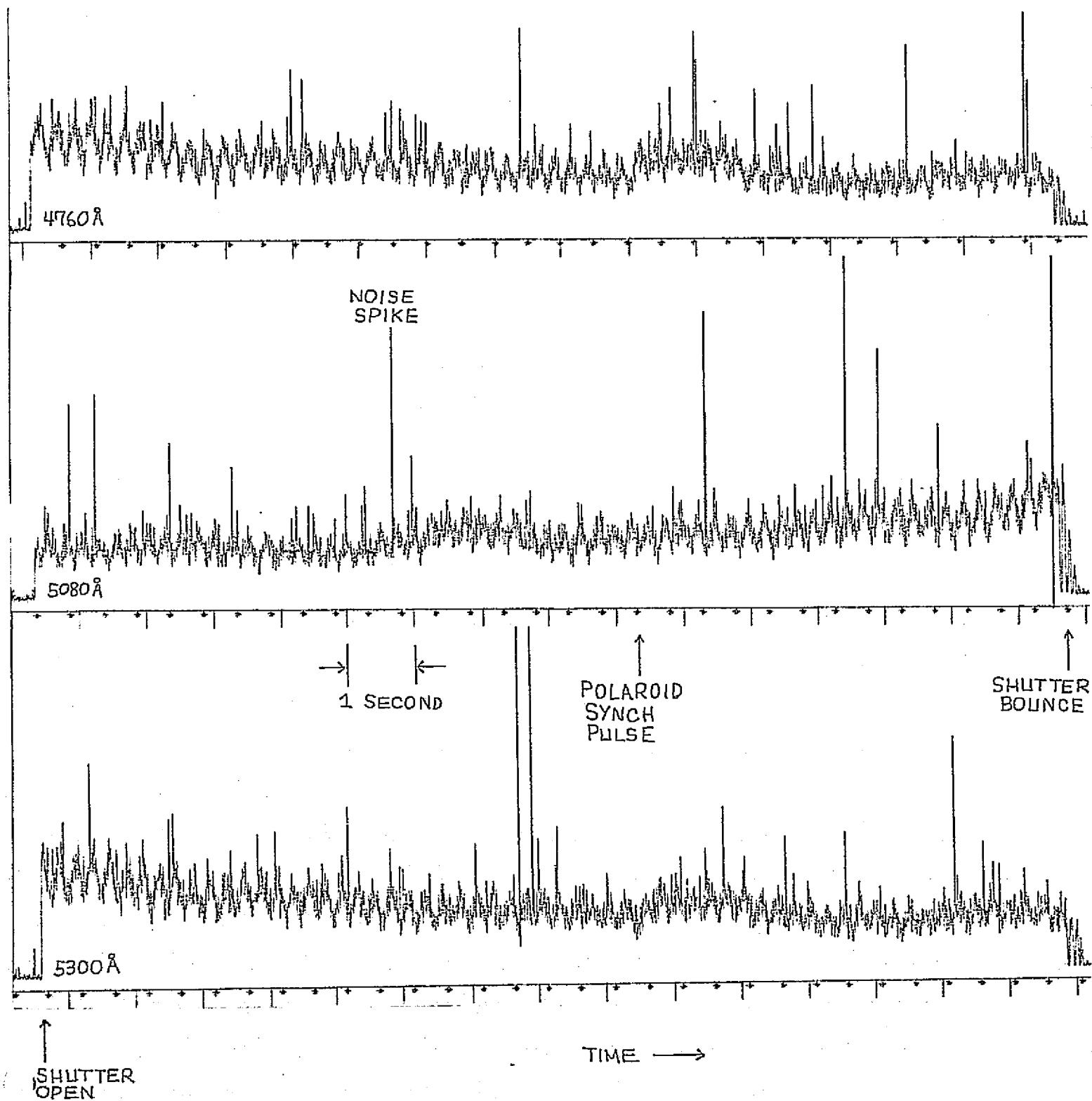


Figure 4. Representative computer-generated plots of detector output versus time (polaroid position) for an azimuth scanning program: 3 colors, run 12, SL-2. These data are contaminated by stray light, but they demonstrate the form of the data.

background starlight and, to some extent, the zodiacal light brightness change rapidly with azimuth angle during the sky mapping programs and, therefore, with time in the above expression; a linear slope suffices provided a fit is attempted only over a relatively small interval of time, say one second. The phase angle "D" can be related to the orientation of the plane of polarization, which in general corresponds to that of the zodiacal light.

Much of the telemetry data was seriously degraded as a result of the introduction of an amplitude compression factor during transmission of the data between ground stations prior to preparation of experimenter tapes; changes in photomultiplier output voltage that did not exceed 4 units (full scale range 253 units) were ignored. Since the amplitude of the sinusoidal (polarized) signal component was often less than this, much of the data could not be analyzed properly. Measurements during which the photometer remained pointed at fixed directions on the celestial sphere were not affected as much as the mapping programs since 10 seconds of sky measurement data are available for a given filter between dark current readings; with these data digital synchronous detection could be used. Initial results from the fixed position data have been presented on the spacecraft corona and on the polarized brightness of the zodiacal light (see later).

Figure 5 outlines the various steps involved in the handling, processing, and reduction of experiment data. Circles represent existing software; triangles represent hard copy. The various modules that comprise this reduction system are listed and described below.

73 MAIN or 73 MAIN/ENG. These programs are nearly identical with the

ORIGINAL PAGE IS
OF POOR QUALITY

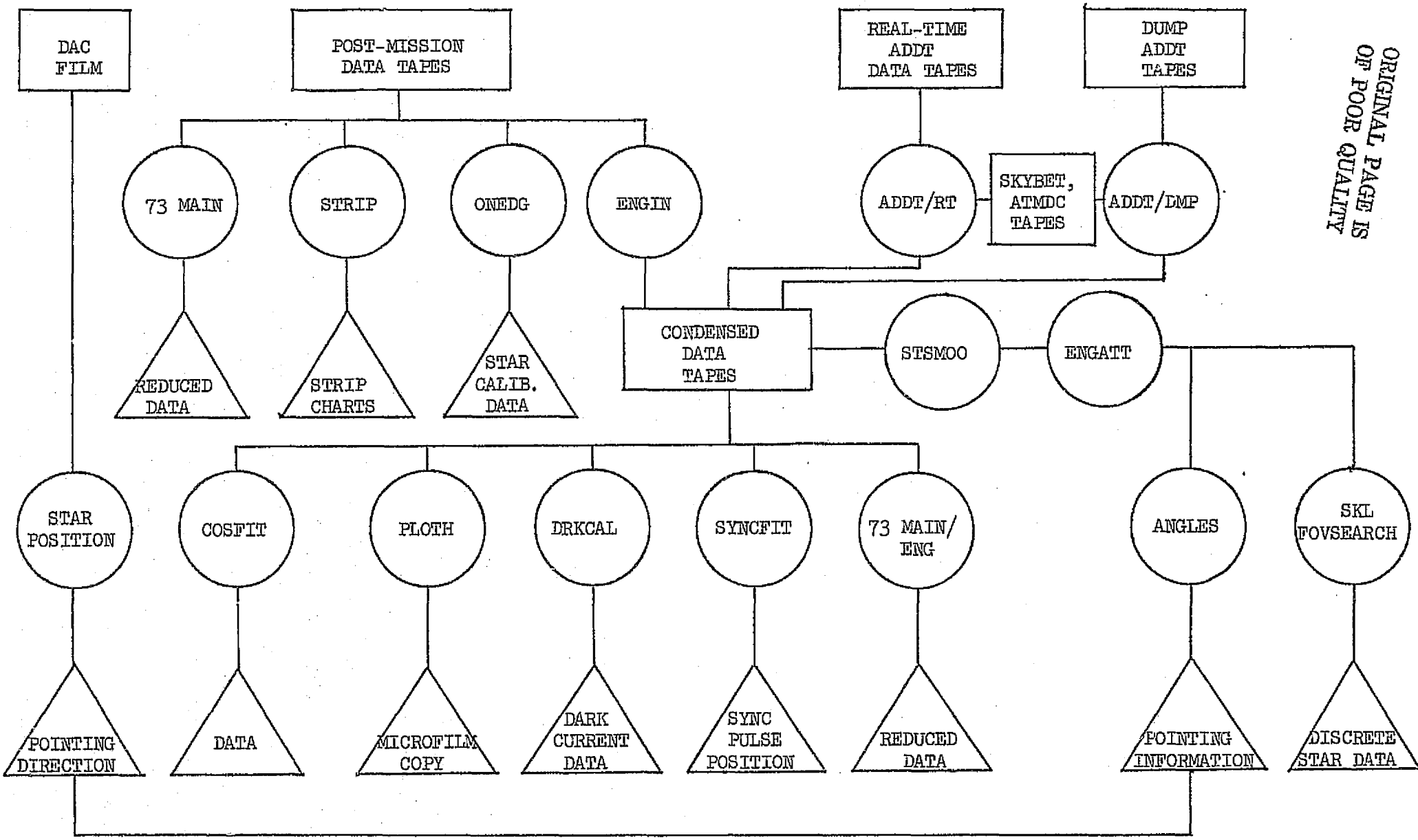


Figure 5. Steps in the handling and processing of photometer and camera data.

exception that 73 MAIN reads the Post-Mission tapesⁱ and 73 MAIN/ENG reads the condensed data tapes. These programs accept the raw data, make the necessary corrections, and call a computational routine which provides the following:

- a) Total measured brightness in $S_{10}(\text{vis})$ units
- b) Brightness of the polarized component
- c) Orientation of the plane of polarization
- d) Pointing direction
- e) Engineering information (instrument parameters)
- f) Diagnostic information.

These programs utilize a vector analysis routine (digital synchronous detection) to compute the polarization information.

STRIP. Accepts the raw signal data (detector output in volts) and provides a plot of signal versus time for visual analysis.

ONEDG. Analyzes the raw signal data in small time blocks (detector output is sampled at 320 SPS) to provide data on total measured brightness as bright stars pass through the field of view; this is required for calibration.

ENGIN. Reformats the raw data on approximately 200 tapes and places them on 7 condensed data tapes.

ADDT/RT and ADDT/DMP. These programs accept data from the ADDT tapes (raw data without compression) and Skybet and ATMDC tapes (position data), apply engineering unit conversions and time conversion, and reformat the data onto condensed data tapes.

STSMOO. Accepts the raw values of azimuth and elevation telemetry data and applies corrections for data scatter and drop-outs and provides an improved set of instrument coordinates for further computations.

ENGATT. Processes azimuth and elevation data along with vehicle position data to provide pointing data in terms of right ascension and declination.

ANGLES. Transforms instrument pointing to both galactic (systems I and II) and ecliptic coordinates. It also computes the angle between the look direction and the moon, sun, and earth.

ⁱ Post-Mission tapes refer to experimenter data tapes. As noted earlier, these data were degraded by use of a data compression scheme. The result was that these Post-Mission data consist of a piece-by-piece reconstruction of data fragments with different quality down to msec intervals; i.e., we could not "process through" much of the data, and much of the data were not capable of analysis. Also, 25% of the data were never received and many of the tapes contained problems (incorrect time, data outages, other experimenter's data, etc.) which prevented any processing. These were the only data available, however, and we used them to develop and test our reduction software and to examine some of the engineering and science data that were less affected by these problems.

SKL FOVSEARCH. Uses the final computed/verified pointing directions to identify all "resolved" stars in the field of view. Since a suitable star catalog does not exist, it was necessary to create one. This was done by merging and editing the Yale Observatory Bright Star Catalog and U.S. Naval Observatory Photoelectric Catalogue, eliminating all stars with V magnitude greater than 8.0, adding several hundred stars from the Moscow Variable Star Catalog, etc. Our merged star catalog is also being used by the Max Planck Institute for Astronomy, Heidelberg, for reduction of data from their Helios A/B zodiacal light experiment.

COSFIT. As noted earlier, the photometer output data are being analyzed by digital synchronous detection and by a least squares fit (COSFIT) to an expression of the form

$$\text{PMT output} = A + Bt + C \sin(\omega t + D).$$

PLOTH. Accepts the condensed data tapes and reformats the data for microfilm hard copy of the raw data (down to the level of individual samples).

DRKCAL. Applies smoothing and rejection sampling routines to the raw dark current (shutter closed) data. This supplements the dark current routine which is in SO73MAIN.

SYNCFIT. Applies smoothing techniques to the raw sync pulse data. This is necessary because some samples in this telemetry channel were used for other data, resulting in the possibility that a sync pulse could be lost or translated in time.

Except for refinements needed in processing observations in the South Atlantic anomaly and when applying COSFIT to data in regions of small polarization and rapidly changing background, the following major steps in the reduction system are operational:

- absolute calibration data are available to convert to absolute values of total brightness (starlight plus zodiacal light) and polarized brightness (only zodiacal light, except at low galactic latitudes) and, therefore, to determine total degree of polarization;
- the observed and predicted directions of polarization can be determined;
- the position of each instantaneous field of view can be determined in the spacecraft, celestial, ecliptic, and galactic coordinate systems;
- all stars in each instantaneous field of view can be identified using our merged star catalog;
- using semi-automatic methods, the brightness contribution of these stars can be determined and subtracted from the total brightness, leaving zodiacal light plus background starlight.

These data can be derived for each observation; i.e., for each observed position and color in these observations. Some additional work is required

to fully automate the procedure for removing the brightness contribution of "resolved" stars from the data numbers associated with each instantaneous field of view. A similar code has been developed for use with our Pioneer 10/11 zodiacal light data; it needs only minor modification to permit its use with the Skylab data. Still further work is required to separate the background starlight and zodiacal light.

2. Data Acquisition Camera.

A 16 mm Data Acquisition Camera (DAC) was boresighted with the photometer to provide information on anomalous results obtained with the photometer and to provide backup information on instrument pointing. The DAC and film type 2485 combined to provide excellent data: the film was not adversely affected by radiation, many frames contain sharp starfields suitable for use in determining pointing, the airglow banding is clearly visible in a number of frames, the exposure durations are for the most part excellent, and a number of frames are "clean" enough to permit photometric analysis via digitization. On the negative side, there appear to be some cracks in the film and, in some portions of the film, electrostatic "fogging".

The camera was programmed to expose a frame with every filter change in the fixed-pointing programs and with every 45° of azimuth motion or 22.5° of elevation motion in the scanning programs. 3154 frames were exposed during SL-2. Because the instrument was jettisoned during SL-3, the film from that mission was not recovered. Since the DAC had no capability for coding the various frames, the first task was to catalogue all frames and separate them into frames for smeared starfield - position use, frames containing anomalous data or frames obtained when the photometer obtained anomalous results, and frames con-

taining "clean" scientific data (e.g., the airglow banding, regions of sky devoid of bright stars, etc.). The first step involved quick-look numbering and identification of each frame, including determination of the astronomical coordinates of the center of frame, identification of airglow, horizon cuts, bright planet transits, anomalies, mount jiggle, etc. This cataloguing showed that the camera was not light-tight and, therefore, that the frame in position during orbital hold periods was always overexposed.

The exposure time (2.375 sec) was chosen as a compromise between obtaining sufficient density for weak stars and minimizing the smearing due to camera scanning motion. Stars down to V magnitude 5 and 6 were able to be identified in frames taken during the scanning and fixed-position programs, respectively. Because of this sensitivity limitation, many of the scanning frames do not contain readable images. The useable frames were noted in a master log.

For those frames which contained readable images, a microfilm reader-printer was arranged to project the frame on a view glass which was calibrated in an arbitrary x-y coordinate system. Each star was identified and its position noted on the arbitrary scale. A computer program was written which compared the distance between any two stars in the arbitrary system with the true distance computed from the known right ascension (RA) and declination (DEC). By suitable weighting and averaging of the results obtained from each pair of stars, a scale factor (arbitrary units to actual distance) was determined. The program then used this scale factor to determine the center of the frame (0,0 in the arbitrary scale) in RA and DEC from each star in the frame and the logged positions of the stars in the frame. These results were again weighted and averaged, and the

best determination of the RA and DEC of the center of the frame was made. The orientation of the frame was determined in a similar manner, and the azimuth to true north was computed. Frames which contained smeared stars were read at both the beginning and end of the smears, and the center of frame was determined for the times of shutter opening and shutter closing.

Approximately 90% of the readable frames were read and 20% computed when this effort was terminated due to funding limitations. The conversion of telemetry values of azimuth and elevation to equatorial coordinates involves a complex series of transformations utilizing both matrix and quaternion arithmetic (see Appendix 3). The DAC pointing data were sufficient to permit a comparison with results derived from telemetry data and to pinpoint problems in the telemetry pointing computations.

Analysis of star positions in the SL-2 Maurer photographs enabled the right ascension and declination of the camera pointing direction to be determined generally within $\pm 0.2^\circ$, provided that at least 3 or 4 stars could be identified. Comparison with the orientation of the photometer calculated using the attitude of the ATM coordinate axes showed agreement usually within $\pm 0.5^\circ$. On some occasions, however, the two methods gave discrepant results. Several possible sources are being investigated: differences in rigidity or lack of reproducibility in the direction of extension of the boom for the 1.0 m and 5.5 m extensions; errors in telemetry data on the various ATM or vehicle reference directions and their transformations; and errors in telemetered data on photometer azimuth and elevation.

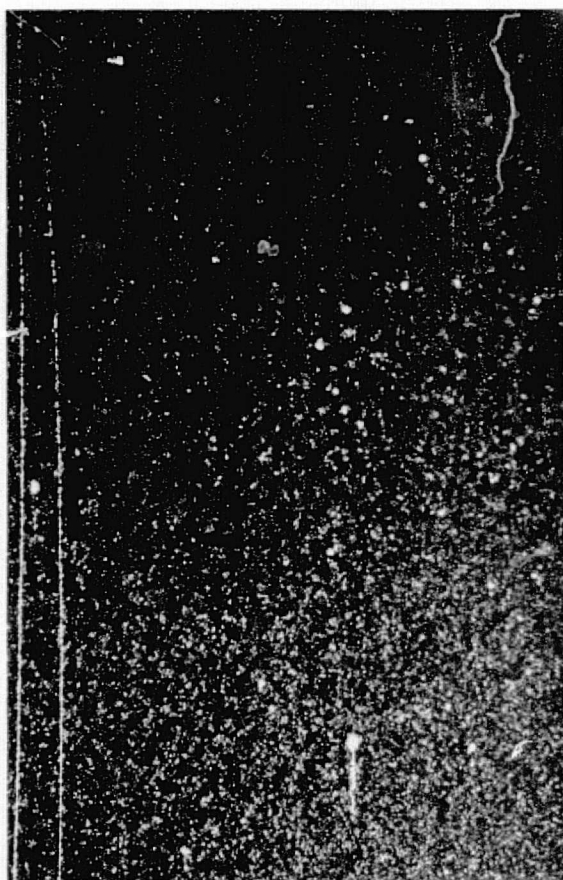
Many of the frames were invaluable for diagnostic purposes. Anomalously high photometer signals were often seen to be a result of stray light from

the earth or part of the illuminated spacecraft. Representative photographs are shown in Figure 6.

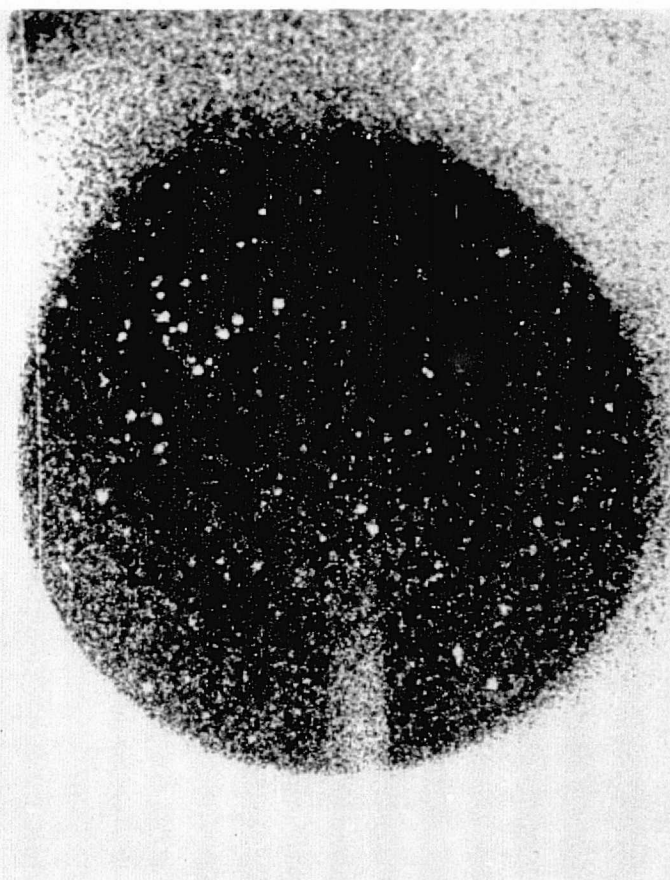
After the photometer and extension mechanism were jettisoned, attempts were made to recover some of the lost experiment opportunities by using on-board photographic equipment. Five photographs were made of the Gegenschein during SL-3 using experiment T025 equipment. During SL-4 35 contamination photographs and 62 photographs of scientific targets (Gegenschein, zodiacal light, Comet Kohoutek tail, lunar libration regions L_4 and L_5 , and various astronomical objects) were taken. Unfortunately, the film pressure plate appears to have separated from its location in the camera back, resulting in every frame of the SL-4 data being out of focus. A great deal of work was done to evaluate these photographs and to see what would be required to salvage some of the data. The results are given in the attached Preliminary Experiment Report for Skylab Mission SL-4.

Calibration

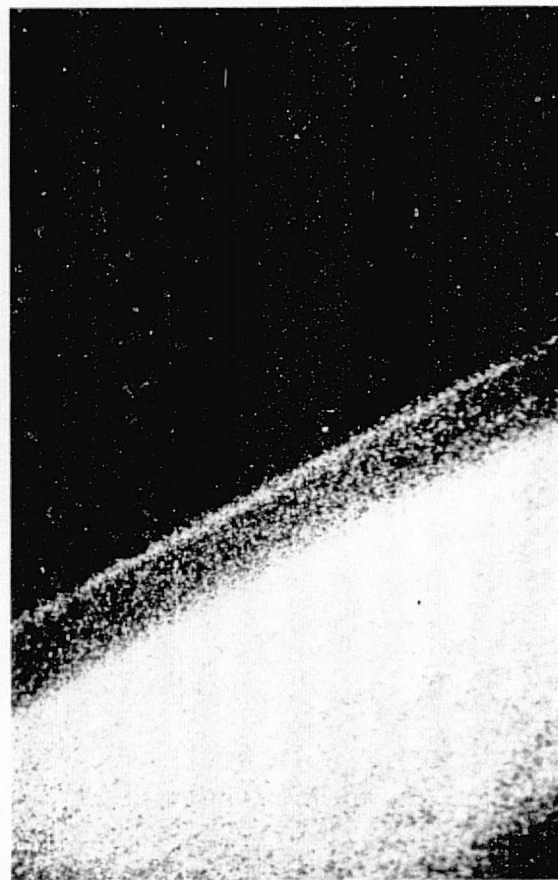
Absolute calibration of diffuse field photometers used in zodiacal light studies is usually achieved by one of two methods: laboratory calibration using a radioactively excited phosphor or diffuse source which has been previously related to a standard lamp, or field calibration using star crossings and the area and response of the photometer field of view. Our intent was to use an absolute calibration based on a secondary standard (a 15cm luminous diameter, C^{14} - activated phosphor source), supplemented by calibrations obtained from star crossings. The Pm^{147} source mounted on the cap (Figure 2) was to be used to measure changes in the photometer during flight and changes between final calibration and initial instrument turn-on. From the Fritz Peak Observatory



i



ii



iii

Figure 6. Representative 16 mm photographs taken during fixed-position programs in Skylab mission SL-2 with the camera that was mounted parallel to the photometer:

- i A typical 2.375 second photograph showing a grouping of well-defined star images.
- ii An example of the effect of stray light. In this case, the sunlit Earth illuminated part of the spacecraft, which, in turn, illuminated the sunshield baffles. Note that the sky background is still dark and that the star field is still well defined.
- iii The Earth's limb and airglow layer. Note the presence of star images above and below the airglow layer.

Photometry Laboratory and the Max Planck Institut für Astronomie, Heidelberg, each of which has primary standards and experience in diffuse source calibration and intercomparison, we obtained absolute calibrations of our laboratory C^{14} source and several other sources, including the Pm^{147} flight source. In our laboratory we determined the change of brightness with temperature of these sources as well as the irradiance ratio between the C^{14} source and several Pm^{147} sources at wavelengths ranging from 4000\AA to 8200\AA .

The thermoelectric heater/cooler maintained the photomultiplier photocathode near -10°C after equilibrium was achieved in space; however, during ground calibration the photocathode temperature was at times as high as 15°C . The manufacturer's data for this type of photomultiplier tube (EMR 541E) indicate that this 25°C change in temperature would cause a photocathode sensitivity change of less than 1%. The photomultiplier dynode chain temperature remained significantly higher than the photocathode temperature by virtue of the heat generated by the surrounding electronics. The estimated dynode temperature difference of 55°C between ground calibration and inflight operation would, according to the manufacturer, cause a gain change of about +10%. It should be noted that the use of "mean" tube temperature coefficients can cause significant errorsⁱ.

The nominal temperature of the interference filters in flight was -32°C . The wavelengths of peak transmission of the various filters were shifted by up to 15\AA by this decrease in temperature from nominal 25°C , as calculated from the filter temperature coefficients given by Bliffordⁱⁱ. This was particularly significant for the two narrow bandpass filters.

ⁱYoung, A. T., Appl. Opt. 2, 51-60 (1963).

ⁱⁱBlifford, Jr., I. H., Appl. Opt. 5, 105-111 (1966).

Changes in bandwidth and peak transmission are not of consequence for similar "Thin Films" filtersⁱ. The large temperature-brightness coefficient of the Pm^{147} source (as much as $-0.28\%/^{\circ}\text{C}$ at some wavelengths), coupled with unexplained differences in the output of the source at similar temperatures in ground calibration and in-flight measurements just after launch, made it difficult to use the flight source for relative calibration. These uncertainties and unexplained differences between the Heidelberg and Fritz Peak calibrations of the C^{14} source made us reject this method of calibration and use, instead, a calibration obtained from star crossings.

With a 6° diameter field of view, there are only a few bright stars that can be used for calibration, particularly because of the relatively small area of sky covered during the sky mapping programs. Thus we have based the calibration upon the readings obtained during crossings of Vega, Arcturus, and Spica; each star was scanned at least twice at all ten wavelengths except 8200\AA , and the photometer star signal was related to the star's magnitude at each filter wavelength. The magnitude was determined from a $1/\lambda$ curve fit to the Johnson, et al.ⁱⁱ and Mitchell and Johnsonⁱⁱⁱ photometric data. Comparison was also made with calibrations based on flux measurements made by Hayes and Latham^{iv} for Vega, Bahner^v and Aller, et al.^{vi} for Spica, and Schild^{vii} for Arcturus. Since

ⁱBlifford, Jr., I. H., Appl. Opt. 5, 105-111 (1966).

ⁱⁱJohnson, H. L., R. I. Mitchell, B. Iriarte, and W. Z. Wisniewski, Commun. Lunar and Planet. Lab. No. 63, Univ. of Arizona (1966).

ⁱⁱⁱMitchell, R. I. and H. L. Johnson, Commun. Lunar and Planet. Lab. No. 32, Univ. of Arizona (1969).

^{iv}Hayes, D. S. and D. W. Latham, Astrophys. J. 197, 593-601 (1975).

^vBahner, K., Astrophys. J. 138, 1314-1315 (1963).

^{vi}Aller, L. H., D. J. Faulkner, and R. H. Norton, Astrophys. J. 144, 1073-1100 (1966).

^{vii}Schild, R., unpublished measurements, reproduced in Breger, M., Commun. in Astronomy No. 1, State Univ. of New York at Stony Brook (1971).

Spica is a variable (binary) with a total range of 0.09 magⁱ, the calibration for this star was based on the mean value. Conversion to a calibration in units of $S_{10}(V)$ ⁱⁱ was obtained using the absolute flux of Vega given by Hayes and Lathamⁱⁱⁱ, the absolute solar flux given by Johnson^{iv}, and the apparent solar visual magnitude of -26.73^v.

The field of view of the Skylab photometer was calculated from laboratory measurements, in one color, of the sensitivity across the field; these indicated that the field was sensibly flat with little vignetting. Later measurements at all wavelengths on a duplicate photometer gave the same result.

We do not expect to incur an error of more than 2-3% due to the Vega fluxes we have chosen, except at 4000Å and 8200Å where reliable flux estimates are difficult due to the convergence of the Balmer and Paschen lines, respectively^{vi}. The precision of the star calibrations is better than $\pm 6\%$ at all wavelengths except 6300Å and 8200Å where it is $\pm 10\%$. Thus, anticipating no significant error in the field of view measurement, we estimate the uncertainty of our calibration at each wavelength as not more than: 8200Å $\pm 20\%$; 4000Å $\begin{matrix} +10 \\ -20 \end{matrix} \%$; 4760Å $\begin{matrix} +6 \\ -12 \end{matrix} \%$; 6300Å $\pm 10\%$; and $\pm 6\%$ at all other wavelengths. Agreement between the Johnson^{iv} solar flux values and the more recent data of Labs and Neckel^{vii} gives us confidence

ⁱShobbrook, R. R., D. Herbison-Evans, I. D. Johnston, and N. R. Lomb, Mon. Not. Roy. Astr. Soc. 145, 131-140 (1969)

ⁱⁱEquivalent number of 10th magnitude solar (G2V) stars per square degree at mean solar distance.

ⁱⁱⁱHayes, D. S. and D. W. Latham, Astrophys. J. 197, 593-601 (1975).

^{iv}Johnson, F. S., J. Meteorol. 11, 431-439 (1954).

^vStebbins, J. and G. E. Kron, Astrophys. J. 126, 266-280 (1957).

^{vi}Oke, J. B., Absolute Spectral Energy Distribution in Stars, in Annual Review of Astronomy and Astrophysics, Vol. 3 (L. Goldberg, editor), 23-46, (Palo Alto: Annual Reviews, Inc.), (1965).

^{vii}Labs, D. and H. Neckel, Solar Phys. 15, 79-87 (1970).

that the uncertainty in solar flux does not contribute significantly to our error except at 4000Å and 4760Å; at these wavelengths it is probable that we have introduced an error of about 10% by using the Johnson data. In subsequent studies we will make use of the Labs and Neckel data, following the recommendations of Sparrow and Weinbergⁱ.

Measurements of the orientation of the polaroid with respect to the time of the synchronous pulse had been made in the laboratory five months before launch utilizing a pile of plates polarizerⁱⁱ. Evidence for birefringence within the optical train was indicated by a difference of up to 2° in the orientation angle with wavelength. Similar measurements two months later with the photometer mounted in the spacecraft did not show this effect, nor was it seen during flight observations. Instrumental polarization was less than 1% at all wavelengths.

ⁱSparrow, J. G. and J. L. Weinberg, The S₁₀(V) Unit of Surface Brightness, in Proc. IAU Colloq. No. 31, Lecture Notes in Physics, Number 48, 41-44, (Springer-Verlag, Heidelberg), 1976.

ⁱⁱWeinberg, J. L., Appl. Opt. 3, 1057-1061 (1964).

Initial Results

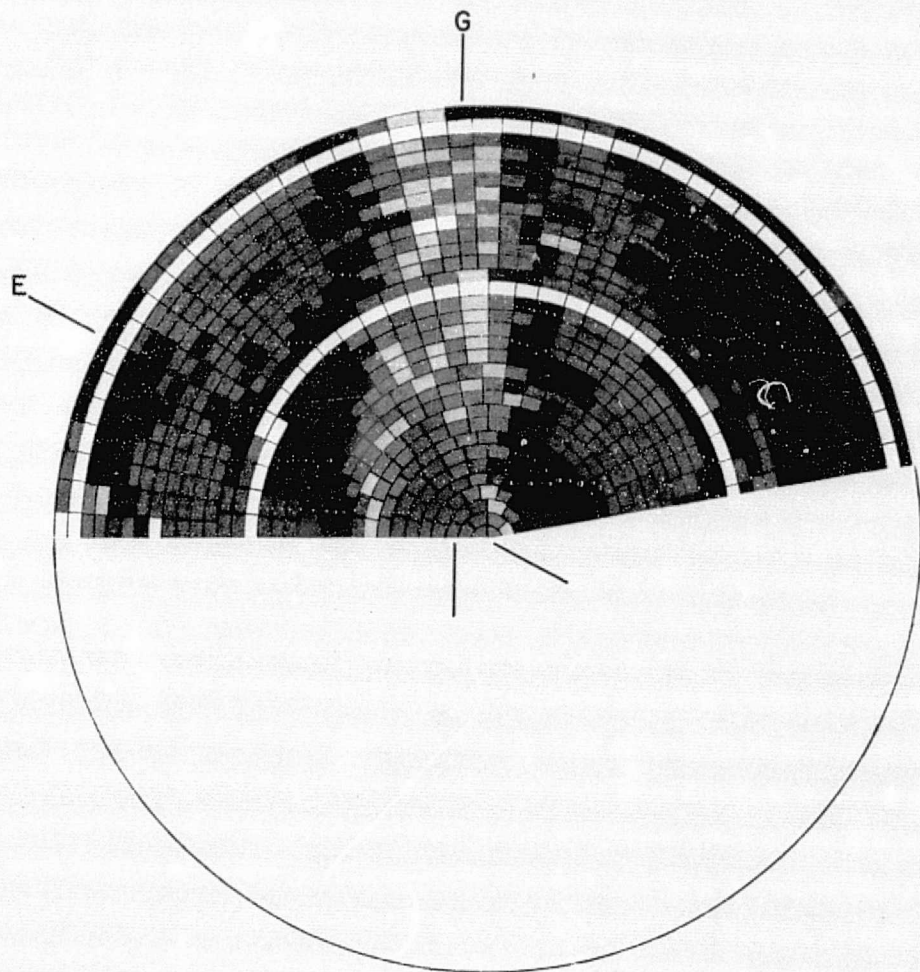
Data from a partial sky map during Skylab mission SL-2 are used in Figure 7 to illustrate the form of the photometer data and one method used to display it. The brightnesses and polarizations are "total"; they include zodiacal light, background starlight (integrated starlight and diffuse galactic light), and the contribution of individually-resolved stars. With the 6° field of view used for most of the zodiacal light observations, a 6th magnitude star contributed an equivalent brightness of approximately $1 S_{10}(V)$. A protective shutter was activated when the brightness exceeded a fixed threshold such as Jupiter (inner white band) or the illuminated earth (outer white band). Some of the complex structure in the total polarization arises from the use of a small increment size in percent polarization and from the effects of individual stars. The relatively large increment used in the total brightness masks the contribution of individual stars.

This figure is shown to illustrate the form of the data, not the science therein. But even in this raw form, a number of features can be seen:

- (1) The Gegenschein is included in the bright region at and to the left of elevation zero.
- (2) The region of minimum zodiacal light brightness in the ecliptic is relatively narrow compared to the minima above and below the ecliptic.
- (3) Total brightness is not a minimum at the ecliptic pole due to the contribution of light at low galactic latitudes.
- (4) The total degree of polarization is a minimum in the ecliptic at small elevations (large elongations).
- (5) To a first approximation, the total degree of polarization is symmetric about the antisolar point (i.e., dependent on elongation, not ecliptic latitude) except for a general depolarization in the Milky Way. This suggests that the degree of polarization of the zodiacal light is larger at high ecliptic latitudes than at similar elongations near the ecliptic.

BRIGHTNESS $S_{10}(\text{vis})$

100-199	████████
200-299	████████
300-399	████████
400-499	████████
500-599	████████
600-699	████████
700-799	████████
>800	████████



POLARIZATION %

<2	████████
2-29	████████
3-39	████████
4-49	████████
5-59	████████
6-69	████████
7-79	████████
8-99	████████
>10	████████

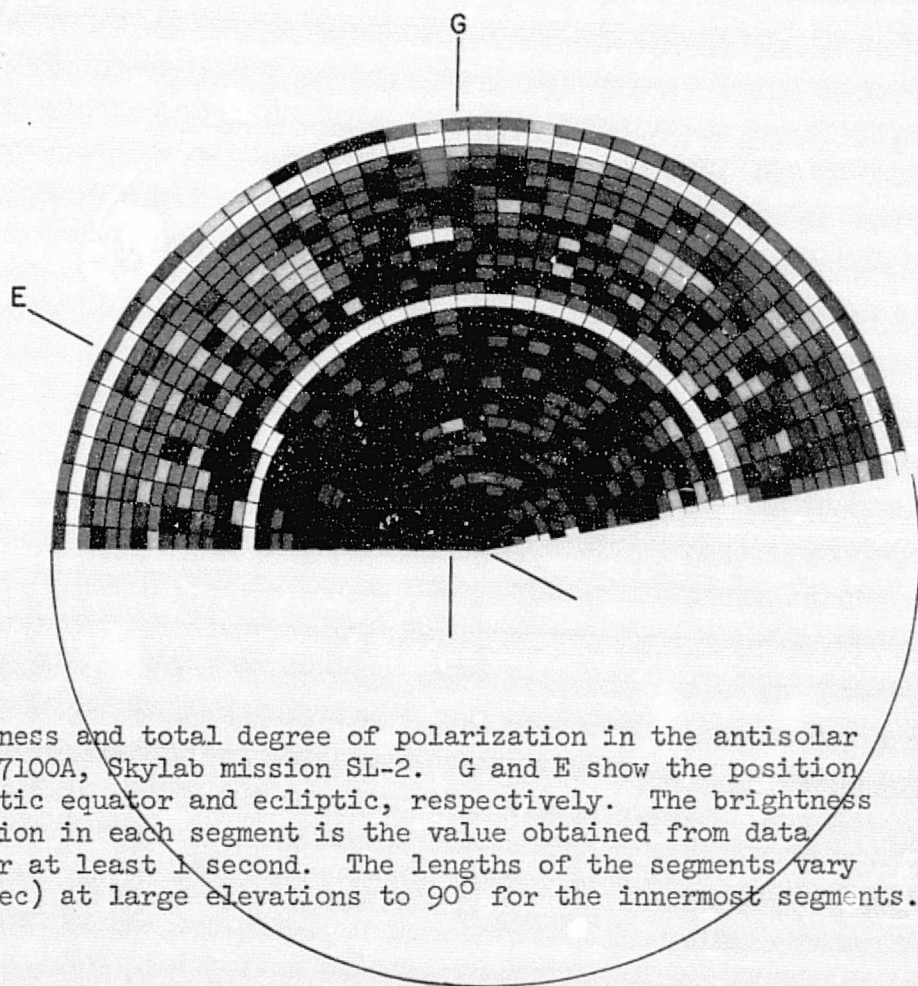


Fig. 7. Total brightness and total degree of polarization in the antisolar hemisphere, 7100A, Skylab mission SL-2. G and E show the position of the galactic equator and ecliptic, respectively. The brightness or polarization in each segment is the value obtained from data measured over at least 1 second. The lengths of the segments vary from 4° (1 sec) at large elevations to 90° for the innermost segments.

As noted earlier, subsequent steps in the analysis involve removing the equivalent brightness contributed by individually resolved stars and separating background starlight and zodiacal light.

To provide information on the spacecraft corona in near real time, the photometer was fixed in position at approximately 95 degrees from the sun, and 10-color observations were made on SL-2 mission day 19 starting with the spacecraft in the earth's shadow and ending in daylight. The reverse sequence was performed later in the same orbit; i.e., day to night. Comparison of the data, day/night or night/day, gives the characteristics of the spacecraft corona directly. In a preliminary analysis of these dataⁱ we found that there were levels of sky brightness in daylight only 5% above those at night, indicating that the spacecraft corona was minimal. Subsequently, total instrument reproducibility and the method of differencing day/night or night/day sky brightnesses were found to give a minimum detectable brightness change of from 1 to 3 $S_{10}(V)$; in a more detailed analysisⁱⁱ, we found no evidence for integrated light from contaminant particulates down to this column brightness threshold for detection (see Appendix 5).

Included among the fixed-position regions that were observed are the north celestial pole, south ecliptic pole, two regions near the north galactic pole, and 90 degrees from the sun in the ecliptic. The polarized brightnesses (Stokes parameter Q) of the zodiacal light were found to have the color of the sun at each of these positionsⁱⁱⁱ; the mean values

ⁱWeinberg, J. L., R. D. Mercer, and R. C. Hahn, Bull. Am. Astron. Soc. 6, 337 (1974).

ⁱⁱSchurman, D. W. and J. L. Weinberg, Preliminary Study of Contaminant Particulates around Skylab, NASA contractor report, State Univ. of New York at Albany, May 1976.

ⁱⁱⁱSparrow, J. G., J. L. Weinberg, and R. C. Hahn, Polarization of the Zodiacal Light: First Results from Skylab, in Proc. IAU Colloq. No. 31, Lecture Notes in Physics, Number 48, 45-51, (Springer-Verlag, Heidelberg), 1976.

in $S_{10}(V)$, in the order given above, are $19.5 \pm .2$, $12.4 \pm .2$, $17.1 \pm .3$, $18.1 \pm .2$, and $26.5 \pm .3$. Since previous observers had found the total brightness (Stokes parameter I) to have the color of the sun from the near ultraviolet out to $2.4 \mu\text{m}$, the degree of polarization of the zodiacal light is independent of wavelength from 4000\AA to 8200\AA . Information on the sizes of the particles would be available from polarization observations in the ultraviolet, especially if the degree of polarization was found to change with wavelength in that region.

Fortunately, the Skylab analog data, without data compression, are still available, and new experiment data tapes were generated. Most of these tapes were made available between September 1975 and January 1976, and it will now be possible to derive results from the scanning programs and to complete the analysis of fixed-position data.

Publications Related to the Experiment

J. L. Weinberg, Current Problems in the Zodiacal Light, in Space Research X, (T. M. Donahue, P. A. Smith, and L. Thomas, eds.), 233-243, (North Holland, Amsterdam), 1970.

M. S. Hanner, Zodiacal Light Models based on Scattering by Silicate Particles, Bull. AAS, 2, 319, 1970.

J. L. Weinberg, A Coordinated Program of Satellite and Ground-Based Observations of the Zodiacal Light, in Trans. IAU, XIV B, 166, 1971.

M. S. Hanner, Physical Properties of the Interplanetary Dust, in Physical Studies of Minor Planets, (T. Gehrels, ed.), 377-388, (NASA SP-267), 1971.

C. Leinert*, Stray Light Suppression in Sunshields and Optical Systems: Measurements on Three Space Experiments, Dudley Observatory Report No. 6, December 1971.

R. H. Giese*, Single-Component Zodiacal Light Models, Dudley Observatory Report No. 7, September 1972.

K. G. Henize and J. L. Weinberg, Astronomy through the Skylab scientific airlocks, Sky and Telescope, 45, 272-276, 1973.

R. H. Giese*, M. S. Hanner, and C. Leinert*, Colour dependence of zodiacal light models, Planetary Space Sci., 21, 2061-2072, 1973.

J. L. Weinberg, Polarization of the zodiacal light, in Planets, Stars and Nebulae studied with Photopolarimetry (T. Gehrels, editor), 781-793, University of Arizona Press, 1974.

D. Clarke*, Nomenclature of polarized light: linear polarization, Applied Optics, 13, 3-5, 1974.

D. Clarke*, Nomenclature of polarized light: elliptical polarization, Applied Optics, 13, 222-224, 1974.

J. L. Weinberg, R. D. Mercer, and R. C. Hahn, The optical environment of Skylab, mission SL-2, Bull. AAS, 6, 337, 1974.

J. G. Sparrow*, Solar radiation induced rotational bursting of interplanetary particles, Geophys. Res. Letters, 2, 255-257, 1975.

N. Y. Misconi and M. S. Hanner, On the possibility of detecting solar flare effects in the zodiacal light, Planetary Space Sci., 23, 1329-1335, 1975.

J. G. Sparrow* and J. L. Weinberg, Variations in gegenschein polarization?, Astron. and Astrophys., 41, 475-476, 1975.

N. Y. Misconi, Solar flare effects on the zodiacal light, Ph.D. Dissertation, State University of New York at Albany, September 1975.

*Visiting Astronomer

J. L. Weinberg, J. G. Sparrow*, and R. C. Hahn, The Skylab ten color photoelectric polarimeter, Space Science Instr., 1, 407-418, 1975.

J. L. Weinberg and R. C. Hahn, Multicolor photometry of low light level phenomena from Skylab, in Proceedings, ATAA/AGU Conference on Scientific Experiments of Skylab, in press.

J. L. Weinberg, Space observations of the zodiacal light, in Proceedings, IAU Colloquium No. 31, Interplanetary Dust and Zodiacal Light, Lecture Notes in Physics, Number 48, (H. Elsässer and H. Fechtig, eds.), 3-18, (Springer-Verlag, Heidelberg), 1976.

J. G. Sparrow* and J. L. Weinberg, The $S_{10}(V)$ unit of surface brightness, in Proceedings, IAU Colloquium No. 31, Lecture Notes in Physics, Number 48, 41-44, 1976.

J. G. Sparrow*, J. L. Weinberg, and R. C. Hahn, Polarization of the zodiacal light: first results from Skylab, in Proceedings, IAU Colloquium No. 31, Lecture Notes in Physics, Number 48, 45-51, 1976.

J. G. Sparrow*, J. L. Weinberg, and R. C. Hahn, The 10 color Gegenschein/zodiacal light photometer, Applied Optics (special Skylab issue), in press.

J. L. Weinberg, D. W. Schuerman, and D. E. Beeson, Comments on "Photometer Calibration Problem for Extended Astronomical Sources", Applied Optics, in press.

N. Y. Misconi, Solar flare effects on the zodiacal light?, Astron. and Astrophys., in press.

J. L. Weinberg, J. G. Sparrow*, and D. E. Beeson, Calibration and use of diffuse sources, submitted to Planetary Space Sci., 1976.

N. Y. Misconi, On the rotational bursting of interplanetary dust particles, Geophys. Res. Letters, in press.

D. W. Schuerman and J. L. Weinberg, Preliminary study of contaminant particulates around Skylab, NASA Contractor Report CR - 2759, 1976.

*Visiting Astronomer

Appendix 1. Summary of Photometer Observations.

SL-2 Observations

<u>RUN NO.</u>	<u>MODE</u>	<u>START</u>	<u>STOP</u>	<u>COMMENT</u>
1	0a	162:18:53	162:20:25	Majority of data invalid due to cap light leakage.
2	0a	162:23:46	163:00:06	At night but through SAA.
3	4a	163:1:15	163:11:01	Only seven filters. Post mission data good for 5 of 7 reps.
4	1e(W)	163:13:55	163:14:23	Simultaneous observations from Pioneer 10 & 11 and Mt. Haleakala, Maui. Data look good.
5	1d(S)	163:19:55	163:20:07	Available data look good.
6-1	1a	163:20:14	163:20:32	Available data look good.
6-2	1a	163:21:24	163:21:42	Available data look good.
7	0a	165:21:33	165:22:45	Some data lost due to cap light leakage.
8	4a	166:00:45	166:13:30	Post mission data good for only 4 of 9 reps. ADDT data appear good for all 9 reps.
9	1d	166:14:55	166:15:08	Post mission data good for only 2 of 6 reps. ADDT data might be O.K.
10	2c	166:19:15	166:19:40	Data O.K.
11	4a	166:21:05	167:09:43	Post mission data good for 7 of 9 reps. ADDT data might be O.K.
12	3d	167:09:56	167:19:23	Data not processed.
13	3d	167:21:44	168:11:50	Data not processed.

SL-3 Observations

<u>RUN NO.</u>	<u>MODE</u>	<u>START</u>	<u>STOP</u>	<u>COMMENT</u>
1	4a	213:23:07	214:13:47	Crew error--two reps entered instead of ten; only two colors completed.
2	1b	215:13:53	215:14:46	Filter wheel out of sync. Data useless.
3	1a	215:15:59	215:16:17	Reflection from spacecraft closes shutter after sunrise.
4	1a	215:17:28	215:18:51	Program was started 28 minutes late--went into day--reflections closed shutter.
5	1b	215:19:01	215:19:19	Data appear O.K.
6	2b	215:23:50	216:12:27	Daylight reflections closed shutter halfway through each rep as sun rose.

Appendix 2. Status of the Photometer Data.

Early in this experiment we developed and wrote a program to accept the digital data tapes (Post Mission Tapes) to be supplied by MSFC and to perform the necessary computations through a digital synchronous detection routine. This program was used to screen the tapes as they were received and resulted in reports to MSFC that approximately 25% of the tapes had various problems which prevented processing. It was also noted that the Post Mission Tapes were compiled from both real-time and dump data as expected. It was found, however, that if both real-time and dump data were available for any particular time period, the real-time data were used, contrary to earlier agreement. This was unfortunate since the real-time data had a compression factor, K, of 3, which prevented transmission of subsequent data numbers unless they were at least 80 mv different in level. Because much of our polarization information was in this 80 mv differentiation, the "K" factor effectively erased much of the most important information in our measurements.

Fortunately, the Skylab analog data, without data compression, were still available, and the Skylab Program Office agreed in late 1974 to our having new digital data tapes (ADDT's) created from the analog mission tapes and to our taking over from MSFC all the processing associated with this effort. With the assistance of MSFC and GSFC, arrangements were made for the Bermuda Tracking Station (BDA) to work with us to create new ADDT's, with no data compression, for all experiment real-time and dump data. Although promised by January 1975, the conversion process at BDA was slow due to their work load, and they were unable to provide more than one batch of ADDT's until October 1975. In order to determine the quality of the data in this first batch of tapes and to determine the time periods covered on each tape, a special interrogation

code had to be developed. Because of anomalies in the data, this code had to be able to handle data drop-outs, sync errors, and differences in format for data on different recorders, and also convert the recorded time to GMT. Since the documentation was incomplete and the data were "raw", we had to figure out a solution to each problem as it was encountered. It took a major effort by our staff, but we are now able to start with raw ADDT's from BDA and process all the way from checking, correction, reformatting, condensing, applying engineering unit conversions and time coding through software which determines pointing directions and performs coordinate transformations, applies absolute and relative calibrations, determines the Stokes parameters of the total radiation, identifies "resolved" stars in each field of view, etc. At the same time, we worked to derive results on selected data to show that we are able to handle the entire data handling and processing in-house and to show the importance of these unique data. The last of these data were received in January 1976. Table 2-1 summarizes the history and condition of experiment data tapes as of the end of the contract.

Table 2-1. Summary of S073 Data Tapes

SL-2

Run/REP	Post Mission Tape #	% K1	Rcvd	REAL	Rcvd	AMP-2	Rcvd	AMP-3	Rcvd
				TIME		ADDT		ADDT	
				Tape #		Tape #		Tape #	
1	1072	?	5/21/74	1217	3/5/75	1292	9/22/75	1301	9/22/75
	1073	"	"			1293	9/22/75	1306	9/22/75
	1074	"	"						
	1075	"	"						
	1076	"	"						
	1077	"	"						
	1078	"	"						
	1079	"	"						
2	1080	5	5/21/74	1200	3/5/75	1303	9/22/75	1302	9/22/75
	1081	5	5/21/74	1198	3/5/75				
3-1	932	65	4/30/74	1218	3/5/75	1303	9/22/75	1291	9/22/75
	933	65	4/30/74					1306	9/22/75
	934	65	4/30/74						
3-2	937	90	4/30/74	1214	3/5/75	1303	9/22/75	1291	9/22/75
	938	90	4/30/74						
	939	90	4/30/74						
	940	90	4/30/74						
3-3	941	91	4/30/74	1221	3/5/75	1305	9/22/75	1304 ²⁾	9/22/75
	942	91	"	1222	3/5/75				
	943 ¹⁾	91	"						
3-4	945 ³⁾	93%	4/30/74	1211	3/5/75	429	2/4/76		4)
	946 ³⁾	93%	4/30/74						
3-5	1055	95%	5/21/74	1206	3/5/75	1308	9/22/75	1307	9/22/75
	1056	95%	"						
	1057	95%	"						
3-6	1063	75%	5/21/74	1201	3/5/75	1310	9/22/75	1309	9/22/75
	1064	"	"						
	1065	"	"						
3-7	1069	56%	5/21/74	1227	3/5/75	1312	9/22/75	1311	9/22/75
	1070	"	"	1202	3/5/75				
	1071	"	"						
4	929	50%	4/30/74	1204	3/5/75	349	11/4/75	1314 ⁵⁾	9/22/75
	930	"	"	1205	3/5/75				
	931	"	"						
5	1176	100%	5/21/74			1352	9/22/75		4)
	1177	100%	"						
6-1	1178	100%	5/21/74			1352	9/22/75		4)
	1179	100%	5/21/74						

<u>Run/REP</u>	<u>Post Mission Tape #</u>	<u>% Kl</u>	<u>Rcvd</u>	<u>REAL TIME ADDT Tape #</u>	<u>Rcvd</u>	<u>AMP-2 ADDT Tape #</u>	<u>Rcvd</u>	<u>AMP-3 ADDT Tape #</u>	<u>Rcvd</u>
6-2	1180 1181 1182	33% " "	7/1/74 7/1/74 7/1/74			1352	9/22/75	1316	9/22/75
7	972 973 6)		5/15/74 5/15/74	1233	4/7/75	1353 1354	9/22/75 9/22/75	1317	9/22/75
8-1	1151 ³⁾ 1152 ³⁾	82% "	6/17/74 "			1318	9/22/75	1319	9/22/75
8-2	1152	100%	6/17/74			1321	9/22/75	1320	9/22/75
8-3	1153 ³⁾ 1154 ³⁾	100% "	6/17/74 "	1243 1245	4/7/75 4/7/75	1321	9/22/75	1323	9/22/75
8-4	1156 ³⁾ 1157 ³⁾	100% "	6/17/74 "			1324	9/22/75	432	2/4/76
8-5	1020 1021	100% "	5/21/74 "			1327	9/22/75	1328	9/22/75
8-6	1023 1024 ²⁾	89% 89%	5/21/74 "	1253	4/7/75	1329	9/22/75	433	2/4/76
8-7	1025 ³⁾	56%	5/21/74	1251 1254	4/7/75 4/7/75	1331	9/22/75	1330 433	9/22/75 2/4/76
8-8	1028 1029	17% "	5/21/74 "	1258 1259	4/7/75 4/7/75	1331 1332	9/22/75 9/22/75	1330 ²⁾	9/22/75
8-9	1084 1085 1086	59% " "	5/24/74 " "	1299	9/22/75	1332	9/22/75	1333	9/22/75
9	1089 ⁵⁾ 1090	100% "	5/24/74 "			4)		1335	9/22/75
10	1141 1142	100% 100%	5/28/74 5/28/74			1355	9/22/75	435	2/4/76
11-1	1142 1143	100% "	5/28/74 "			1355	9/22/75	1336	9/22/75
11-2	1144 1145	81% "	5/28/74 "			4)		436	2/4/76
11-3	948 949	90% "	5/13/74 "			1337	9/22/75	1356	9/22/75
11-4	952 ³⁾	91%	5/13/74			437	2/4/76	438	2/4/76
11-5	955 956	78% "	5/13/74 "			1339	9/22/75	1338	9/22/75

<u>Run/REP</u>	<u>Post Mission Tape #</u>	<u>% KI</u>	<u>Rcvd</u>	<u>REAL TIME ADDT Tape #</u>	<u>Rcvd</u>	<u>AMP-2 ADDT Tape #</u>	<u>Rcvd</u>	<u>AMP-3 ADDT Tape #</u>	<u>Rcvd</u>
11-6	959 960	87% "	5/13/74 "			1339	9/22/75	439	2/4/76
11-7	1120 1121	100% "	5/28/74 "			1340	9/22/75	1342	9/22/75
11-8	1125 ³⁾ 1126 ³⁾	? "	5/28/74 "			1345	9/22/75	1346	9/22/75
11-9	1130 ⁷⁾	94%	5/28/74			1345 ⁷⁾	9/22/75	1346 ⁷⁾	9/22/75
12-1	1131	?	5/28/74			1345	9/22/75	1346	9/22/75
12-2	1133 1134	?	5/28/74 "			1347	9/22/75	1348	9/22/75
12-3	454	?	5/20/74			1357	9/22/75	1349	9/22/75
12-4	055	?	5/20/74			4)		1349	9/22/75
12-5	800	?	5/20/74			1359	9/22/75	1360	9/22/75
12-6	534	?	5/20/74			1361	9/22/75	4)	
12-7	4)	?				1361	9/22/75	1362	9/22/75
13-1	1050	?	5/21/74			1363	9/22/75	4)	
13-2	1053	?	5/21/74	256	11/4/75	1364	9/22/75	4)	
13-3	989	?	5/20/74			1369	9/22/75	1368	9/22/75
13-4	992	?	5/20/74			1369	9/22/75	1371	9/22/75
13-5	993 994	? ?	5/20/74 "			1374	9/22/75	1371	9/22/75
13-6	0063	?	5/20/74	261	11/4/75	1376	9/22/75	1375	9/22/75
13-7	979	?	5/16/74	264	11/4/75	1376	9/22/75	1378	9/22/75
13-8	983	?	5/16/74	267	11/4/75	1379	9/22/75	4)	
13-9	984	?	5/16/74	269	11/4/75	4)		4)	
13-10	985	?	5/16/74			4)		4)	

<u>Run/REP</u>	<u>Post Mission Tape #</u>	<u>% Kl</u>	<u>Rcvd</u>	<u>REAL TIME ADDT Tape #</u>	<u>Rcvd</u>	<u>AMP-2 ADDT Tape #</u>	<u>Rcvd</u>	<u>AMP-3 ADDT Tape #</u>	<u>Rcvd</u>
1-1	1164 1165 1166 1167	? " " "	7/1/74 " " "			1383	9/22/75	1382	9/22/75
1-2	1170 ⁵⁾ 1171 1172 ⁵⁾ 1173 1174	? " " " "	7/1/74 " " " "			1383 ₄₎	9/22/75	1384	9/22/75
2	1031 ⁸⁾ 1032 ⁸⁾ 1033 ⁸⁾ 1034 ⁸⁾ 1035 ⁸⁾ 1036 ⁸⁾	? ? ? ? ? ?	5/21/74 5/21/74 " " " "			1393	9/22/75	1394	9/22/75
3	1040	61%	5/21/74	677	11/4/75	4)		1394	9/22/75
4	1043 1044 1045 1046 1047 1048	? " " " " "	5/21/74 " " " " "	679 680 681 682 683	11/4/75 11/4/75 11/4/75 11/4/75 11/4/75	4)		1397	9/22/75
5	1096 1097	? "	5/25/74 "			4)		1397	9/22/75
6-1	1098 ³⁾		5/25/74			4)		4)	
6-2	1102 ³⁾		5/25/74			1398	9/22/75	4)	
6-3	1103	? "	5/27/74 "	693 694	11/4/75 11/4/75	1400	9/22/75	441	9/22/75
6-4	1104		5/28/74	695 696	11/4/75 11/4/75	1400	9/22/75	441	9/22/75
6-5	1105	? "	5/28/74 "	697 698 699	11/4/75 11/4/75 11/4/75	442	9/22/75	443	9/22/75
6-6	1136	? "	5/28/74 "	700 701	11/4/75 11/4/75	444	9/22/75	443	9/22/75
6-7	1137 ³⁾		5/28/74	703 704	11/4/75 11/4/75			445	9/22/75
6-8	1138 1139	? ?	5/28/74 5/28/74	796	11/4/75	447	9/22/75	450	9/22/75
6-9	1139 1140	? ?	5/28/74 5/28/74	797 798	11/4/75 11/4/75	449	9/22/75	450	9/22/75

Notes to Tape Summary Table

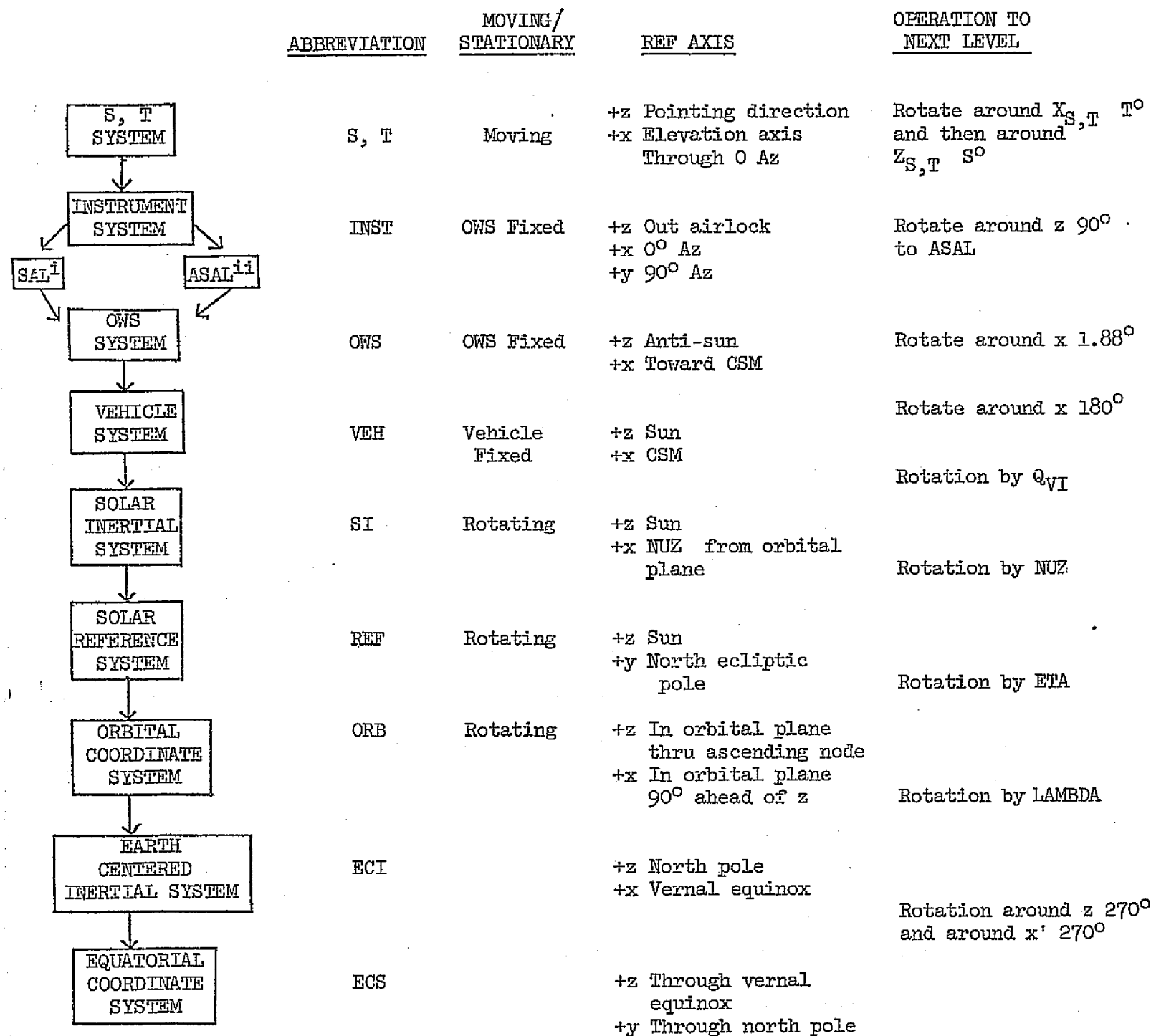
- 1) 10 minutes missing
- 2) 4 minutes missing
- 3) No useable data in tape
- 4) Not received
- 5) Poor quality data
- 6) 40 minutes missing
- 7) 11 minutes missing - turned off early by crew
- 8) instrument not operating correctly - data unuseable

Appendix 3. Pointing Direction Computations

The conversion of azimuth and elevation values obtained from telemetry to celestial coordinates involves a complex series of coordinate transformations utilizing both matrix and quaternion arithmetic. A block diagram of this procedure is shown in Figure 3-1; the accompanying matrix transformations give the details.

Data from Skylab Best Estimate Trajectory (SKYBET) and from the ATMDC were used by MSFC to perform pointing computations for us, and the results were included on the Post-Mission tapes. The computations were incorrect for a number of reasons, including the fact that the input data had errors from the data sources. We attempted to create another program which used these raw data, and we did obtain partially successful results. This program was different from the equations in Figure 3-1 because of the difference in reference points used in the raw data but did not always give consistent results due to incorrect raw data. When new data became available (SKYBET REV 2 and improved ATMDC), the program shown in Figure 3-1 gave correct results; however, there is still an indication of some errors in the new raw data.

As a check on the overall system, the results obtained from the computation program were checked against the DAC film results and seemingly random differences as large as 4° were noted. A recheck of the DAC film method uncovered some human errors on certain frames. An extensive review of the computational program assured that when the raw data were good the answers were correct. The differences which then remained had to be instrumental, either electrical or mechanical. As can be seen from the equations, we assumed that the instrument was orthogonal to the spacecraft and differed only by the known 1.88° offset of the anti-solar scientific



ⁱSolar airlock
ⁱⁱAnti-solar airlock

Figure 3-1

For details see following pages.

ORIGINAL PAGE IS
OF POOR QUALITY

and

$$\begin{matrix} & \boxed{\text{ZN}} & \\ \text{REF} & & \text{SI} \end{matrix} = \begin{bmatrix} \cos \gamma_z & \sin \gamma_z & 0 \\ -\sin \gamma_z & \cos \gamma_z & 0 \\ 0 & 0 & 1 \end{bmatrix}$$

where γ_z (NUZ) is the angle between the orbital plane and the +x axis of the solar inertial system.

and

$$\begin{matrix} & \boxed{Q} & \\ \text{SI} & & \text{VEH} \end{matrix} = \begin{bmatrix} 2(Q_4^2 + Q_1^2) - 1 & 2(Q_1Q_2 + Q_3Q_4) & 2(Q_1Q_3 - Q_2Q_4) \\ 2(Q_1Q_2 - Q_3Q_4) & 2(Q_4^2 + Q_2^2) - 1 & 2(Q_1Q_4 + Q_3Q_2) \\ 2(Q_2Q_4 + Q_1Q_3) & 2(Q_2Q_3 - Q_1Q_4) & 2(Q_4^2 + Q_3^2) - 1 \end{bmatrix}$$

where $Q_1 = QVI_1$, $Q_2 = QVI_2$, $Q_3 = QVI_3$, $Q_4 = QVI_4$ and QVI_1 , QVI_2 , QVI_3 , QVI_4 are the four elements of the quaternion which relates the vehicle coordinate system to the Solar Inertial Coordinate system.

and

$$\begin{matrix} & \boxed{B} & \\ \text{VEH} & & \text{INST} \end{matrix} = \begin{bmatrix} 1 & 0 & 0 \\ 0 & -.99946 & +.03286 \\ 0 & -.03286 & -.99946 \end{bmatrix}$$

and

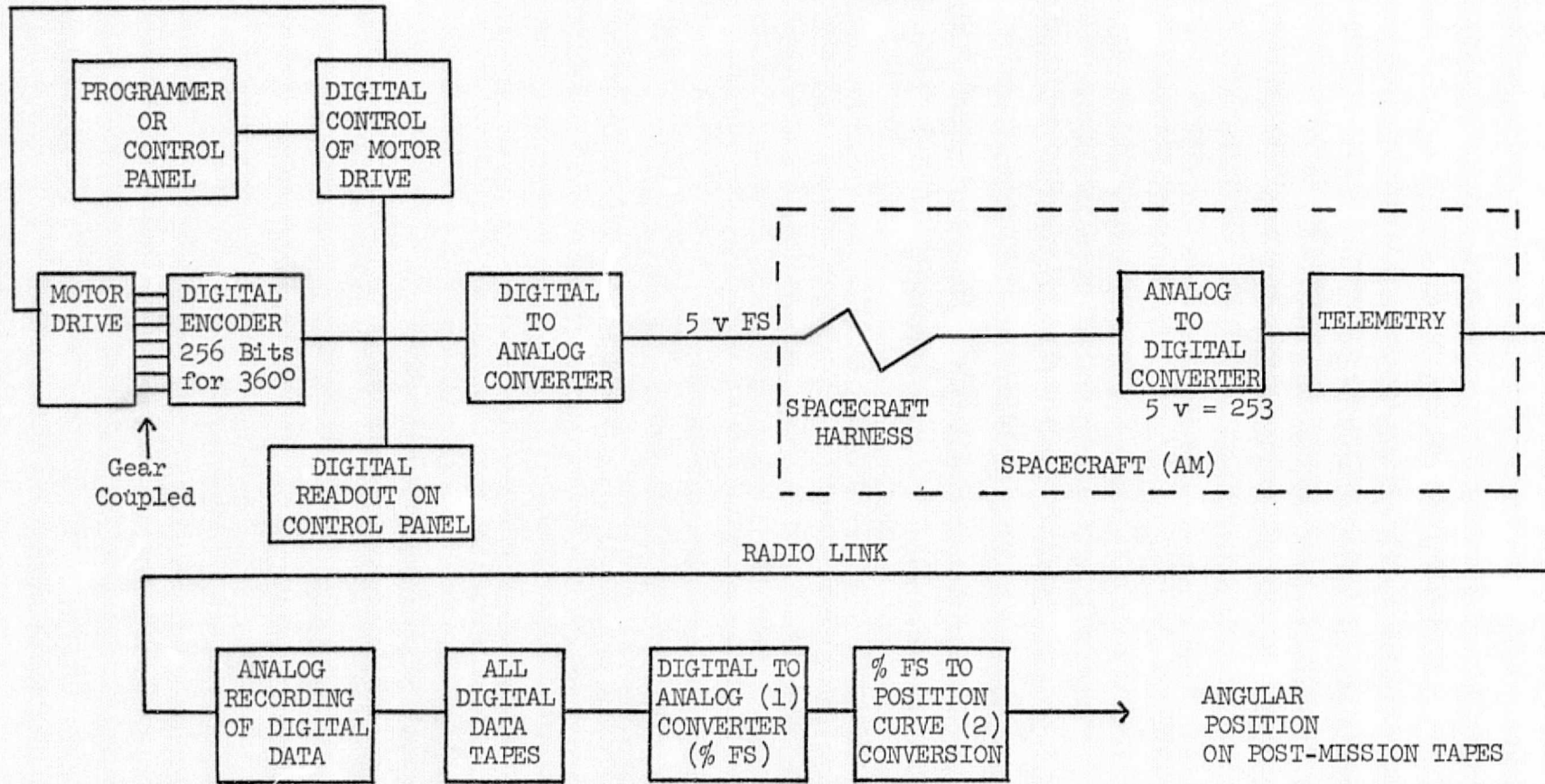
$$\begin{matrix} & \boxed{A} & \\ \text{INST} & & \text{ST} \end{matrix} = \begin{bmatrix} \cos s & -\sin s \cos t & -\sin t \sin s \\ \sin s & \cos s \cos t & \sin t \cos s \\ 0 & -\sin t & \cos t \end{bmatrix}$$

where s and t are the shaft and trunnion values respectively.

airlock (SAL) from the spacecraft -z axis. This did not allow for boom instability, mounting misalignment, or manufacturing tolerances which would not place the 0 azimuth (shaft, S), 0 elevation (trunnion, T) photometer pointing direction in the expected direction. No tests were made on the instrument prior to flight to determine these parameters because of the need for a zero gravity test facility. Because an averaging technique was used to reduce the effects of telemetry data jitter, it was assumed that the values of shaft and trunnion fed to the computational program truly represented the position of the photometer; these assumptions are now subject to question.

Since the instrument was digitally controlled, we must assume, with certain exceptions, that if the crew or automatic programmer directed the photometer to a certain position it did, in fact, go to that position. In most, but not all, cases the telemetry did not report the position of the photometer equal to the input program. For the fixed-pointing modes this was easy to check; for the scanning modes we used check points determined by camera shutter (0, 45, 90, 135, 180° shaft) or by the discrete steps in trunnion (0, 2.8, 5.6, 8.4, 11.2°, etc.). By forcing the computational program to accept the PAD or expected values of shaft and trunnion, the resulting answers compared much more favorably to the DAC results, but differences still occurred in certain cases. In an attempt to create a correction factor for the telemetry values, the differences were examined at many points in the map. This study included histograms of the telemetry samples for fixed modes, best-fit straight lines between expected and determined values for the scanning modes, and a review of the system for converting position to ground telemetry (Figure 3-2). The histograms did not always show a normal distribution as would be expected

FIGURE 3-2



(1) $\% FS = \frac{PCM - 1}{2.53}$

- (2) Developed by calibration of the
 0 → 5.0 v output of the instrument
 D-A to the digital readout of position on control panel.

ORIGINAL PAGE IS
 OF POOR QUALITY

if the variations were random or statistical. Some of the histograms were skewed to the left and some to the right. A simple average of the values, therefore, gave values both above and below the "correct" value. The skewing pattern is not random but has a periodic variation which we ascribe to the beating of the 255 bit D to A output with the 253 bit A to D. An exact method of correcting for this problem is yet to be determined.

Study of the expected vs. telemetry values revealed an offset and slope problem. The offset of slightly less than 1 bit (1.4°), where the telemetry values were always higher than the expected values could be attributed to noise pickup on the spacecraft harness (≈ 20 mv). The slope difference could be attributed to the fact that the calibration was not done through the entire system as shown in Figure 3-2. Exact correction for these errors requires the analysis of more data.

It was also determined that when the boom was extended to 7 rods, an additional shaft correction of $+3.6^{\circ}$ was required to make the telemetry results agree with the DAC film. It is possible that a torsion or twist in the boom occurred when fully extended which offset the 0 shaft position by 3.6° .

Although we believe we have discovered all of the problems associated with determining the pointing direction on the sky, a significant effort is still needed to create the appropriate correction factors which will achieve the required accuracy of $\pm 0.2^{\circ}$ from the telemetry data.

Appendix 4. Miscellaneous Operational Difficulties or Anomalies

1. Light leak. On the first attempt to operate the instrument on SL-2, a program Oa System Monitor (Mode 0, code a; shutter open, cap closed), it was very obvious that the cap was not light tight when closed and that a large amount of light was leaking into the detector when the instrument was pointed at or near the sun-lit earth. This leakage invalidated most of the measurements and made it impossible to achieve the intended results on instrument performance. At first the engineering support group believed that the extreme temperatures had created the problem. The crew was asked to manually operate the cap to see if it could be closed by repeated operations. This was unsuccessful. Several points of information relate to this problem:
 - i. During instrument testing by MMC a photometer head was subjected to various conditions of illumination. The test report indicated that exposure to 1.0 solar constant resulted in an appreciable leakage, whereas exposure to 0.2 solar constant was almost undetectable. The conclusions were questioned by MSFC and within the group at MMC, and we could never determine the actual results of the tests. They were not able to be repeated prior to launch.
 - ii. The flight unit had been mechanically modified during manufacture to solve a cap sticking problem. This modification involved enlarging mechanical clearances in the light trap area and could have reduced the light-tightness.
 - iii. It is not clear whether the instrument which was tested was similarly modified.
 - iv. After SL-2, light leak tests were performed at MMC and observed by us. These tests on the backup unit proved that the design of the cap light seal was inadequate to allow a Mode 0 operation when the telescope was pointed within 19° of the sun or sun-lit earth.
 - v. During DOY/MD 167/23 the crew reported that the brightness (output voltage) indicator was over range during an orbital wait period (i.e., voltage exceeded 5.0 volts with cap and shutter closed). When they reduced the gain to low, the indicator read 2.4 volts. The pointing direction during this period has not yet been determined.

This problem was not unexpected, since our criteria for acceptable light leakage were not accepted. Any daylight operation of the instrument in Mode 0 must be evaluated with care because of this failure.

2. Shaft motor operation. Near the end of SL-2 the shaft motor control malfunctioned such that it would always go to the high limit when not manually directed to reverse direction. It could be driven to the minimum limit by manually setting the shaft switch, but on release it would again drive to its maximum limit. In attempting to retract the instrument, the crew accidentally hit the side of the spacecraft and the anomaly disappeared. After that the shaft drive operated correctly and the instrument was able to be retracted using Mode 6.

No further use of the instrument was scheduled for SL-2. A cursory examination and malfunction procedure performed at the beginning of SL-3 failed to indicate the cause of the failure and, in fact, the first use of the instrument during SL-3 was satisfactory.

3. Shutter bounce. Throughout final calibration and test and during mission operations an excessive photometer shutter bounce on closure was noted. Special data handling techniques had to be developed to remove the effects of this anomaly from the data.
4. Apparent noise on the azimuth and elevation telemetry lines caused errors in the decoding of pointing information.
5. In addition to electronics problems in the pointing telemetry (4, above) comparison of the DAC film and the telemetry-derived pointing direction shows errors which appear to be of a mechanical nature. Whether this is due to a boresight problem, a structural rigidity problem, or an instrument mounting problem is not yet determined. There is evidence, however, that the error is increased (to as much as 4 deg.) when the boom was extended to 7 rods.
6. Extra scans were noted in 3 sky maps; these were apparently due to forces applied to the head by the connecting cables.
7. On one occasion there appears to have been an incorrect start of the instrument by the automatic programmer. The run was made in daylight and the instrument was overloaded (high brightness) but was not damaged.
8. There was an apparent early termination of one run by the crew which resulted in the loss of some data.
9. A small error, 1 data point out of 2000, was discovered in the dump data when compared to the real time data. This is ascribed to the on-board tape recorder but is not considered significant.
10. A significant drift in the spacecraft orientation was noted by the DAC film on one of the fixed pointing programs.
11. Inability to drive in shaft. During SL-3 the shaft drive appeared to stick at its high limit. No action by the crew, even tapping the photometer against the side of the spacecraft, could correct the malfunction. In a coordinated effort by the crew and by ground personnel, many attempts were made to correct or to by-pass the malfunction - without success. After several additional observations were obtained which did not require shaft motion, the instrument was jettisoned on DOY 216. Subsequent studies have indicated that the similar failure on SL-2 may have been related but apparently was not identical.

II. Analysis of Selected Photometer Data on Contamination, Experiment S073

Introduction

When experiment S073 was initially proposed by Prof. E. Ney of the University of Minnesota in June 1967, it had two objectives: 1. measurement of the surface brightness and polarization of the night sky light over as large a portion of the celestial sphere as possible at several wavelengths in the visible spectrum, and 2. performance of the same experiment with sunlight on the spacecraft to determine the extent and nature of the spacecraft corona. Although the Minnesota hardware concept, a hand-held Gegenschein-zodiacal light-airglow photometer ("GZAP gun"), bears no resemblance to the actual instrumentation flown on Skylab, the dual objectives were maintained; this resulted in a sharing of hardware and operations with Skylab experiment T027 and some duplication in the analysis of the data. In this report we present results on four programs performed during mission SL-2 that were designed to provide data on the spacecraft corona. These programs are outlined in Table 1.

Analysis of SL-2 Contamination Programs

The first contamination program (6-1) was performed on SL-2 mission day 19 with the photometer fixed in position at approximately 95 degrees from the sun. Observations were made in all 10 colors* from 4000A to 8200A, starting with the spacecraft in the earth's shadow and ending in daylight. The reverse sequence (6-2) was performed later in the same orbit; i.e., daylight to shadow. This program was designed to provide information in near real time on the level of scattered light by particulate material around Skylab; our quick-look analysis at JSC indicated that

*4000, 4760, 5080, 5300, 5577, 6080, 6300, 6435, 7100, 8200Å.

Table 1

Selected SL-2 observing programs containing photometric data on the optical environment of Skylab

<u>Run number</u>	<u>Mode</u>	<u>Photometer Extension (distance from spacecraft)</u>	<u>Program description</u>
6-1	1a	5.5m	Fixed in position at 95 degrees from the sun as vehicle moved from night to day; 9 cycles of 10 colors: 7.5 night, 1.5 day.
6-2	1a	1m	Fixed in position at 95 degrees from the sun as vehicle moved from day to night; 9 cycles of 10 colors: 2.5 day, 6.5 night.
12	3d	1m	Scan in azimuth at fixed elevation, during satellite day. 10 colors per orbit, 8 orbits.
13	3d	5.5m	Scan in azimuth at fixed elevation, during satellite day. 10 colors per orbit, 8 orbits.

the spacecraft corona was minimal. A more detailed, but still preliminary, analysis of these data (Weinberg, et al., 1974) indicated that there were levels of sky brightness in daylight only 5% above those at night; i.e., low light level astronomical observations were able to be made from outside the earth's shadow. Subsequent fixed-position and sky scanning programs measured higher levels of daytime sky radiance, but analysis of those programs could not be completed until additional data were obtained on program timing and on illumination conditions of the vehicle and photometer/camera system.

In an independent study of the data from these programs (Table 1), Muscari and Jambor (1975) conclude that factor-of-100 brightness changes observed in runs 6-2 and 12 are a result of sunlight scattered by a contaminant cloud around Skylab. We have evaluated these data in detail; we find that the observed changes in brightness are a direct result of stray light from illuminated parts of the vehicle outside the photometer field of view. We find no evidence for a spacecraft corona to the photometer's limit of detection of a change in background (see section III of this report). In the following we examine each of these runs (Table 1) in detail.

A. Run 6-2

As noted earlier, the photometer was fixed in position at 95 degrees from the sun (toward the north galactic pole) as the vehicle moved from day to night. The measurements are tabulated as a function of color, GMT time, and time from sunrise/sunset in Appendix 1. The occasional groupings of high dark current indicate times when the spacecraft was near the South Atlantic anomaly.

In Figure 1 we have plotted day sky brightness normalized to the night value as a function of time for four of the 10 observed wavelengths. It is unfortunate that the program was started at the wrong time; thus, there are only a few data points in daylight. Examination of all the data indicates that the sky signal was decreasing as early as five minutes before sunset. The nature of this time decay, its rate of change and its position, is of particular interest.

Since data concerning the characteristics of sunrise/sunset were not readily available, we determined the apparent altitude versus time of

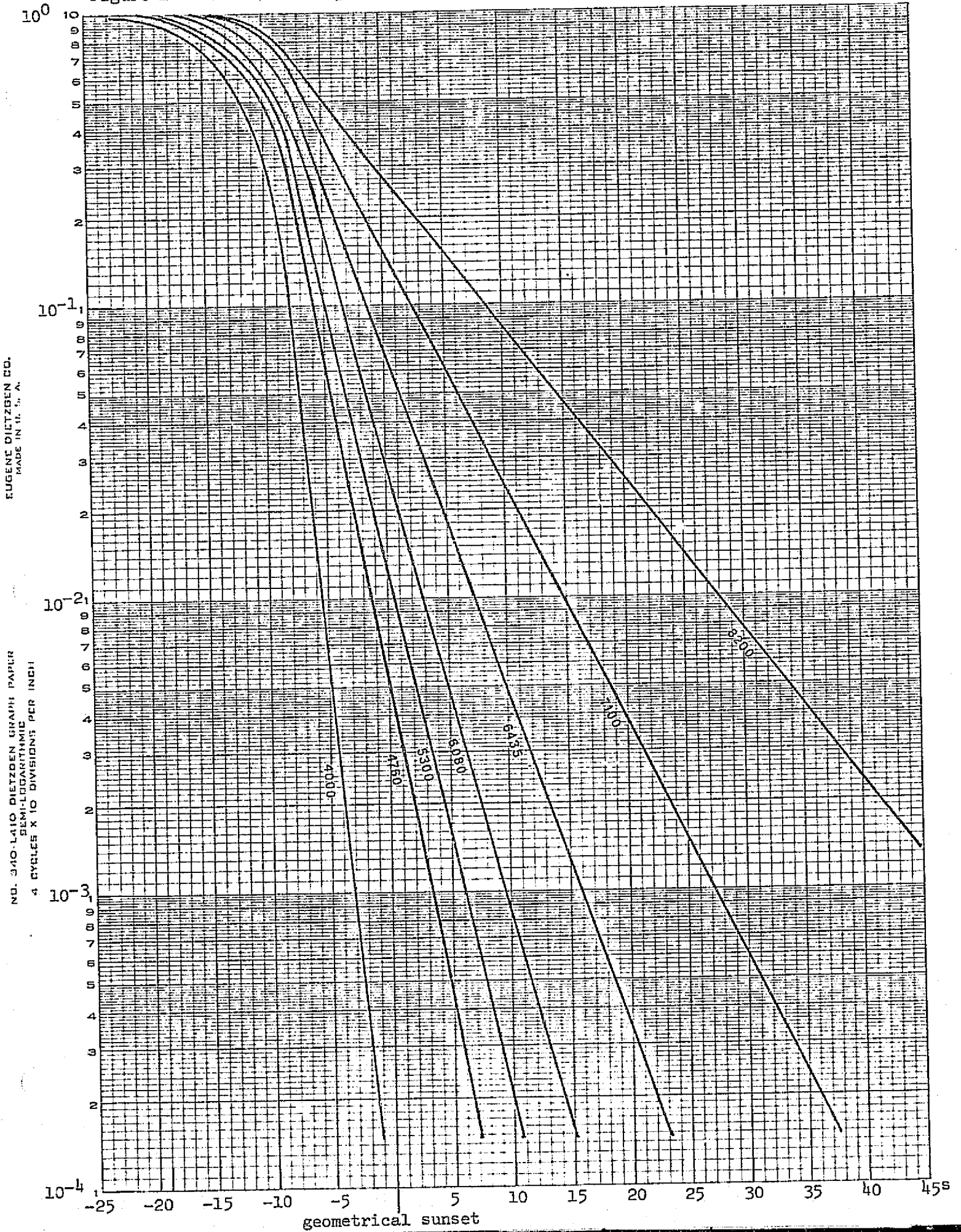
sunrise/sunset as a function of beta angle (see Appendix 2). For each altitude, we calculated the number of air masses traversed by the sun's rays and, using the atmospheric transmission given by Allen (1973), the color and time characteristics of apparent sunrise/sunset. The results are shown in Figure 2. No attempt was made to model the day/night 5577 and 6300 airglow characteristics. These data, as expected, have a different time rate of change than the data at continuum wavelengths. Note that the decay rates shown in Figure 2 begin only 20 seconds before geometrical sunset and continue for more than 50 seconds after geometrical sunset. A comparison with the observations shown in Figure 1 indicates that sunrise/sunset is not responsible for the observed rate of change of sky brightness.

The next step in the analysis involves a determination of the irradiance due to the sunlit earth. The time period from terminator set (line of demarcation of sunlit earth directly below spacecraft) to sunset was chosen for this modeling. Since the irradiance is proportional to both the area of the sunlit earth seen by the spacecraft and the absorption of the atmosphere as the sun's rays penetrate and are reflected back to the spacecraft, the modeling must include both effects. The reflection characteristic of the earth was assumed to be wavelength independent; thus, the irradiance at the spacecraft is

$$I(T) \propto A(T)e^{-\tau_{\lambda} m(T)},$$

where $A(T)$ is the relative projected area of the illuminated earth as a function of the solar depression angle T , τ_{λ} is the absorption per unit air mass at wavelength λ , and $m(T)$ is the number of air masses traversed as a function of T (see Appendix 3). The solar depression angle can be

Figure 2. Color/time dependence of apparent sunrise/sunset.



EUGENE DIETZGEN CO.
MADE IN U. S. A.

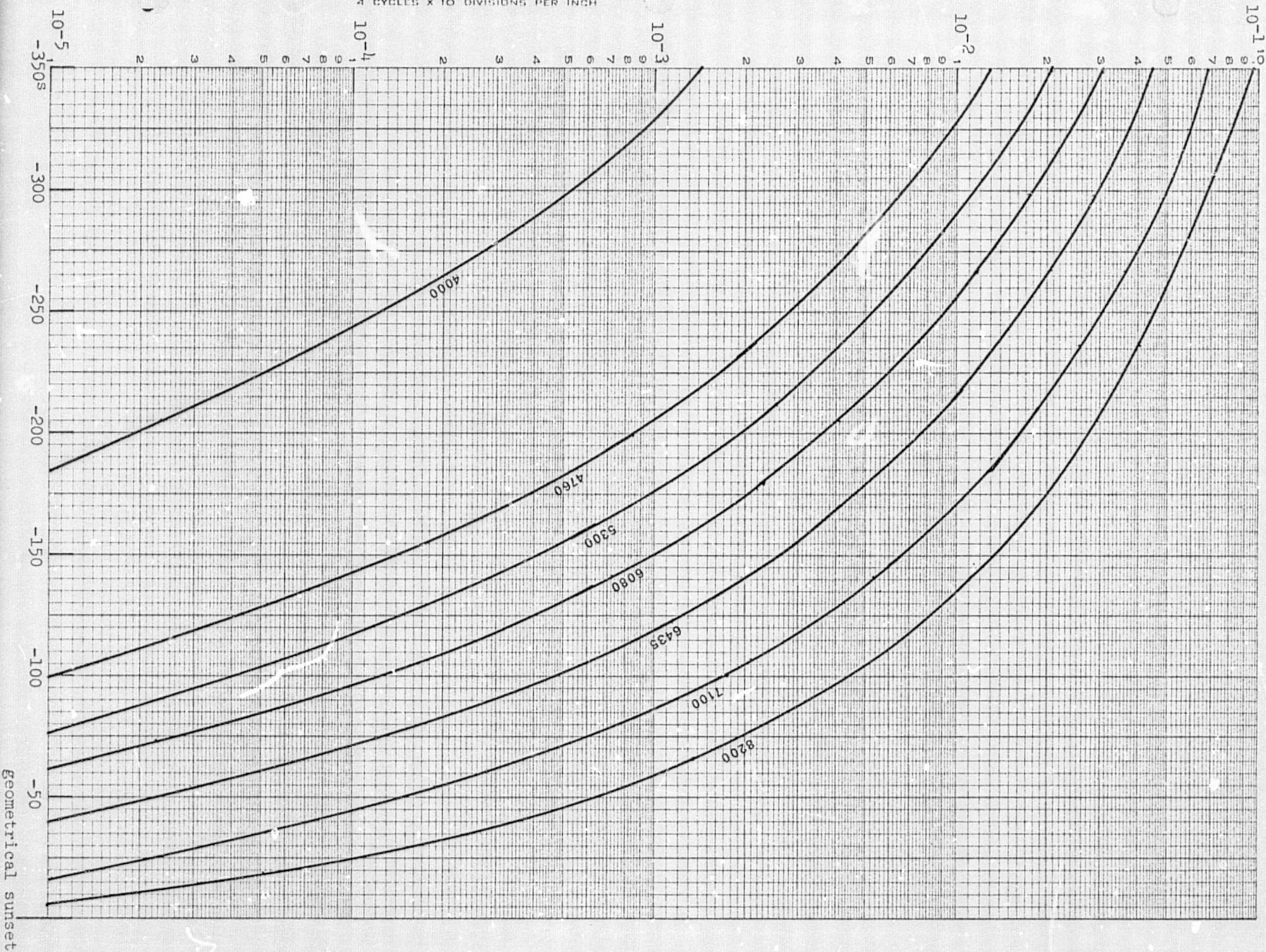
NO. 340-LA10 DIETZGEN GRAPH PAPER
SEMI-LOGARITHMIC
4 CYCLES X 10 DIVISIONS PER INCH

related to time through the orbital angular velocity and beta angle, and thus the relative irradiance can be determined as a function of time. The result is plotted in Figure 3 for the beta angle during Run 6-2. As in the case of direct sunrise modeling, the effect on the airglow lines was not considered.

As in Figure 2, there is a strong wavelength dependence in the time decay characteristic. Note that a significant rate of decay is occurring as early as 300 seconds before sunset and that the blue end of the spectrum is diminished before the red end by as much as 50 to 100 seconds before sunset. The similarity of these time characteristics to the observed decay rates (Figure 1) suggests strongly that the sunlit earth is the primary source of the observed changes.

We also investigated the possibility that the change in signal was caused by direct (on-axis) earthlight. The earth was "behind" the photometer, i.e. more than 90° from the line of sight at all times. Conclusive evidence for the source being "off-axis" is shown in Figure 4, which is a copy of a photograph taken during the "high signal" period with the 16 mm Data Acquisition Camera (DAC) that was boresighted with the photometer. Note that the sky region defined by the camera sunshield was exposed correctly; i.e., the sky is dark, and stars are as clearly visible as they are at night. Note, also, that the inner portions of the sunshield are overexposed; this can only be caused by the sunshield's knife edges being illuminated by a source outside the field of view (the camera and photometer fields of view are 15 and 6 degrees, respectively). A study of the geometry indicates that the spacecraft dish antenna was approximately opposite the bright corner and was therefore responsible for some and perhaps all of the off-axis brightness seen by the camera and the

Figure 3. Color/time dependence of the irradiance of the sunlit earth.



photometer.

Various parts of the illuminated (by the sunlit earth) spacecraft were found to be within 90° of the line of sight, with the discone antenna being approximately 50° from the line of sight. The short, low-rejection sunshield was used for these observations, and this sunshield does not have adequate rejection for bright sources this close to the line of sight.

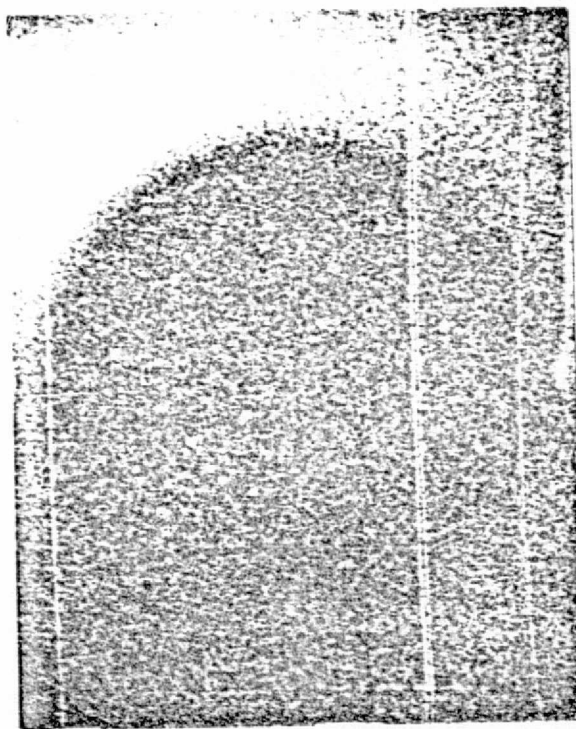


Figure 4. One of a series of DAC photographs taken during run 6-2. Note the dark sky at the center and the illuminated portion of the sunshield in the upper left.

B. Run 6-1

Muscari and Jambor (1975) reported that there was no night/day change in signal for this observation; this is expected, because the last data group was taken only 60 seconds after sunrise. Curves similar to Figures

2 and 3 for sunrise show that significant earthlight was not present until more than 100 seconds after sunrise. Full direct sunlight was present within 20 seconds after sunrise.

C. Run 12

The analysis of these data are more complex, because the photometer was scanning in azimuth (i.e., in a plane approximately perpendicular to the direction to the sun) during the measurement cycle. In this program the photometer observed over a range of azimuth at fixed elevation; the scan was made in a particular color, the photometer retraced its scan at the next color, etc., until all 10 colors were used. The photometer then waited until it reached the same starting place in the next orbit and it repeated the cycle. Multicolor scans of a 60° region of azimuth were obtained in this program on successive orbits, some scans with the photometer 1 m from the spacecraft and some (run 13) at 5.5 m from the spacecraft.

As noted by Muscari and Jambor (1975), each scan was started (and completed) during spacecraft day. The program was initiated only 11 seconds after sunrise, however; in orbit 1 it stopped at sunrise plus 110 seconds and in orbits 2 and 3 it stopped at sunrise plus 182 seconds. This difference was due to an anomaly in the instrument preparation routine; in the first orbit only the last 5 filters were used. This difference is important since the 8200A data in orbit 1 were taken starting only 80 seconds after sunrise; in orbits 2 and 3 these data were taken starting 150 seconds after sunrise. This is the filter that showed the largest rise in signal, and these are the data that Muscari and Jambor use to determine the level of "contamination".

Figure 5 is a computer-generated plot of output signal versus time

for orbits 2 and 3. The signal shown at the left of each plot is the output at 7100A with the azimuth moving towards its upper limit. At the upper limit the shutter closed (dark current level is shown left of center), the 8200A filter moved into position, the shutter opened, and the azimuth (after a 1 sec delay) moved toward its lower limit. The scanning rate was $3.87^{\circ}/\text{sec}$. The sinusoidal variation of output at the higher levels is due to the modulation of the polarized component by the rotating polaroid; the large amplitude indicates that the signal was highly polarized. Brightnesses marked along the baseline correspond to data averaged over $\frac{1}{4}$ -second intervals ending at the position of the value; also indicated are the relative phase angles of the polarized component. The limiting effect of the telemetry system (5 volts) is clearly visible on the high signal levels in Figure 5. The difference in levels of the maximum signal between the two orbits is probably due to the fact that the azimuth control was accurate only to ± 1.4 degrees. At the large rate of increase of signal, even a small difference in azimuth could produce the difference in signal level between the two orbits. Muscari and Jambor claim that this difference is due to the gradual dissipation of the contaminant cloud between orbits 2 and 3.

Characteristics similar to Figures 2 and 3 were derived for the beta angle during run 12. They show that the earthlight at 8200A increases by a factor of 3 between 80 and 140 seconds after sunrise; thus, the signals at any particular point in the scan should differ by that amount between orbits 1 and 2. Muscari and Jambor's data show a difference of a factor of 2.5 at azimuth 185° between orbits 1 and 2. The fact that the signal increase was a strong function of azimuth also suggests that the source is light reflected off the spacecraft. Difficulties

in the telemetry system require that the raw azimuth data be corrected. When these corrections are made, the signal increases as a function of azimuth for orbits 2 and 3 are almost identical, not significantly different as indicated by Muscari and Jambor. Other differences noted by Muscari and Jambor, especially the spectral differences, can also be shown to be similar to the earthlight color/time characteristics.

The difference in direction of polarization of the enhanced signal (Figure 5) is still further evidence against contamination as the source of the enhancement. The direction of polarization for the zodiacal light or for scattering by particulates near the spacecraft is the same - perpendicular to the direction to the sun. Only multiply-scattered light (e.g., light scattered off the vehicle and seen by the sunshield baffles) can give a different direction of polarization.

In summary, there is firm evidence for stray light from the sunlit earth in the SL-2 photometer observations analyzed by Muscari and Jambor (1975); we find no evidence for a detectable spacecraft corona in these observations. In the subsequent section we show further that the photometer would not detect the column brightness from the typical level of particulates observed by the S052 coronagraph.

References

- C. W. Allen, *Astrophysical Quantities*, 3rd edition, the Athlone Press, 1973.
- J. A. Muscari and B. Jambor, Final Report, Skylab Experiment T027, ED-2002-1776, Martin-Marietta, June 1975.
- J. L. Weinberg, R. D. Mercer, and R. C. Hahn, The optical environment of Skylab, Mission SL-2, Bull. AAS, 6, 337, 1974.

APPENDIX 1

Run 6-1

GMT day	time with respect to sunrise (sec)	color, nominal	total signal (volts)	dark current (volts)	net signal (volts)	net signal (S ₁₀ (V))
163	20:14:27.9	4000 Å	>10			
	:39.9	4760	>10			
	:51.9	5080	>10			
	15:03.9	5300	>10			
	15:15.9	5577	1.32	.10	1.22	13788
	:29.9	6080	1.02	.1	1.01	3222
	:41.9	6300	.43	.1	.33	5763
	:53.9	6435	.68	.11	.57	1721
	16:05.9	7100	.48	.11	.37	1235
	:17.9	8200	.63	.10	.53	2876
	:31.9	4000	.19	.10	.09	595
	:44.0	4760	.40	.10	.30	690
	:56.0	5080	.23	.11	.12	302
	17:08.0	5300		gain change		
	:20.0	5577	.42	.11	.31	350
	:34.0	6080	1.05	.11	.94	300
	:46.0	6300	.33	.12	.21	367
	:58.0	6435	1.07	.12	.95	287
	18:10.0	7100	1.03	.11	.92	307
	:22.0	8200	.80	.11	.69	374
	:35.9	4000	.52	.11	.41	271
	:47.9	4760	1.10	.12	.98	256
	:59.9	5080	1.12	.12	1.00	252
	19:11.9	5300	1.18	.11	1.07	256
	:23.9	5577	.36	.11	.25	282
	:38.9	6080	.90	.11	.79	252
	:49.9	6300	.31	.11	.20	349
	20:01.9	6435	.96	.11	.85	256
	20:13.9	7100	.92	.11	.81	270
	:25.9	8200	.65	.11	.54	293
	:40.0	4000	.51	.11	.40	264
	:52.0	4760	1.05	.11	.94	216
	21:04.0	5080	1.09	.11	.98	247
	:16.0	5300	1.11	.11	1.00	239
	:28.0	5577	.35	.11	.24	271
	:42.1	6080	.88	.11	.77	246
	:54.0	6300	.31	.11	.20	349
	22:06.0	6435	.85	.11	.84	254
	:18.0	7100	.91	.11	.80	267
	:30.0	8200	.65	.11	.54	293
	:44.1	4000	.51	.11	.40	264
	:56.1	4760	1.06	.11	.95	218
	23:08.1	5080	1.08	.11	.97	245
	:20.1	5300	1.14	.11	1.03	246
	:32.1	5577	.34	.11	.23	260

GMT day	hr:min:sec	time with respect to sunrise (sec)	color, nominal	total signal (volts)	dark current (volts)	net signal (volts)	net signal (S ₁₀ (V))
163	20:23:46.1		6080 Å	.88	.11	.77	246
	:58.1		6300	.30	.11	.19	332
	24:10.1		6435	.94	.11	.83	251
	:22.1		7100	.91	.11	.80	267
	:34.1		8200	.63	.10	.53	288
	:48.1		4000	.50	.11	.39	258
	25:00.2		4760	1.05	.11	.94	216
	:12.2		5080	1.10	.11	.99	250
	:24.2		5300	1.13	.11	1.02	244
	:36.2		5577	.34	.11	.23	260
	:50.2		6080	.88	.11	.77	246
	26:02.2		6300	.30	.11	.19	332
	:14.2		6435	.94	.11	.83	251
	:26.2		7100	.91	.11	.80	267
	:38.2		8200	.63	.10	.53	288
	:52.2		4000	.50	.11	.39	258
	27:04.2		4760	1.05	.11	.94	216
	:16.2		5080	1.09	.11	.98	247
	:28.2		5300	1.13	.11	1.02	244
	:40.2		5577	.34	.12	.22	249
	:54.3		6080	.88	.11	.77	246
	28:06.2		6300	.28	.11	.17	297
	:18.2	- 110	6435	.93	.11	.82	247
	:30.2	- 99	7100	.90	.11	.79	264
	:42.2	- 86	8200	.64	.11	.53	288
	:56.3	- 72	4000	.50	.11	.39	258
	29:08.3	- 60	4760	1.05	.11	.94	216
	:20.3	- 48	5080	1.09	.11	.98	247
	:32.3	- 36	5300	1.13	.11	1.02	244
	:44.3	- 22	5577	.34	.12	.22	249
	:58.3	- 10	6080	.88	.11	.77	246
	30:10.3	+ 2	6300	.29	.11	.18	314
	:22.3	+ 14	6435	.96	.11	.85	257
	:34.3	+ 26	7100	.94	.11	.83	277
	:46.3	+ 38	8200	.78	.11	.67	363
	31:00.4	+ 52	4000	.51	.12	.39	258
	:12.4	+ 64	4760	1.07	.12	.95	218
	:24.4	+ 76	5080	1.16	.11	1.05	264
	:36.4	+ 88	5300	1.29	.12	1.07	256
	:48.4	+ 100	5577	.42	.12	.30	339
	32:02.4	+ 114	6080	.90	.11	.79	252
	:14.4	+ 126	6300	.32	.12	.20	349
	:26.3	+ 138	6435	.96	.11	.86	260
	:38.3	+ 150	7100	.93	.11	.82	274
	:50.3	+ 162	8200	.85	.11	.74	401

Run 6-2

GMT day	hr:min:sec	time with respect to sunset (sec)	color, nominal	total signal (volts)	dark current (volts)	net signal (volts)	net signal (S ₁₀ (V))
163	21:24:23.0	- 296	4000 Å	.58	.11	.47	310
	:35.0	- 284	4760	1.02	.11	.91	209
	:47.0	- 272	5080	1.25	.11	1.14	288
	:59.0	- 260	5300	1.16	.11	1.05	250
	25:11.0	- 248	5577	.41	.11	.30	338
	:25.0	- 234	6080	.66	.10	.56	180
	:37.0	- 222	6300	.33	.11	.22	390
	:49.0	- 210	6435	.73	.11	.62	188
	26:01.0	- 198	7100	.78	.11	.67	223
	:13.0	- 186	8200	.84	.11	.73	398
	:27.1	- 172	4000	.39	.11	.28	184
	:39.1	- 160	4760	.75	.12	.63	144
	:51.1	- 148	5080	.79	.10	.69	174
	27:03.1	- 136	5300	.82	.10	.72	172
	:15.1	- 124	5577	.30	.12	.18	203
	:29.1	- 110	6080	.62	.12	.50	161
	:41.1	- 98	6300	.27	.12	.15	261
	:53.1	- 86	6435	.67	.13	.54	163
	28:05.1	- 74	7100	.68	.13	.55	182
	:17.1	- 62	8200	.60	.14	.46	249
	:31.2	- 48	4000	.46	.20	.26	175
	:43.2	- 36	4760	.83	.22	.61	141
	:55.2	- 24	5080	.85	.25	.60	151
	29:07.2	- 12	5300	.93	.30	.63	151
	:19.2	0	5577	.44	.34	.10	119
	:33.2	+ 14	6080	.83	.39	.44	142
	:45.2	+ 26	6300	.55	.45	.10	176
	:57.2	+ 38	6435	.99	.50	.49	147
	30:09.2	+ 50	7100	1.04	.55	.49	163
	:21.2	+ 62	8200	.94	.61	.33	177
	:35.2	+ 76	4000	.96	.66	.30	198
	:47.2	+ 88	4760	1.34	.74	.60	139
	:59.2	+ 100	5080	1.46	.79	.67	168
	31:11.2	+ 112	5300	1.54	.83	.71	169
	:23.2	+ 124	5577				
	:37.2	+ 138	6080	1.51	1.01	.50	160
	:49.2	+ 150	6300	1.16	1.06	.10	176
	32:01.2	+ 162	6435	1.65	1.12	.53	159
	:13.2		7100	1.71	1.19	.52	175
	:25.2		8200	1.01	1.25	.36	198
	:39.3		4000	1.63	1.30	.33	220
	:51.3		4760	1.95	1.35	.60	139
	33:03.3		5080	2.01	1.40	.61	155
	:15.3		5300	2.13	1.44	.69	164
	:27.3		5577	1.68	1.47	.21	233

GMT day	hr:min:sec	time with respect to sunset (sec)	color, nominal	total signal (volts)	dark current (volts)	net signal (volts)	net signal (S ₁₀ (V))
163	21:33:41.3		6080 Å	2.04	1.50	.54	172
	:53.3		6300	1.76	1.52	.24	414
	34:05.3		6435	2.08	1.54	.54	163
	:17.3		7100	2.06	1.54	.52	174
	:29.3		8200	1.90	1.54	.36	196
	:43.3		4000	1.88	1.53	.35	234
	:55.3		4760	2.07	1.51	.56	129
	35:07.3		5080	2.14	1.49	.65	165
	:19.3		5300	2.14	1.44	.70	168
	:33.9		5577	1.58	1.40	.18	209
	:45.3		6080	1.91	1.35	.56	179
	:57.3		6300	1.52	1.33	.19	330
	36:09.3		6435	1.84	1.26	.58	174
	:21.3		7100	1.72	1.20	.52	175
	:33.3		8200	1.54	1.16	.38	206
	:47.3		4000	1.38	1.10	.28	187
	:59.3		4760	1.63	1.02	.61	141
	37:11.3		5080	1.54	.95	.59	148
	:23.3		5300	1.51	.90	.61	147
	:35.3		5577	.98	.79	.19	214
	:49.4		6080	1.19	.69	.50	159
	38:01.4		6300	.81	.60	.21	373
	:13.3		6435	1.01	.53	.48	145
	:25.3		7100	.91	.45	.46	153
	:37.3		8200	.69	.35	.34	183
	:51.5		4000	.53	.28	.25	166
	39:03.5		4760	.84	.28	.56	129
	:15.5		5080	.83	.22	.61	153
	:27.5		5300	.83	.19	.64	152
	:39.5		5577	.30	.17	.13	149
	:53.5		6080	.62	.15	.47	149
	40:05.5		6300	.22	.13	.09	166
	:17.5		6435	.63	.12	.51	154
	:29.5		7100	.60	.12	.48	159
	:41.5		8200	.44	.11	.33	180
	:55.5		4000	.36	.11	.25	163
	41:07.6		4760	.70	.11	.59	136
	:19.6		5080	.72	.11	.61	154
	:31.6		5300	.74	.11	.63	151
	:43.6		5577	.26	.11	.15	169
	:57.6		6080	.56	.10	.46	148
	42:09.6		6300	.21	.10	.11	198
	:21.6		6435	.61	.10	.51	153
	:33.6		7100	.58	.10	.48	161
	:45.6		8200	.44	.10	.34	182

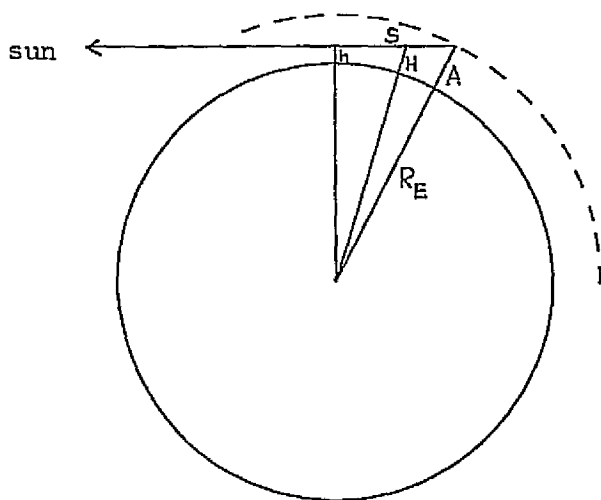
Preliminary Study of Contaminant Particulates around Skylab

APPENDIX 2

Air Mass versus Altitude and Apparent and Geometric Sunrise and Sunset seen from Skylab

Utilizing techniques given in Schuerman, et al. (1975)* the apparent altitude of the rising/setting sun was calculated as a function of time (Table 1), taking account of the effects of beta angle and refraction. To illustrate use of the table, the apparent sunrise at beta angle 30° is 27 seconds before geometric sunrise, and the sun is at an apparent altitude of 10 km 26 seconds after apparent sunrise.

At each altitude the sun's rays are seen through a different air mass. The geometry used to determine the appropriate air mass is shown below.



- A spacecraft altitude
- h apparent altitude of sun
- s $1/2$ the path traversed by the sun's rays
- H altitude at any point along s
- h_T extent of atmosphere ≈ 120 km

* D.W. Schuerman, F. Giovane, and J.M. Greenberg, Stellar Refraction: A Tool to Monitor the Height of the Tropopause from Space, J. Appl. Meteorol. 14, 1182-1186, 1975.

The total air mass m along path s is

$$\frac{2 \int_h^{h_T} \rho(H) ds(H)}{\int_0^{h_T} \rho(H) dH},$$

where $\rho(H)$ is taken from the U.S. Standard Atmosphere Supplements, 1966.

Since

$$ds(H) = \frac{(H + R) dH}{\sqrt{(H + R)^2 - (h + R)^2}},$$

$$m = \frac{2 \int_h^{h_T} \rho(H) (H + R) dH}{\int_0^{h_T} \rho(H) dH}.$$

m was calculated at 2 km intervals of altitude H from 0 to 70 km; the results are given in Table 2.

Table 1

Apparent Sun Rise/Set Time versus Altitude

beta angle	T(0)	ΔT_{10}	20	30	40	50	60	70	80	90	100
0	:23	:22	:30	:34	:38	:42	:46	:50	:54	:58	1:02
5	:23	:22	:30	:34	:38	:42	:46	:50	:54	:58	1:03
10	:23	:23	:30	:35	:39	:43	:47	:51	:55	:59	1:03
15	:24	:23	:31	:36	:40	:44	:48	:52	:56	1:01	1:05
20	:25	:24	:32	:37	:41	:45	:49	:54	:58	1:03	1:07
25	:26	:25	:33	:38	:43	:47	:52	:56	1:01	1:05	1:10
30	:27	:26	:35	:40	:45	:50	:54	:59	1:04	1:09	1:14
35	:29	:28	:38	:43	:48	:53	:58	1:03	1:08	1:14	1:19
40	:32	:31	:41	:47	:53	:58	1:03	1:09	1:14	1:20	1:26
45	:35	:34	:45	:52	:58	1:04	1:10	1:16	1:22	1:29	1:35
50	:41	:39	:52	:60	1:07	1:13	1:20	1:27	1:34	1:41	1:48
55	:48	:46	1:02	1:11	1:19	1:27	1:35	1:43	1:51	1:59	2:08
60	1:03	1:00	1:20	1:31	1:42	1:52	2:02	2:12	2:22	2:32	2:42
61	1:07	1:04	1:25	1:38	1:49	1:59	2:10	2:20	2:31	2:41	2:52
62	1:12	1:10	1:32	1:45	1:57	2:08	2:19	2:30	2:42	2:53	3:04
63	1:19	1:16	1:40	1:55	2:07	2:19	2:31	2:43	2:55	3:07	3:19
64	1:28	1:25	1:51	2:07	2:20	2:33	2:46	2:59	3:12	3:25	3:38
65	1:40	1:37	2:06	2:23	2:38	2:52	3:07	3:21	3:35	3:48	4:02
66	1:59	1:55	2:28	2:48	3:05	3:21	3:36	3:52	4:07	4:22	4:38
67	2:35	2:30	3:10	3:32	3:52	4:10	4:28	4:45	5:02	5:19	5:36
68		5:04	5:55	6:23	6:47	7:08	7:20	7:50	8:10	8:29	8:48
69		2:37	4:04	4:44	5:16	5:44	6:11	6:36	7:00	7:23	7:46
70				1:36	2:49	3:39	4:20	4:56	5:28	5:59	6:27

T(0) is the difference between the time of apparent sunrise (sunset) and the time of geometric sunrise (sunset). Geometric rise and set have SA (solar depression angle) = 110.5957 deg. for OWS alt. of 435 km., while apparent rise and set have SA = 112.0854 deg.

T10, 20, etc., are the time intervals between apparent rise (set) and the time the sun appears to be at 10, 20, etc. km. Times are in min:sec.

Air Mass versus Altitude

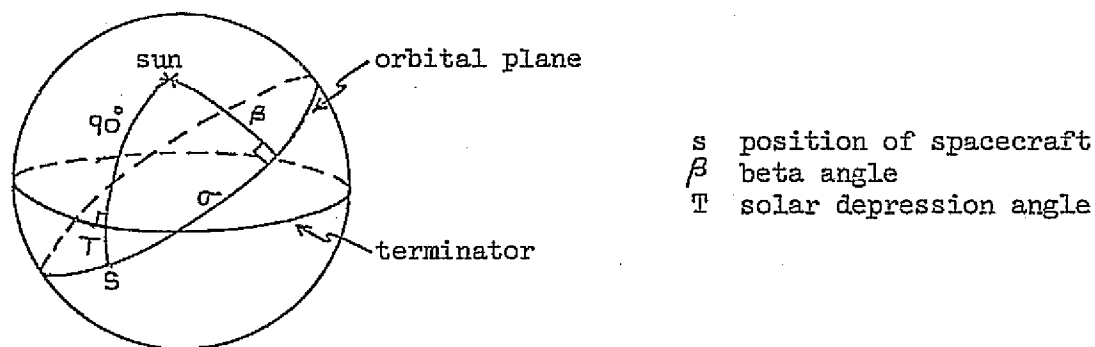
<u>Altitude(km)</u>	<u>Total air mass</u>	<u>Altitude(km)</u>	<u>Total air mass</u>
0	78.0	36	.41
2	63.2	38	.31
4	50.16	40	.23
6	39.32	42	.17
8	30.38	44	.13
10	23.04	46	.10
12	16.96	48	.08
14	12.38	50	.06
16	9.04	52	.05
18	6.60	54	.04
20	4.82	56	.03
22	3.52	58	.02
24	2.58	60	.02
26	1.88	62	.01
28	1.38	64	.01
30	1.02	66	.01
32	.76	68	.00
34	.56	70	.00

Preliminary Study of Contaminant Particulates around Skylab

APPENDIX 3

Irradiance at the Spacecraft due to the Sunlit Earth as a Function of Time

The solar depression angle T is defined in the following figure:



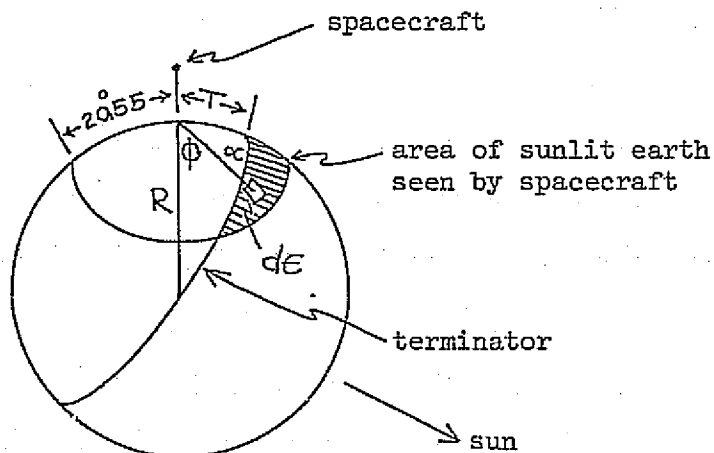
From the above, we obtain

$$\cos (90^\circ + T) = \cos \sigma \cos \beta \quad (1)$$

$$\text{or } \sin T = -\cos \sigma \cos \beta. \quad (2)$$

T is 20.55° at sunrise/sunset and 0° at terminator rise. Since $\frac{d\sigma}{dt}$ is known to be $3.87^\circ/\text{min}$ (orbital angular velocity), $\frac{dT}{dt}$ can be calculated from (2).

The area of the sunlit earth seen by the spacecraft is illustrated below.



To derive this area as a function of solar depression angle T , we note that

$$dE = R^2 \sin \alpha \, d\alpha \, d\phi. \quad (3)$$

The total area A is then

$$A(T) = \int dE = R^2 \int_{T_1}^{T_2} \sin \alpha \, d\alpha \int_{\phi_1}^{\phi_2} d\phi. \quad (4)$$

To determine the value of A at any value of T , the appropriate limits of integration are:

$$T_1 = 20.55^\circ$$

$$T_2 = T$$

$$\phi_1 = \sin^{-1} \frac{\tan T}{\tan \alpha} \quad (\text{equation of terminator})$$

$$\phi_2 = \pi.$$

The area A' projected on a plane perpendicular to the spacecraft-earth line is

$$A'(T) = 2R^2 \int_{20.6}^T \cos \alpha \sin \alpha \, d\alpha \left[\frac{\pi}{2} - \sin^{-1} \left(\frac{\tan T}{\tan \alpha} \right) \right]. \quad (5)$$

The brightness of the area A is a function of the reflection coefficient $F(\lambda)$ and the irradiance of the sun on the area:

$$B_A \propto I_\odot F(\lambda) e^{-\tau(\lambda) m(T)}, \quad (6)$$

where $\tau(\lambda)$ is the absorption of unit air mass, $m(T)$ is the number of air masses traversed, and I_\odot is the solar irradiance. The irradiance at the spacecraft is then

$$I_s(T) \propto B_A A' e^{-\tau(\lambda)} m(T) \quad (7)$$

or

$$I_s(T) \propto A'(T) F(\lambda) I_0 e^{-2\tau(\lambda)} m(T). \quad (8)$$

$F(\lambda)$ is assumed to be a constant and I_0 is known. Thus

$$I_s(T) \propto A'(T) e^{-2\tau(\lambda)} m(T). \quad (9)$$

The function $m(T)$ can be determined from

$$\cos(T + 2\theta) = \frac{R}{R + h} \cos\theta, \quad (10)$$

where θ is the solar elevation angle, R is the radius of the earth, and h is the spacecraft altitude.

(T) is determined from (10) and $m(\theta)$ is obtained from Allen (1973). Therefore, $m(T)$ is the product of the functions $\theta(T)$ and $m(\theta)$, and $I_s(T)$ can be determined. Since $T(t)$ can be determined from (2), $I_s(t)$ can be determined for each color of interest. This function is plotted in section II of the text (Figure 3) with reference to sunrise/sunset.

III. The Composite Picture

Photographs obtained with the S052 coronagraph and photoelectric data obtained with the photometer of experiments S073 and T027 contain unique data on the Skylab spacecraft corona. Particle tracks on the S052 photographs have provided data on discrete contaminant particulates at small scattering angles: number, size, distance, velocity. Further analysis of selected photometric data from Mission SL-2 showed no evidence for integrated light from contaminant particulates down to our threshold of detection of a few $S_{10}(V)^*$. It is of interest to determine the approximate sensitivity of the photometer to the brightness contributed by individual particles and to compare the photographic (small angle) and photoelectric (large angle) results.

We make the following assumptions:

1. The average particle size ρ is 25 microns in radius;
2. The particles are uniformly distributed out to a distance L of 200 meters from the spacecraft;
3. The energy scattered from each particle at scattering angles of $90^\circ \pm 10^\circ$ is .05 of the energy of an isotropic scatterer whose scattering cross section is assumed to be equivalent to its geometrical cross section.

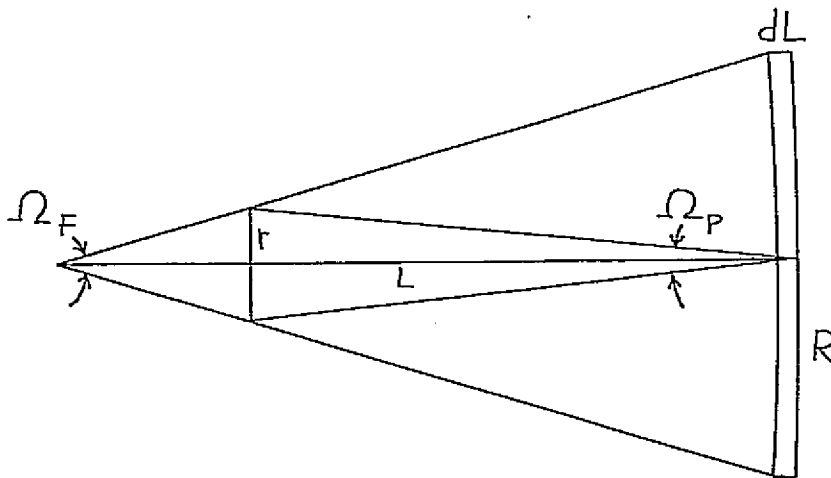
The scattered energy E_s at the photometer objective lens is

$$.05 \int_0^L I_\odot \pi \rho^2 \frac{1}{4\pi} \frac{\pi r^2}{L^2} \sigma \, dv,$$

where σ is the number density of particles, ρ is the particle radius, and I_\odot is the solar flux per unit area.

* Equivalent number of 10th magnitude solar (G2V) stars per square degree at mean solar distance. At 5300A, $1 S_{10}(V) = 1.30 \times 10^{-9}$ ergs/cm² sec sterad Å = $4.5 \times 10^{-16} B_\odot$.

Figure 1.



- r radius of photometer objective lens
 Ω_F solid angle of the photometer field of view
 Ω_P solid angle subtended by the objective at distance L
 R radius of photometer area of view at L
 A photometer area of view at L

$$dV = A dl = L^2 dl$$

Referring to Figure 1, this reduces to

$$E_s = .05 \int_0^L I_0 \frac{\rho^2}{4} \pi r^2 \sigma \Omega_F dl$$

or

$$E_s = .05 I_0 \frac{\pi \rho^2 r^2}{4} \sigma \Omega_F L.$$

The energy at the photometer due to the direct solar radiation is

$$E_0 \pi r^2 \Omega_F$$

or

$$\frac{I_0}{\Omega_0} \pi r^2 \Omega_F.$$

Normalizing the radiation from the particles to the direct solar radiation gives

$$\frac{.05 I_0 \frac{\pi \rho^2 r^2 \sigma}{4} \Omega_F L}{\frac{I_0}{\Omega_0} \pi r^2 \Omega_F}$$

$$= \frac{.05 \rho^2 \sigma L \Omega_0}{4}.$$

Using the values assumed earlier for ρ and L and the solid angle Ω_0 of the sun, we obtain $1.06 \times 10^{-7} \sigma$.

The photometer output is calibrated in $S_{10}(V)$ units (see earlier). After subtracting the brightness contribution of resolved stars, the total sky brightness for the region in question is approximately 100 $S_{10}(V)$. Total instrument reproducibility and the method of differencing day-night or night-day sky brightness combine to give a minimum detectable brightness change of from 1 to 3 $S_{10}(V)$. Using the value of 3 $S_{10}(V)$, we obtain a minimum detectable number density of particulates of

$$= \frac{3 S_{10}(V) \times 4.5 \times 10^{-16} B_0/S_{10}(V)}{1.06 \times 10^{-7}}$$

$$= 1.27 \times 10^{-8} \text{ particles/cm}^3.$$

The number of particles per S052 field (see Figure 9 of section I) ranged from 5 to 100. For the typical number of 10 particulates in the S052 volume of view out to 200 m, the number density is $2 \times 10^{-9} \text{ cm}^{-3}$.

Our inability to distinguish a day-night or night-day change in brightness which could be attributed to contamination is therefore consistent with the SO52 analysis which finds the typical number density to be below our column brightness threshold for detection. However, there were periods of a factor-of-ten higher concentration that would bring the particulate background up to the level of detectability of the photometer. Since this increased level of particulates had no preferred direction, we do not associate these levels with dumps or thruster firings.

THE SKYLAB TEN COLOR PHOTOELECTRIC POLARIMETER

J. L. WEINBERG, J. G. SPARROW* and R. C. HAHN

Space Astronomy Laboratory, State University of New York at Albany, U.S.A.

(Received 5 May, 1975)

Abstract. A 10-color photoelectric polarimeter was used during Skylab missions SL-2 and SL-3 to measure sky brightness and polarization associated with zodiacal light, background starlight, and the spacecraft corona. A description is given of the instrument and observing routines together with initial results on the spacecraft corona and on the polarization of the zodiacal light.

1. Introduction

A ten color photoelectric polarimeter was flown during the first two Skylab missions (SL-2 and SL-3) to measure sky brightness and polarization as well as to investigate optical contamination surrounding the spacecraft. The Saturn workshop was launched on May 14, 1973 into a 435 km circular orbit inclined at 50 degrees to the equator.

The photometer and a 16 mm camera were designed to operate from an alt-azimuth mounting at the end of a universal extension mechanism (Figure 1) and were designed to be deployed up to a distance of 5.5 m beyond the spacecraft using scientific airlocks (SAL's) in either the solar or antisolar directions (Figure 2). The 5.5 m extension was required to permit daylight observations from the solar SAL out to 90 degrees from the Sun without obstruction from the spacecraft. The SAL's and the extension mechanism/mounting were designed for use by several experiments [1]. Unfortunately, the solar SAL could not be used because a permanent heat shield was deployed out the solar SAL following the loss of the spacecraft meteoroid shield during launch. Therefore all observations with the photometer were obtained from the antisolar SAL.

The observations contain information on the Gegenschein, zodiacal light, and integrated starlight in the antisolar hemisphere. Comparison with simultaneous measurements from a ground station in Hawaii may help to elucidate the problem of airglow subtraction from ground observations of the nightglow.

2. Instrument Description

The photometer-camera system consisted of a photoelectric photometer, a parallel 16 mm Maurer camera, and sunshields. The photometer (Figure 3) was similar to that used by one of us in ground-based studies [2, 3] and consisted of a sunshield, a telescope cap, Fabry optics with a 6.35-cm primary objective, two six-position wheels containing interference filters, a rotating polaroid, a field of view wheel, a shutter, and a detector package.

* On leave from Aeronautical Research Laboratories, Melbourne, Victoria, Australia.

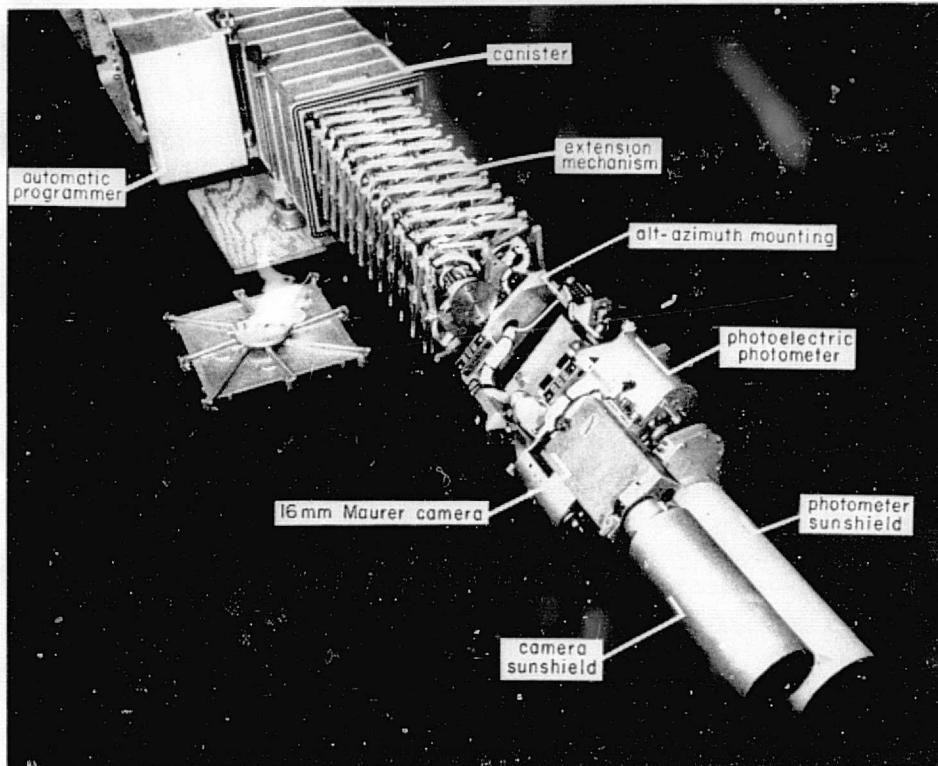


Fig. 1. The universal extension mechanism and photometer-camera system. The canister and attached panels contain power supplies, automatic and manual control equipment, and the universal extension mechanism.

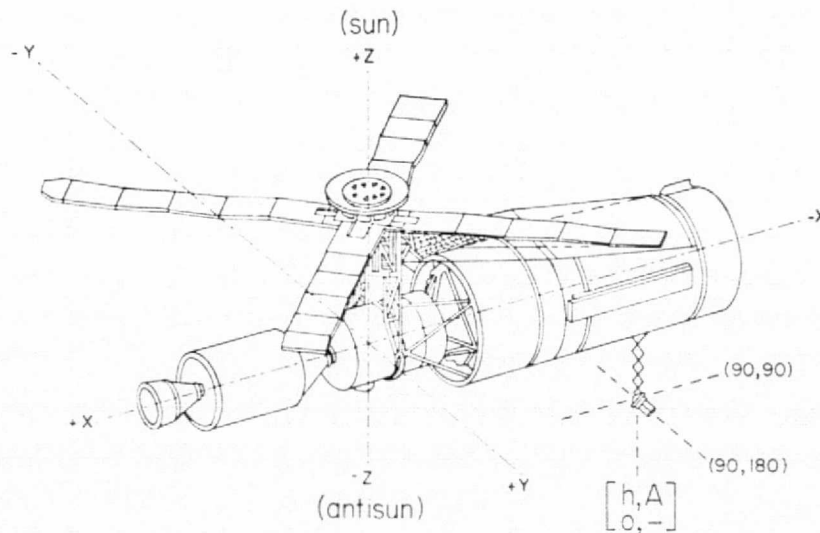


Fig. 2. The Skylab orbital assembly and reference directions. The photometer-camera system is shown deployed through the antisolar scientific airlock.

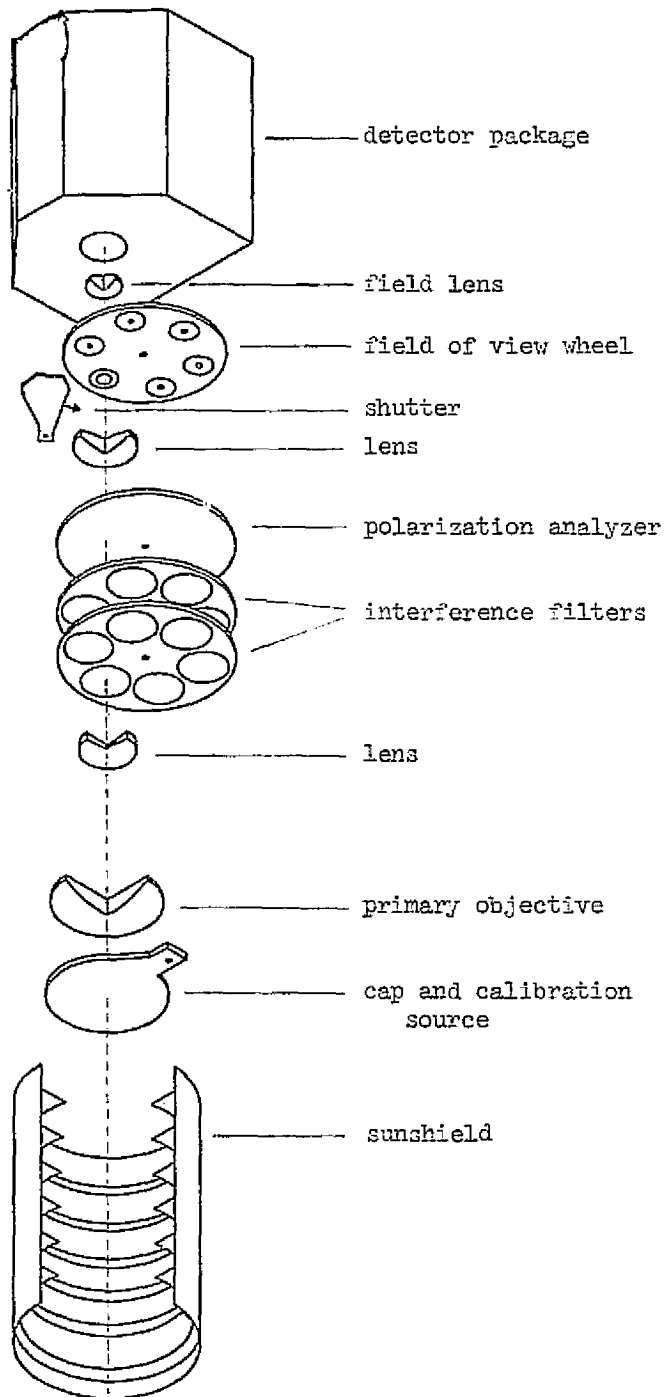


Fig. 3. Exploded, oblique view of the photometer head.

TABLE I
Interference filter characteristics

Color, nominal (Å)	Central wavelength ^a (Å)	Bandwidth at $\frac{1}{2}$ peak transmission ^a (Å)
4000	4001	110.0
4760	4748	47.5
5080	5068	49.7
5300	5294	61.0
5577	5562	17.0
6080	6063	83.0
6300	6286	20.0
6435	6427	108.2
7100	7093	135.0
8200	8160	220.0

^a At center of filter, -32°C .

The sunshield had two parts: a short baffle section for observations from the antisolar SAL and for limited observations from the solar SAL, and a longer, aperture-restricting section for use in observing close to the Sun. Since all observations were made from the antisolar SAL, only the short baffle was used. The cap protected the optical system when not in use. Mounted on the inside of the cap was a Pm^{147} -activated phosphor source for monitoring instrument performance. Shutter closure permitted measurement of the photomultiplier dark current. Each filter wheel contained five filters (Table I) and an open position. The filter bandwidths (except the two airglow filters) were chosen to give approximately the same photomultiplier output signal for a source having the solar color. The field of view wheel contained six different aperture/neutral density filter combinations, although most of the observations were obtained with a 6 degree diameter field without neutral density filter.

The detector package contained an EMR 541E photomultiplier (S20 response tube selected for high red sensitivity), a high voltage supply, and an output voltage differential amplifier. A thermoelectric cooler kept the photomultiplier photocathode at a temperature of approximately -10°C . Detector gain settings of 10^5 , 10^6 , and 10^7 could be selected, although in general the observations were taken with the middle gain. The time constant for the detector and preamplifier was approximately 2 ms. Temperature sensors were positioned near the cathode of the photomultiplier, near the interference filters, and near the cap source.

The HN 32 polaroid was driven at approximately 2 rps by an induction motor while a signal pulse was generated once per mechanical cycle as the polaroid rotated past a fixed point. The photomultiplier output was sampled at 320 sps while a similar channel was used to record the polaroid position pulse. These two channels, together with other instrument data sampled less frequently, were stored by an onboard digital tape recorder and subsequently telemetered to the ground. Alternatively, the data could

be telemetered in real time. The telemetry word size was nominally 2^8 (256) although the photomultiplier and synchronous pulse channels were limited to a data word range of 5 to 253 by telemetry constraints (5 volts full scale).

The elevation and azimuth of the pointing direction of the photometer were recorded 20 and 10 times per second, respectively, with a precision set by the bit size of 1.4 degrees.

The camera was included to provide information on possible anomalous results obtained with the photometer and to provide refined information on instrument pointing. Photographs were taken automatically every 11.25 degrees in elevation* and every 45 degrees in azimuth* or, for fixed position programs, at each filter change of the photometer (every 12 seconds). Kodak film type 2485 was used with exposures of $2\frac{3}{8}$ seconds. The field of view of the camera with baffle was approximately 15 degrees. The right ascension and declination of the center of the camera field of view (and therefore the photometer) could be determined to within ± 0.2 degrees provided that the field was well populated with stars that could be identified. The orientation of the field was also determined.

Control equipment for the photometer and camera was located on the canister shown in Figure 1. Instrument displays on the control panels included the output voltage, photometer coordinates, and data on the filters, field of view, shutter, and cap.

An automatic programmer was designed to operate the photometer manually or in any of seven automatic modes:

- 0 calibration
- 1 fixed position
- 2 vertical circle (scan in elevation at fixed azimuth)
- 3 almucantar (scan in azimuth at fixed elevation)
- 4 limited-area sky map (almucantars separated 2.8 degrees in h)
- 5 all-sky map (almucantars separated 5.6 degrees in h)
- 6 stowage position return.

Modes 0 and 1 were used for fixed position observations: of the cap source (Mode 0) or of the sky (Mode 1). One sequence of 10 filters took 2 minutes: 10 seconds on each filter interspersed with 2 seconds of dark current measurement. Modes 2 through 5 were used for scanning selected regions of the sky at approximately 4 deg s^{-1} . Only one of the azimuth and elevation drive stepping motors could operate at a time. The logic for termination of a traverse was based on elevation and azimuth readout. Mode 6 returned the mounting to the azimuth and elevation required for retraction into the canister.

A program could be operated any number of times from 1 to 64 and through the use of an orbital period counter could be performed automatically during parts of consecutive orbits. The elevation and azimuth range could be selected by the astronaut to provide scans over any portion of the sky. The mounting could scan through 354 degrees in azimuth and up to 112.5 degrees in elevation from the direction of

* Zero elevation (h) is the direction of the extension mechanism (approximately toward the Sun or anti-Sun); the azimuth (A) plane is perpendicular to the direction of zero elevation (Figure 2).

extension. The automatic programmer and other instrument controls were set up by an astronaut according to programs and times specified in the flight plan or in real time flight plan updates. After actuating a program, the astronaut went on to other activities not related to the experiment, and the instrument operated unattended.

Part of a typical Mode 4 scan sequence is shown schematically in Figure 4. A sample of PMF output from a Mode 4 program is shown in Figure 5. In this mode the selected region of sky was mapped in one color per orbit with the two second dark current measurement taken at the end of each traverse in azimuth. If the photomultiplier signal exceeded 10 volts in a scanning program for longer than 100 ms, the shutter closed and remained closed for the remainder of the scan; in a fixed pointing program, the shutter remained closed until the next filter was positioned.

3. Instrument Calibration

The photometer was calibrated prior to launch by viewing a diffuse source (C^{14} -activated phosphor) whose output had been measured relative to a secondary absolute standard. Any change in the sensitivity of the detector subsequent to this measurement could then be monitored by reference to the signal obtained when the internal Pm^{147} source was viewed. Corrections were made to the Pm^{147} source brightness for radioactive half life (2.67 years) and for change of brightness with temperature. Temperature coefficients determined in the laboratory for sources similar to that flown in Skylab were found to range between $0.09\%/^{\circ}C$ (at 5300 \AA) and $0.28\%/^{\circ}C$ (at 4000 \AA). Since the time from prelaunch calibrations to flight measurements was up to six months and the Pm^{147} source temperature difference ranged to $55^{\circ}C$, both these corrections are significant.

An alternative method of calibration is based upon the signals measured in flight as known bright stars traversed the field of view. Coupled with a prelaunch measurement of the photometer field of view which showed that the field response was essentially uniform with little vignetting, this enabled the response of the instrument to a diffuse source to be calculated. The radiant sensitivity calibration of the photometer is discussed in more detail in [4].

The orientation of the polaroid with respect to the time of the synchronous pulse was determined by allowing the instrument to view a source polarized in a known plane. This latter was derived from a pile of plates polarizer as discussed in [5]. A difference in orientation angle of up to 2 degrees as a function of wavelength indicated some birefringence within the optical train during laboratory measurements made five months before launch. Similar tests two months later with the instrument mounted in the spacecraft did not show this effect, nor was the birefringence present when the instrument was used in flight. Measurements of an unpolarized source showed that the instrumental polarization was significantly less than 1%.

The temperature of the filters was not controlled and dropped to $-30^{\circ}C$ during SL-2, although at times the heat input from the filter changing motor raised this temperature above $0^{\circ}C$. Corrections therefore had to be made for changes in filter

characteristics with temperature. Blifford [6] measured the temperature coefficients for wavelength of maximum transmission, transmittance and bandwidth for a number of commercial interference filters from different manufacturers. We have applied Blifford's temperature coefficients for wavelength of maximum transmission of Thin Film Products filters (Table I), the possible small correction for transmittance and bandwidth being ignored since its effect contributed only in the second order to our measurements (except for the airglow filters).

A limit on total sunshield length and diameter, the need to include a removable sunshield insert for planned observations near the Sun, and the pre-flight plan to only observe within ± 1 week of new Moon, led to the short sunshield's having limited off-axis rejection. The rejection ratio for an off-axis light source has been determined for the photometer [7, 8] and for the short sunshield used during SL-2 and SL-3 [9]. Combining these measurements indicates that the instrument could be expected to view within 21 degrees of the full Moon without adding more than 1 $S_{10}(\text{vis})^*$ to the sky reading. Since the SL-2 observations were taken when the Moon was between 88% and 100% illuminated, the data from each program must be carefully examined for contamination by stray light whenever the Moon or the illuminated Earth were approached.

TABLE II
Observations with the photometer

Mission	Mission day	1973 date	Mode	Program ^a	
SL-2	19	June	12 4	sky map (7 colors, 5300-8200)	
	19		12 1	I north celestial pole	
	19		12 1	II south ecliptic pole	
	19		12 1	III contamination, 2 parts: night/day, day/night	
	22	15 4	sky map (9 colors, 4000-7100)		
	22	15 1	IV north galactic pole		
	22	15 2	V elevation scans		
	22	15 4 ^b	sky map (4000, 4760)		
	23	16 4 ^b	sky map (7 colors, 5080-7100)		
	23	16 3	azimuth scans (5 colors, 4000-5577)		
	23	16 3 ^b	azimuth scans		
	24	17 3 ^b	azimuth scans		
	SL-3	5	August	1 4 ^b	sky map (4000)
		6		2 4 ^b	sky map (4760)
7		3 1		Gegenschein (5 colors, 4000-5577)	
7		3 1		contamination, night/day	
7		3 1		night/day scan, gravity-oriented	
7		3 1		Gegenschein	
7		3 2 ^b		elevation scans	
8		4 2 ^b		elevation scans	

^a 10-color observations, unless otherwise indicated.

^b Program started one day and ended the following day.

* One 10th magnitude (visual) star of solar color per square degree.

4. Observations

Table II summarizes observing programs which were performed with the photometer during the first (SL-2) and second (SL-3) missions. The sky maps were programmed to cover the largest possible part of the antisolar hemisphere given mechanical scanning constraints and the need to avoid the Earth, Moon, and spacecraft. Some scanning programs were designed to provide data on contamination. Others were designed to provide data on the background sky. Those programs which observed from night to day or day to night contain data on both. Since all observations were made from the antisolar SAL and the spacecraft corona was minimal, the 6 degree field of view was used for most of the observations. Figure 6 illustrates the areas of the antisolar hemisphere for which useful data have been obtained from SL-2. The universal

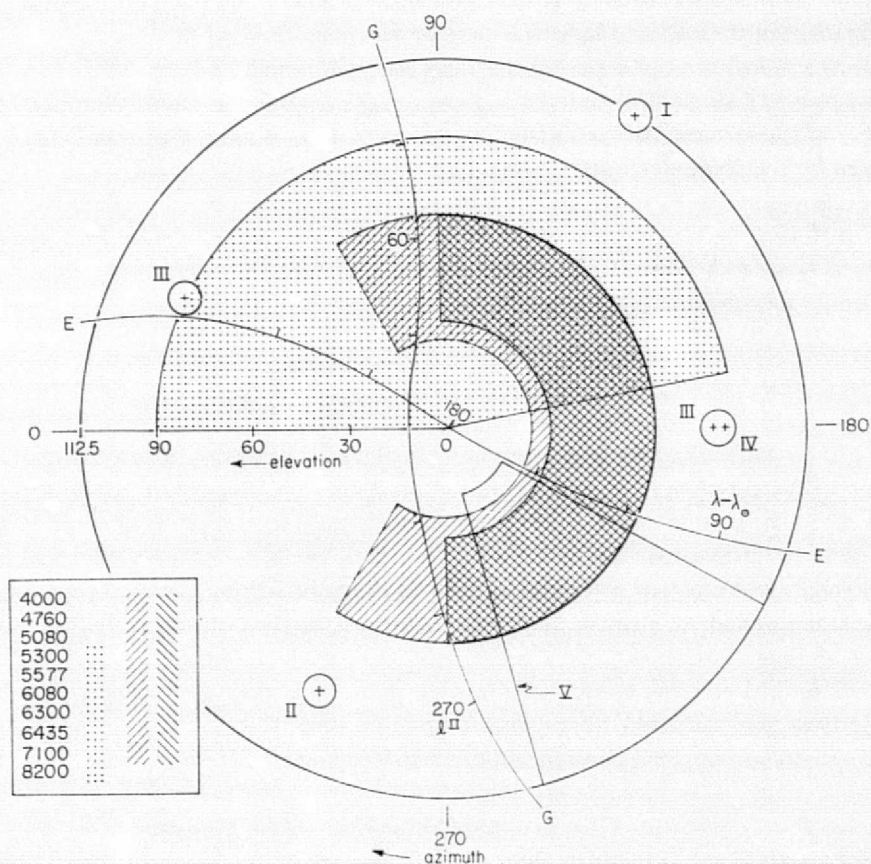


Fig. 6. Regions of the antisolar hemisphere for which useful data were obtained during SL-2 (see, also, Table II). G and E show the positions of the galactic equator and ecliptic, respectively. l^{II} refers to system II galactic longitude in degrees and $\lambda - \lambda_{\odot}$ refers to the ecliptic longitude of the observed point with respect to the Sun, in degrees. The inset shows the filters used with the sky-mapping programs.

extension mechanism/mounting facility failed early in mission SL-3 and could not be retracted, resulting in jettison of the facility and the attached photometer-camera system on August 4, 1973.

5. Data Handling

Data from the spacecraft were telemetered to ground in two different formats; one of these corresponded to data transmitted directly without being recorded onboard, while the second format corresponded to a dump of the tape recorders. Prior to transmission of experiment real time data between ground stations, an amplitude change compression factor was applied to reduce the bandwidth required for transmission. This resulted in the removal of all changes of the photomultiplier output voltage that did not equal or exceed 80 mV (4 bits). Since the amplitude of the sinusoidal signal component was often less than this, much of the information on the polarized component of the zodiacal light was thereby lost from the real time data.

During preparation of experimenter tapes, the real time and dump data were combined to give a single time-ordered sequence of data. Unfortunately, when both real time and dump data were available for the same time period, real time data were chosen by the computer during generation of the experimenter tapes. Furthermore, intervals as small as 50 ms of real time data were interspersed when available without regard to time butting, even though the spacecraft and ground station time systems differed by up to at least 38 ms. These problems have delayed analysis of much of the data until new experimenter tapes become available.

6. Data Analysis and Preliminary Results

The pointing direction of the photometer was obtained using the three axis directions of the workshop on the sky, the position of the antisolar airlock with respect to these axes, and the elevation and azimuth of the photometer. The workshop orientation was derived from gyroscopes reset each orbit from the Apollo telescope mount Sun and star sensors and was well determined. The elevation and azimuth were averaged over one second periods to remove much of the intrinsic scatter introduced by the transducer bit limitation.

During fixed pointing mode programs the spacecraft control moment gyro dump inhibit was activated, and the predicted elevation zero direction (the normal to the SAL) generally remained close to the prelaunch predicted 1.8 degree offset from the antisolar point. This momentum dump is a set of maneuvers applied against the external gravity gradient in the proper sense and timing so as to restore the control moment gyroscopes to their optimum attitude control orientations. In these maneuvers the spacecraft axes' directions changed by as much as 5 degrees. The dump inhibit was not employed during the scanning programs, and the photometer elevation zero direction deviated by up to 7 degrees from the antisolar point.

Preliminary analysis of the correspondence between the calculated pointing direc-

tions of the photometer and the camera shows differences of up to 3 degrees. Whether this is due to elevation/azimuth offsets, a boresight error between photometer and camera, or flexure of the extension mechanism must await further analysis. The absence of short period vibration of the extension mechanism was shown by the lack of jitter of the star images during the $2\frac{3}{8}$ seconds camera exposures at all times except within 10 seconds following completion of a movement in elevation or azimuth.

The photomultiplier data are being analyzed with a least squares fit to the expression

$$\text{PMT output} = A + Bt + C \sin(\omega t + D), \quad (1)$$

where the frequency ω is determined from the polaroid position pulse repetition rate while the time of zero phase angle is referred to the time of this pulse. Since the pulse time is subject to the uncertainty introduced by the sampling interval (3 ms), an improvement in both zero phase time and angular frequency ω can be achieved by averaging over a period of 10 to 30 seconds; i.e., sufficiently long to obtain some smoothing but too short to be affected by fluctuations in the angular frequency of the polaroid motor. Since the scan rate is approximately 4 deg s^{-1} , it is likely that the PMT output will be fitted to one second intervals of data. Digital synchronous detection has been used successfully for fixed position programs where 10 seconds of data are available for a given filter between dark current readings.

The mean value 'A' includes a component consisting of dark current (less than 1 bit) plus a 100 mV (5 bit) offset introduced because of telemetry requirements. The total was measured whenever the shutter was closed and remained constant (within one bit) once the photocathode had reached a stable low temperature. In general, except perhaps near the antisolar direction, we know the direction of polarization of the zodiacal light which is the only source of polarization except near the Milky Way. We may thus use the phase angle D found in Equation (1) to gain confidence in our determination of the amplitude of the polarized component (C), viz: satisfactory agreement between the measured phase angle D and the same angle calculated from the expected direction of zodiacal polarization indicates the efficacy of the least squares (or other) fit and assures that significant spurious (non-zodiacal) polarized light is not contributing to the measured signal.

The first contamination program was performed on SL-2 mission day 19 (III in Table II) with the photometer fixed in position at approximately 95 degrees from the Sun. Observations were made in all colors, starting with the spacecraft in the Earth's shadow and ending in daylight. The reverse sequence was performed later in the same orbit; i.e., daylight to shadow. There were levels of sky brightness in daylight only 5% above those at night, indicating that the spacecraft corona was minimal [10].

The polarized brightnesses of zodiacal light were obtained for the four fixed position programs of SL-2 (I, II, III, and IV of Table II and Figure 6). Except for differences at 4000 Å and 8200 Å, the polarized brightness of zodiacal light has the same color as the Sun [11].

It is hoped that new experimenter tapes will be made available in the near future to permit analysis of the bulk of the data.

Acknowledgements

This research was initiated at Dudley Observatory where it was supported by NASA contract NAS8-24865. Since October 1973 the research has been carried out at the State University of New York at Albany with the support of NASA contract NAS8-30251. Design of the photometer and of the automatic programmer were conceived by J. L. Weinberg and H. M. Mann while at Dudley Observatory. Design of the remaining hardware, including the universal extension mechanism/mounting facility, was performed by Martin-Marietta, Denver, together with the engineering and construction and most of the testing.

At NASA Headquarters we thank M. Dubin of the experiment Sponsoring Office and W. Schneider, J. Lundholm, T. Hanes, and others of the Skylab Program Office for their support and encouragement dating back to early 1969. It would not have been possible to implement this experiment successfully without the efforts of scores of people at the Marshall Space Flight Center and the Johnson Space Center and without the tireless efforts of the SL-2 and SL-3 flight and backup crews. Finally, we thank each member of the zodiacal light group at Dudley Observatory (1969-1973) and at State University of New York at Albany (1973-1974); without their dedicated effort, this experiment would not have made it through the hardware and operations phases.

References

1. Henize, K. G. and Weinberg, J. L.: *Sky Telesc.* 45, 2-6 (1973).
2. Weinberg, J. L.: *Ann. Astrophys.* 27, 718-738 (1964a).
3. Weinberg, J. L. and Mann, H. M.: in J. L. Weinberg (ed.), *Proc. Symposium on the Zodiacal Light and the Interplanetary Medium*, NASA SP-150, pp. 3-8 (1967).
4. Sparrow, J. G., Weinberg, J. L., Beeson, D. E., and Hanner, M. S.: 'Calibration of Zodiacal Light Photometers', to be presented at *IAU Colloquium No. 31 on Interplanetary Dust and Zodiacal Light*, Heidelberg, June 1975.
5. Weinberg, J. L.: *Appl. Opt.* 3, 1057-1061 (1964b).
6. Blifford, Jr., I. H.: *Appl. Opt.* 5, 105-111 (1966).
7. Leinert, C.: *Dudley Observatory Report*, No. 6, Albany, N.Y. (1971).
8. Leinert, C. and Kluppelberg, D.: *Appl. Opt.* 13, 556-564 (1974).
9. Martin-Marietta Corporation: T027 Photometer Head Light Leak and Suppression Test Report ED-2002-1573 (1972).
10. Weinberg, J. L., Mercer, R. D., and Hahn, R. C.: *Bull. Am. Astron. Soc.* 6, 337 (1974).
11. Sparrow, J. G., Weinberg, J. L., and Hahn, R. C.: 'Polarization of the Zodiacal Light: First Results From Skylab', to be presented at *IAU Colloquium No. 31 on Interplanetary Dust and Zodiacal Light*, Heidelberg, June 1975.

SkyLab Experiment S073
Gegenschein/Zodiacal Light

PRELIMINARY EXPERIMENT REPORT

SkyLab Mission SL-4

5 July 1974

Prepared By

Robert D. Mercer

R.D. Mercer
Co-Investigator

Institute for Scientific and
Space Research, Inc.
Delmar, New York 12054

Approved By

J.L. Weinberg

J.L. Weinberg
Principal Investigator

Space Astronomy Laboratory
State University of New York at Albany
Albany, New York 12203

This Report is submitted in accordance with requirements of Exhibit "B", Scope of Work, Task 10, NASA Contract NAS8-30251 to the State University of New York at Albany.

Table of Contents

	page
Background Information	1
Mission Objectives and Constraints	2
Preflight Activities and Flight Planning	6
Operational Accomplishments	10
Data Processing	10
Postflight Activities	19
Preliminary Data Analysis	21

Appendices

- A. Preliminary Quick Look Identification List
- B. Flight Data Calibration Photography
- C. Vignetting Data Identification List
- D. Vignetting Data Calibration Photography
- E. NASA Photographic Technology Laboratory Emulsion Calibration Data
- F. Memorandum on Low Light Level Photography for SL-4

List of Figures

1. Celestial Planning Map
2. Operational Accomplishment Chart
3. Representative S073 Photographic Results from Skylab 4
4. Data Processing and Analysis Flow Chart
5. Experiment S073 Vignetting Test Arrangement with S019 and T025 Equipment
6. Experiment S073 Vignetting Test Arrangement with T025 Equipment
7. Light Source Used to Illuminate Vignetting Test Screen
8. Vignetting Test Screen Measurements

List of Tables

1. S073 Photographic Timeline for SL-4
2. Experiment S073 Astronomical Photography on Skylab 4 by Subject
3. Experiment S073 Contamination Photography on Skylab 4

Background Information

Skylab Experiment S073 was developed to measure color, brightness and polarization of the skyglow over the entire sky to within 15° of the sun with emphasis on the zodiacal light and gegenschein -- faint skyglow brightening toward the sun, antisun (gegenschein) and ecliptic. A small, photoelectric photometer, similar to the one used by the Principal Investigator J.L. Weinberg in ground studies of the skyglow, was designed for use from each of the Scientific Airlocks (SAL). Pointing of the instrument's 1° , 3° or 6° diameter fields of view could be fixed with respect to vehicle axes, or it could be scanned over part or all of 2.719π steradians in any of four scan patterns (the solar SAL was not able to be used). The instrument could be programmed so that any desired portions of the sky could be observed within the constraints of bright celestial object and vehicular obstruction avoidance and earth horizon cutoff. During the Skylab-2 (SL-2) Mission some thirteen observation and/or calibration runs were performed. After the first run on SL-3 the crew reported that the scanning mechanism had become inoperable in one axis at a position that would not permit the photometer to be retracted back through the SAL either for analysis of the equipment problem or to clear the SAL for use by other experiments. An additional five runs were carried out, then the equipment was jettisoned, leaving the experiment with many of its objectives not met. A Preliminary Experiment Report, dated 21 February 1974, gives additional background and preliminary results from SL-2 and SL-3.

A number of circumstances made it possible to try to recover some of the lost observing opportunities by using on-board photographic equipment in missions SL-3 and SL-4. R.D. Mercer, L. Dunkelmann, C.L. Ross and C.L. Wolff had obtained very useful photographs of these and similar phenomena through formal and informal experimental tasks performed by the Apollo Command Module Pilots in lunar orbit using Eastman Kodak type 2485 film in the 35mm Nikon Camera. While that vantage point provided the best elimination of optically contaminating light sources, vehicle stability limitations caused image smear and kept exposure times below five minutes. In the course of that work, new data reduction techniques were developed for analysis of these photographs, although they had not reached production processing status, nor had all available refinements in the computer processing of images been utilized.

Independently, but with some awareness of this Apollo work, D.J. Kessler and H.A. Zook at NASA JSC had requested that the gegenschein be photographed using Skylab Experiment T025 equipment with a few frames of the same high-speed film used on Apollo and available on board Skylab for Experiment S063 requirements. Their specific purpose was to repeat research performed from the ground by R. Roosen to detect the possible presence of the earth's shadow falling on the gegenschein, but at an improved signal-to-noise ratio because the photography would take place above the atmosphere. Atmospheric extinction, scattering and airglow present the ground observer with difficulties that can easily mask the detection of the gegenschein shadowing effect, if, indeed, it does exist. Their proposed photography had been deferred prior to flight. However, the high level of task accomplishments

Background Information, cont'd

on SL-3 permitted that crew to request just this kind of new work; so, this photographic task was added in real time and made a part of Experiment S073 mission requirements. Five photographs were taken on 35mm film cassette BV15 using exposures from 120 to 330 seconds duration. Comparison of the longest two exposures at 300 and 330 seconds indicated that the threshold of detectability continued to be reduced by this additional ten percent time increase; thus, the emulsion's reciprocity failure limits had not been reached. Operationally this photography was quite successful, although it was scheduled when a star of 3.8 magnitude was very near the center of the gegenschein region.

Based on the Apollo and SL-3 results, Mercer took action to add cassettes of the high speed film to the final Skylab mission and, with the backing of the S073 Principal Investigator (PI), gained support for this investigation from the Sponsoring Science and Skylab Program Offices. He also obtained permission from Experiment T025 and S019 PI's to utilize their equipments. Dunkelman had also suggested hand-held, targets-of-opportunity photography of very similar subject matter as a NASA GSFC input to the Skylab missions; now it was possible to elevate these tasks to formal, experiment status through Functional Objectives within the Mission Requirements. A memorandum attesting to this change was jointly executed by Mercer and Dunkelman (see Appendix F). Photographic studies of extensions from galaxies suggested by H.C. Arp of the Hale Observatories and attempted on Apollo lunar flights by Mercer and Dunkelman were easily included. Finally, R.J. Naumann and P. Craven of NASA MSFC requested that contamination studies also be added as a part of the revived S073 requirements. This collection of inputs, then, became the starting point for S073 Experiment photography on SL-4. Also, Mercer, Kessler and Zook were appointed Co-Investigators (Co-Is) responsible for the SL-4 photography tasks.

Mission Objectives and Constraints

The specific objectives of the proposed photography were submitted in October 1973 as a list of Functional Objectives for inclusion in the Mission Requirements Document. Equivalent information, but in greater technical detail, is contained in Table 1, S073 Photographic Timeline for SL-4. The last three columns in this table give the time constraints. These constraints arose from two sources. First, only certain periods are available when the objectives to be photographed are positioned in the celestial sphere so that moonlight, planets, Milky Way, and bright stars are at an acceptable distance away from them and the region around them in the photograph. And second, the antisolar SAL pointing and, when required, the region of the sky available in the S019 Articulated Mirror System (AMS) must provide the capability to point the camera's line-of-sight at the required celestial coordinates. This latter limitation is shown in Figure 1, Celestial Planning Map.

9073 PHOTOGRAPHIC TIMELINE FOR SL-4

FO No.	Objective of Photos	Equipment ¹ Required	Approximate Exposure Durations	Night Passes Required	Approximate Exposures Per Pass	Observational Information		
						First Priority Periods	Second Priority Periods	Useable Periods
1 to 6	Gegenschein and Contamination	ASOL SAL TO25 Can Nikon Vis Lens UV Lens	10 Sec. to 8 Min.	6	5	18 Nov. - 26 Nov. 16 Jan. - 22 Jan.	2 Dec. - 4 Dec. 12 Jan. - 15 Jan. 23 Jan. - 3 Feb.	17 Nov. - 4 Dec. 12 Jan. - 3 Feb.
7 to 10	Zod. Lt East and Contamination	ASOL SAL S019 AMS TO25 Can Nikon Vis Lens UV Lens	10 Sec. to 6 Min.	4	8	18 Nov. - 30 Nov. 18 Dec. - 27 Dec.	1 Dec. - 2 Dec. 28 Dec. - 31 Dec. 16 Jan. - 18 Jan.	17 Nov. - 2 Dec. 17 Dec. - 31 Dec. 16 Jan. - 30 Jan.
11 to 14	Zod. Lt West and Contamination	ASOL SAL S019 AMS TO25 Can Nikon Vis Lens UV Lens	10 Sec. to 6 Min.	4	8	20 Nov. - 1 Dec. 20 Dec. - 30 Dec. 19 Jan. - 29 Jan.	18 Nov. - 19 Nov. 18 Dec. - 19 Dec. 17 Jan. - 18 Jan.	18 Nov. - 2 Dec. 17 Dec. - 31 Dec. 16 Jan. - 30 Jan.
15 to 17	Comet Tail	ASOL SAL S019 AMS TO25 Can Nikon Vis Lens UV Lens	1 Min. to 6 Min.	3	9	20 Nov. - 1 Dec. 20 Dec. - 30 Dec. 19 Jan. - 29 Jan.	18 Nov. - 19 Nov. 18 Dec. - 19 Dec. 17 Jan. - 18 Jan.	18 Nov. - 2 Dec. 17 Dec. - 31 Dec. 16 Jan. - 30 Jan.
18 to 25	Libration L ₄ ² and Contamination	ASOL SAL S019 AMS TO25 Can Nikon Vis Lens UV Lens	10 Sec. to 8 Min.	8	8	28 Nov. 8 ^h - 28 Nov. 20 ^h	27 Nov. 8 ^h - 28 Nov. 8 ^h 28 Nov. 20 ^h - 29 Nov. 20 ^h 28 Dec. 3 ^h - 28 Dec. 15 ^h 26 Jan. 23 ^h - 27 Jan. 11 ^h	27 Nov. 8 ^h - 29 Nov. 20 ^h 27 Dec. 3 ^h - 29 Dec. 15 ^h 25 Jan. 23 ^h - 28 Jan. 11 ^h
26 to 33	Libration L ₅ ² and Contamination	ASOL SAL S019 AMS TO25 Can Nikon Vis Lens UV Lens	10 Sec. to 8 Min.	8	8	20 Nov. 20 ^h - 21 Nov. 8 ^h 20 Dec. 15 ^h - 21 Dec. 3 ^h 19 Jan. 11 ^h - 19 Jan. 23 ^h	19 Nov. 20 ^h - 20 Nov. 20 ^h 21 Nov. 8 ^h - 22 Nov. 8 ^h 19 Dec. 15 ^h - 20 Dec. 15 ^h 21 Dec. 3 ^h - 22 Dec. 3 ^h 18 Jan. 11 ^h - 19 Jan. 11 ^h 19 Jan. 23 ^h - 20 Jan. 23 ^h	19 Nov. 20 ^h - 22 Nov. 8 ^h 19 Dec. 15 ^h - 22 Dec. 3 ^h 18 Jan. 11 ^h - 20 Jan. 23 ^h
34 to 36	NCC 5128 NCC 224 NCC 4472 NCC 3031 Coma Cluster	ASOL SAL S019 AMS TO25 Can Nikon Vis Lens UV Lens	4 Min. to 6 Min.	3	6	28 Jan. - 30 Jan. 20 Dec. - 31 Dec. 16 Jan. - 20 Jan. 18 Nov. - 2 Dec. 16 Jan. - 20 Jan.	25 Jan. - 27 Jan. 1 Jan. - 2 Jan. 1 Jan. - 4 Jan. 3 Dec. - 7 Dec. 1 Jan. - 4 Jan.	25 Jan. - 30 Jan. 20 Dec. - 4 Jan. 1 Jan. - 4 Jan., 15 Jan. - 20 Jan. 17 Nov. - 7 Dec. 1 Jan. - 4 Jan., 15 Jan. - 30 Jan.

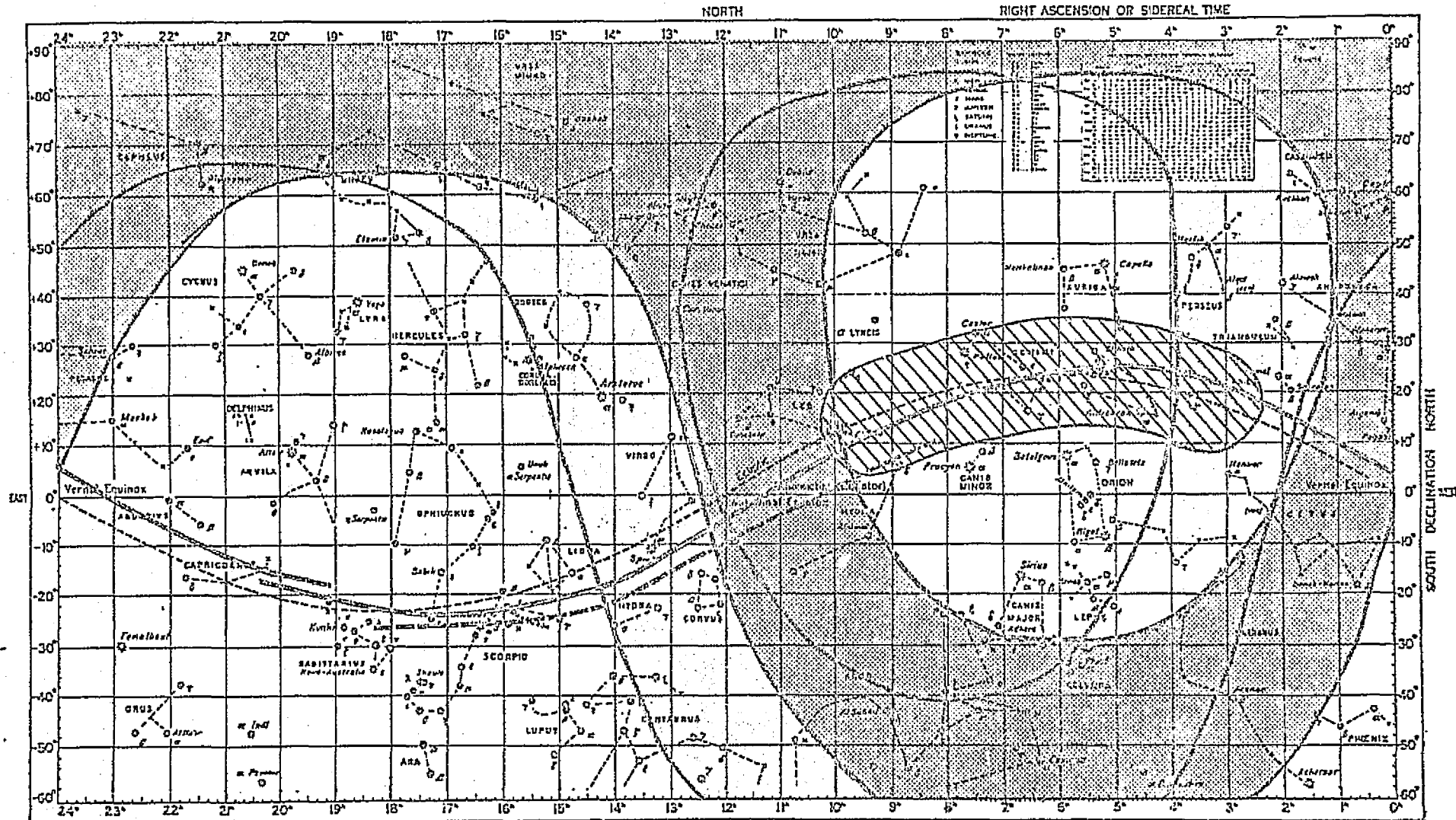
ORIGINAL PAGE IS OF POOR QUALITY

1. Observational periods for photographic tasks utilizing S019's Articulated Mirror System may be further constrained from field-of-view blockage by HF antennae and by the earth's horizon when magnitude of Beta angle exceeds 20°.

2. Libration regions L₄ and L₅ present shortest periods for observations of all tasks. Hours noted are in GMT.

Table 1

WORLD STAR CHART



- S019 AMS Field-of-View on 25 Dec 73
- S019 AMS Field-of-View on 25 Jan 74
- Anti-Solar circular Field-of-View coverage during mission
- Moon and Lunar Libration Points L_4 and L_5 track
- Comet Kohoutek track

Figure 1

ORIGINAL PAGE IS
OF POOR QUALITY

Mission Objectives and Constraints, cont'd

In this figure, the gegenschein lies at a position directly opposite the sun, the antisolar point. This point is 180° distant from the sun. Since the antisolar SAL was always pointed in that direction whenever there was no Control Moment Gyro momentum dump maneuver, gegenschein photography was mostly dependent on celestial lighting constraints, usually moonlight. But, from early December to mid-January the antisolar point passed across the Milky Way; so, altogether, less than one-half of the SL-4 on-orbit time was usable for gegenschein photography. And yet, this represented the easiest objective to photograph.

The shorter exposures represent photography for contamination studies. Photographs of the various celestial objectives taken when the spacecraft was in sunlight as well as in the earth's shadow could reveal any light scattering by particulate material around the spacecraft. Furthermore, it might be possible to determine the extent and periphery of the cloud of this material and the size distribution of its constituent particles. These in-sunlight photographs with ten-second and two-minute exposure durations were taken just prior to spacecraft sunset or just after spacecraft sunrise as added frames to gegenschein, zodiacal light and lunar libration region photography.

Zodiacal light east refers to the light in and near the ecliptic plane from 90° to 120° eastward of the sun, which would be to the left of the sun along the ecliptic in Figure 1. Zodiacal light west would be westward of the sun from 90° to 120° and to the right in the figure. These regions of the ecliptic were the only portions available to the camera's view using the AMS. Moonlight and bright planets further restricted the regions of zodiacal light that could be photographed. In addition, only a small field of view was available with the Nikon-T025-S019 AMS equipment combination, slightly less than 9° in diameter. Overlapping fields were required to cover the fall-off in brightness of the zodiacal light perpendicular to the ecliptic as well as at greater elongations from the sun along the ecliptic. Each photograph was planned to have several minutes of exposure time so it was only possible to obtain two or three photographs over a 20 to 30-minute night side pass of the spacecraft. Even this time period was reduced by one-third to one-half because the earth would occult the ecliptic view for a part of each night pass.

The track of the moon and of comet Kohoutek are also shown. Libration point L₄ lies on the lunar track to the left of the moon's position by 60° ; L₅ lies on track 60° to the right. Therefore, the moon's position at any given time can be used to compute the L₄ and L₅ positions. Only when the libration points were in the AMS field could they be photographed. The same holds true for comet Kohoutek's tail, which was always nearby the comet track, and for the galaxies.

Thirty-six night passes were required to complete the entire list of objectives. Over the 84-day mission period there were at least 60 days when some photography would be possible. This represented over 900 night

Mission Objectives and Constraints, cont'd

pass opportunities. This also takes into account those periods when the beta angle, the orbital-plane-to-sun angle, is so large that very short night passes or no night passes occur. Unfortunately, it does not take into account the competition for crewmen's time to carry out this photography versus the many other experimental and operational tasks on-board. While the S073 requirements represented four percent of the available night-times, that level was considered optimistic. In fact, it turned out that a little more than one percent of the usable night passes were actually devoted to S073 photography.

Preflight Activities and Flight Planning

The most crucial factor in the acceptance of the use of on-board equipment to continue Experiment S073 was the launch stowage weight on-board the SL-4 Command Module. Request had been made to carry twelve 35mm film cassettes loaded with Eastman Kodak type 2485 high-speed, black and white, recording film. Ten of these cassettes, with film for 40 exposures on each plus space for the JSC Photographic Technology Division's (PTD) sensitometric calibrations, were to be used for data. The remaining two cassettes were to be used for special preflight and postflight, absolute brightness calibrations required by the investigators. Although these dozen cassettes would weigh a total of just over two pounds, the Command Module was very close to its launch weight limit, and last minute changes in other experiments and operational tasks produced several contenders for this weight margin which was too small to satisfy all comers. The final decision was left to the JSC Program Manager and his Configuration Control Board, but the S073 request was supported from NASA Headquarters and MSFC.

The result was approval to fly eight cassettes, and the investigators reserved one of these for the special calibrations. These calibrations were required to fly with the data cassettes so that they would experience the same history of temperature, humidity, pressure and high energy radiation. The purpose of these calibrations was to record the level of density in the emulsion that had undergone the same exposure durations to known surface brightnesses in the same range of values as expected in the data frames. While JSC's PTD added preflight and postflight exposures of a standard, 22-step, sensitometric wedge for later evaluation of processing, the exposure duration for this wedge was only a one-hundredth of a second. The investigators required exposures to a special step-wedge calibrated in terms of the sun's surface brightness and spectral content. Also, it was very important that the selected exposure times cover the range of every exposure planned for the data frames, so that film reciprocity failure characteristics could be eliminated during the data reduction.

Reciprocity failure refers to the fact that photographic emulsions, like other detectors that integrate photons over time, fail to respond the same to an equal number of incident photons if the period of time over

Preflight Activities and Flight Planning, cont'd

which they arrive is not equal. This is particularly true for long photographic exposure time; thus, the 2485 emulsion will not show as great a signal for an eight-minute exposure to a given intensity as it would for a four-minute exposure to twice that intensity. The reciprocity relationship fails to hold. The very low brightnesses involved in the S073 photography required the use of fast optics and long exposure times, and it was impossible to avoid reciprocity failure effects in the data. But, because the equivalent duration calibration frames experience this same effect, it can be completely eliminated in the data processing, when densities in the data frames get converted to log intensities of the absolute surface brightnesses in corresponding calibration frames.

Flight film stock bearing emulsion number 112-1 was obtained from JSC's PFD, and calibrations were performed at the High Altitude Observatory in Boulder, Colorado on October 23, 1973 using their solar-referenced Sensitometer Box No. 1. Four cassette loads were calibrated to provide one for flight, one for backup, one for PFD control and one for the investigators to use for assessing anomalies, if they should occur. The first ten frames were left blank so that postflight exposures could be added in case some exposure times subsequently used in flight should not match the preflight planning values. The calibration film that actually flew had 32 preflight exposures covering nine minutes to one-eighth second and required ND1, ND2, ND3 neutral density filtering of the illumination source for the calibrated step-wedge as the exposures got longer so that the resulting emulsion densities would permit construction of complete calibration curves (see Appendix B). The flight calibration strip was eventually loaded into cassette BV45, worded "Not for use" and the leader wound completely onto the spool so that it could not accidentally be loaded into the camera in flight. The techniques for this work had evolved and been refined by Ross, Mercer and Dunkelman working closely with JSC's PFD and camera equipment engineers during the last three Apollo lunar missions, and the S073 photography benefitted directly from this work. In addition to the flight film stock, two strips of 107-2 stock were calibrated. These calibrations would be used later to obtain absolute brightness response curves for the lens vignetting test data (see Appendix D) which had that same emulsion number. This completed the preflight preparation phase.

During the mission, it had been agreed among S073, S063, S232 investigators and corollary experiments flight controllers that data for any of these experiments, all of which required use of type 2485 emulsion, could be taken on whatever cassette was loaded. Eighteen cassettes of this film type in 35mm format were carried up on SL-4. They were designated BV22, BV26 through BV29, and BV40 through BV52; for purposes of accountability the first nine were assigned to S063 and the remainder were assigned to S073 except for BV47 which was assigned to S232. The flight usage agreement kept cassette changeovers in flight to a minimum, conserved crew operational time, and thereby reduced the chances for losing data collection opportunities or for inadvertent exposure of the film during hurried cassette changes. The job of sorting out the data frames postflight was considered simple

Preflight Activities and Flight Planning, cont'd

because all three experiments had the same processing requirements, if data collection was nominal.

The first major setback for S073 resulted when the crew reported a much slower adaptation to the level of work schedule accomplishment previously demonstrated by the SL-2 and SL-3 crews. Since S073 had been added very late, it held a low priority and was given no opportunity for performance until well into December. This depleted 30% of the possible celestial opportunities with no data collected. Moreover, it lost the opportunity to photograph gegenschein before it entered the Milky Way and to observe galaxy NGC 3031. When this crew problem stabilized, four photographic passes were completed in December and seven in January. Several more were scheduled but they were scrubbed for higher priority experiments or operations prior to the detailed flight planning. It would be impossible to recount here all details of the scientific/political bargaining and infighting that took place in the course of real-time flight planning at JSC's Mission Control Center. It should suffice to state the obvious -- those with the greatest perseverance and knowledge of tactics walked away with more data collection attempts than others with equal priority and occasionally even more than those with much higher priority. The presence of a champion for an experiment's requirements on the field of battle cannot be overemphasized.

In order to bring some sense to the plethora of priorities, requirements and technical constraints among experiments, a NASA JSC science czar was designated within the Program Management Team. R.A. Parker served in this capacity with J.R. Sevier as his deputy, and every Wednesday and Sunday evening a joint planning meeting was held to review all upcoming experiment requirements, priorities and conflicts. This proved to be a valuable management tool for sensibly resolving conflicts and adjusting priorities over the near term. Nevertheless, each experimenter had to maintain close contact with his controller team to follow hour-by-hour accomplishments on-board Skylab as well as to seize promising opportunities when those activities did not go as planned, and crew time became available unexpectedly. Since Co-I's Kessler and Zook also served as experiment flight controllers, S073 held some advantage in following flight developments. But, because of their relentless schedule on the consoles, often they could not attend the twice-weekly science planning meetings.

Arrangements were made by L. Dunkelman at GSFC for Co-I Mercer to be tied into these two-hour meetings from his home through the Federal Telephone System. Here, again, the objective was to have representation on the field of battle at crucial times when forces were engaged. This arrangement proved quite valuable along with MSFC representation of S073's interests. Success or failure in securing a photographic opportunity usually hinged on a technical detail such as experiment pointing capabilities versus available targets, external lighting on the vehicle or length of nighttime or beta angle constraints, and even information on what film types and number of frames remaining were available in what

Preflight Activities and Flight Planning, cont'd

cameras. Only a dedicated representative for each experiment could follow such intricate matters with full knowledge of their importance to his scientific objectives. Also, the telephone tie-in to these meetings was quite successful for S073 because the distant representative was thoroughly familiar with all procedures and activities that took place during real-time mission control, as well as with most of the other experiment objectives and the general conduct of the science planning meeting itself. The S073 representative could recognize voices of all other attendees at the conference and could relate their interests, requests and comments to matters under discussion. Without such an overview, a distant attendee has very little understanding of the proceedings. Moreover, the other experimenters at the meeting recognized that the telephone attendee was listening to their inputs, and that they must choose their tactics or modify their requests accordingly.

An unusual example of the use of both tactics and scientific exploitation to raise, temporarily, the priority of an experiment was demonstrated in S073's initial photographic pass. The Co-I's noted that there was to be a partial lunar eclipse on December 10, 1973; this meant that the moon was very close to the antisolar point. Just a few hours before this event the earth would pass through the plane of comet Kohoutek's orbit. This edge-on viewing aspect of dust debris from its tail was unquestionably the best opportunity for S073 to observe scattered light from the dust both along and out of the comet's orbit. That is, integration along a common line-of-sight of the scattered light would provide a signal highly peaked in-plane, especially since the observation could not be made closer than 55° to the nucleus of the comet, and at this distance even the brightest signal was expected to be very weak. If such a photograph showed any evidence of the plane, it would have been a scientific "first". However, even partially occulted, the moon would produce considerable light on the antisolar side of the vehicle, but because the moon was close to the antisolar point it would be behind and well within the field-of-view that the camera had of the AMS mirror. So, the direct light would be blocked from view, and, because of the required pointing, no light scattered from the side of the vehicle could be reflected into the scene by the mirrored surface. Furthermore, S073 required no maneuvers of the vehicle or use of control propellants, something that was almost always required for other experiments attempting to photograph the nucleus and adjacent tail. These naturally occurring circumstances were so persuasive that other experimenters vying for this same time period were easily convinced in favor of the S073 comet plane photography. This unique opportunity would have been lost if the investigators had only pointed it out but had not been available to plead their case to the right groups at the right times.

Operational Accomplishments

The number of photographs taken for each task or objective is shown in Figure 2, Operational Accomplishment Chart. The rectangles not lined out represent the times when good celestial viewing of the particular phenomenon was possible. Sixty-two scientific photographs and 35 contamination photographs were taken.

Unfortunately, every frame of data is completely out of focus. This result is depicted in Figure 3, Representative S073 Photographic Results from Skylab 4. For some reason, as yet unexplained, the film pressure plate appears to have become separated from its location in the camera back. The film was not held flat in the image plane, and the resulting exposures have effective focal lengths of about two to five feet, but it varies across the scene and from frame to frame. This effective focal length puts the AMS mirror approximately in focus, but point sources at infinity appear as disks 1.2mm to 1.5mm in diameter. If the data is to be useful, considerable sophistication must be added to the data reduction and analysis phases of the work. For instance, the verification of pointing with identification of star fields has already taken several times longer than it would have if the celestial sphere had been in focus. Table 2, Experiment S073 Astronomical Photography on Skylab 4 by Subject, and Table 3, Experiment S073 Contamination Photography on Skylab 4, provide information on pertinent frames extracted from longer lists (see Appendix A) at their current level of completion.

Data Processing

Because of the out-of-focus problem, the data processing becomes considerably more complex and assumes greater importance in the derivation of significant scientific results. This will not change the expected flow of activities, however, which is shown in Figure 4, Data Processing and Analysis Flow Chart. But, processing through the VICAR Program, particularly removal of stellar images, cannot be expected to eliminate as much of the background noise as had been hoped, because all point source brightnesses have effectively been lowered and distributed over larger areas. Less bright stars can now escape detection and elimination during the application of spike filtering criteria, and their light will be blended into the diffuse, extended light of the gegenschein, zodiacal light or other phenomena under study.

Compilation of Quick Look Identification Lists is nearing completion (see Appendix A). The vignetting tests have been completed and will be reported in more detail below. The longer exposures of gegenschein have been selected for initial processing, because they offer the best chance for producing good scientific results in the shortest time with the least computer processing. The quality of results from this effort will determine what additional subject matter should be processed. Appropriate gegenschein frames, their corresponding calibrations, vignetting data and vignetting

OPERATIONAL ACCOMPLISHMENT CHART

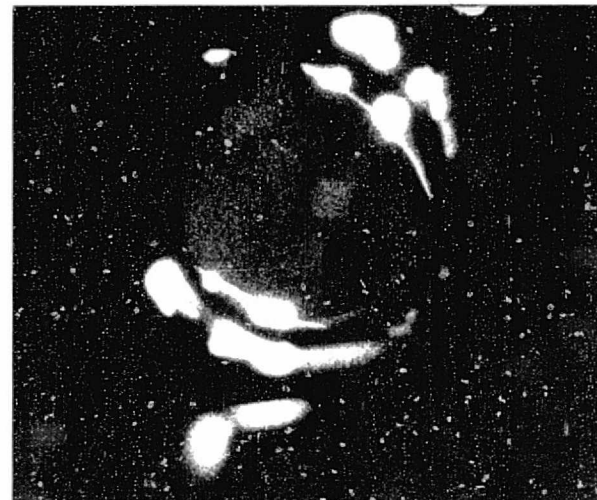
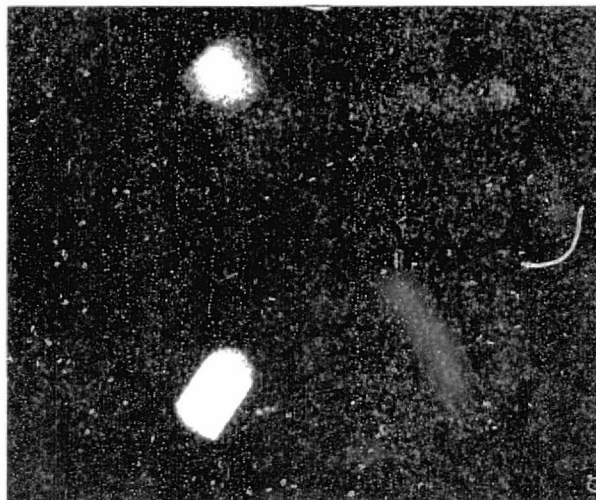
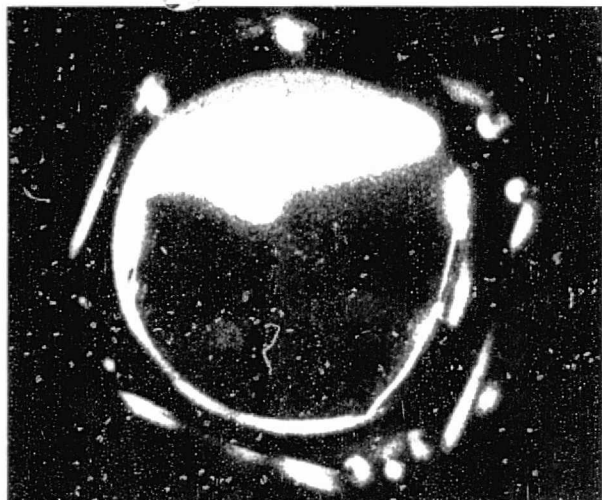
Date	December	01	02	03	04	05	06	07	08	09	10	11	12	13	14	15	16	17	18	19	20	21	22	23	24	25	26	27	28	29	30	31
Day of Year	1973	35	36	37	38	39	40	41	42	43	44	45	46	47	48	49	50	51	52	53	54	55	56	57	58	59	60	61	62	63	64	65
Mission Day	SL-4	6	7	8	9	0	1	2	3	4	5	6	7	8	9	0	1	2	3	4	5	6	7	8	9	0	1	2	3	4	5	6
Task																																
Gegenschein Gegenschein, Contamination																																
Zodiacal Light, East Elongation Zodiacal Light, East Elongation, Contamination																																
Zodiacal Light, West Elongation Zodiacal Light, West Elongation, Contamination																							1	2				2	2			
Kohoutek Comet Plane Kohoutek Comet Plane, Contamination												3	2										1									
Lunar Libration Region L ₄ Lunar Libration Region L ₄ , Contamination												1																2	1			
Lunar Libration Region L ₅ Lunar Libration Region L ₅ , Contamination												1	2										1									
Galaxy NGC 224 Galaxy NGC 224, Contamination																								2	2							
Galaxy NGC 4472 Galaxy NGC 4472, Contamination																														2	2	
Coma Cluster Galaxies Coma Cluster Galaxies, Contamination																																
Galaxy NGC 5128																																
Galaxy NGC 3031																																

Figure 2

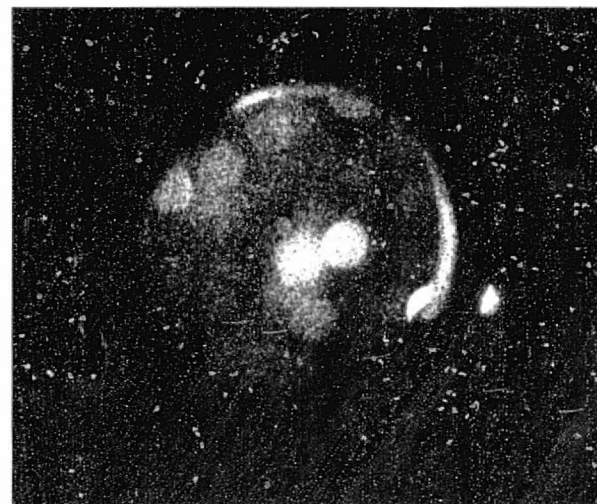
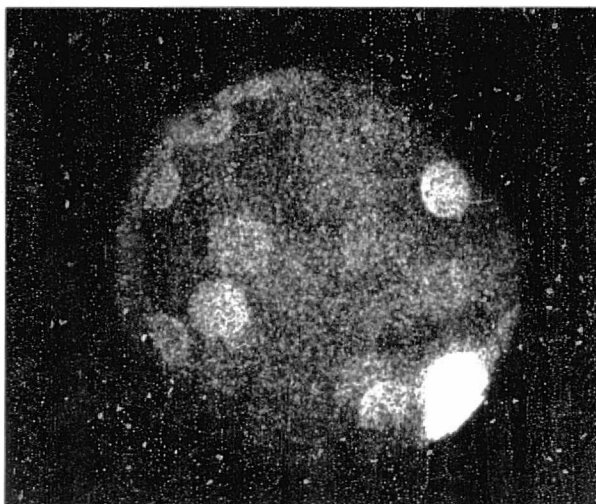
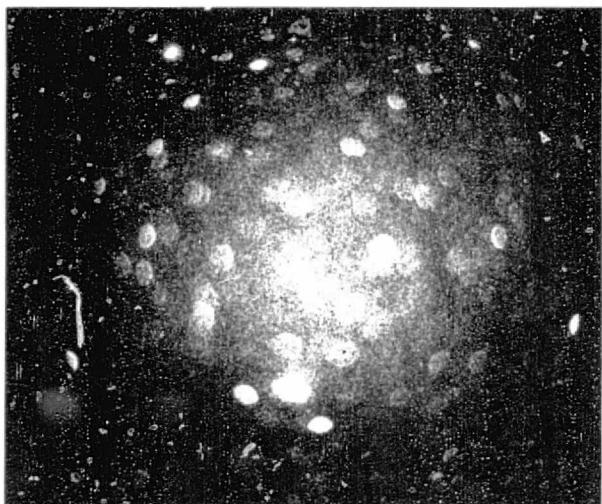
OPERATIONAL ACCOMPLISHMENT CHART

Date	January	01	02	03	04	05	06	07	08	09	10	11	12	13	14	15	16	17	18	19	20	21	22	23	24	25	26	27	28	29	30	31
Day of Year	1974	1	2	3	4	5	6	7	8	9	10	11	12	13	14	15	16	17	18	19	20	21	22	23	24	25	26	27	28	29	30	31
Mission Day	SL-4	47	48	49	50	51	52	53	54	55	56	57	58	59	60	61	62	63	64	65	66	67	68	69	70	71	72	73	74	75	76	77
Task																																
Gegenschein Gegenschein, Contamination																																
Zodiacal Light, East Elongation Zodiacal Light, East Elongation, Contamination																																
Zodiacal Light; West Elongation Zodiacal Light, West Elongation, Contamination																																
Kohoutek Comet Plane Kohoutek Comet Plane, Contamination																																
Lunar Libration Region L ₄ Lunar Libration Region L ₄ , Contamination																																
Lunar Libration Region L ₅ Lunar Libration Region L ₅ , Contamination																																
Galaxy NGC 224 Galaxy NGC 224, Contamination																																
Galaxy NGC 4472 Galaxy NGC 4472, Contamination																																
Coma Cluster Galaxies Coma Cluster Galaxies, Contamination																																
Galaxy NGC 5128																																
Galaxy NGC 3031																																

Figure 2 (Concluded)



Photographs on Eastman Kodak type 2485 emulsion were taken with a 35mm Electric Nikon camera through the T025 cannister and S019 Articulated Mirror System. From left to right, the first two scenes are zodiacal light studies at 90° east elongation using the 55mm UV lens at f/2.0. Scene on right was taken 60° west of comet Kohoutek as earth passed through comet's plane using 55mm visible lens at f/1.2. Out-of-focus condition made point sources at infinity appear as disks. Left photograph was a two minute exposure showing Spica at lower left and side of Orbital Work Shop at top with scattered light from micrometeoroid shield attachment structure and its reflection from gold covered outer skin. Center photograph repeats scene at left for six minute exposure with vehicle in earth's shadow during gyro momentum dump maneuver so that Spica and its image reflected from OWS skin move out of field-of-view. The nine minute photograph at right shows stray light from partially eclipsed moon behind mirror scattered off interior of S019 AMS. (SL4-162-5460 & -5461, SL4-165-5542)



Eight minute exposure with visible lens, f/1.2, at left in antisolar direction using T025 cannister alone shows Pollux at upper left and Beehive cluster in Cancer below center; vignetting distortions in brightnesses and in stellar disk shapes are quite pronounced. Seven minute exposure with same lens, f/1.2, in center shows region 60° eastward along lunar orbit at L4 libration point with Pleides at lower right. Eight minute exposure with same lens, f/2.0, has Andromeda (NGC 224) Galaxy at center, but extensions are not resolvable. (SL4-167-5602, SL4-163-5489, SL4-166-5586)

EXPERIMENT S073 ASTRONOMICAL PHOTOGRAPHY ON SKYLAB 4 BY SUBJECT

Subject	Date & Time (GMT)	Magaz Desig	NASA Frame Number	Lens Type & f/No	Expos Time (Sec)	Cntr Frm Loc	
						Rt Asc (Hr:Mn)	Dec (Deg)
Gegenschein	20 Jan 74 1344	BV 29	SL4-162-5471	Vis 1.2	360	8 ^h 10 ^m	+20.5
Gegenschein	20 Jan 74 1350	BV 29	SL4-162-5472	Vis 1.2	480	8 ^h 10 ^m	+20.5
Gegenschein	20 Jan 74 1359	BV 29	SL4-162-5473	Vis 1.2	240	8 ^h 10 ^m	+20.5
Gegenschein	22 Jan 74 0128	BV 29	SL4-162-5478	Vis 1.2	120	8 ^h 10 ^m	+22.0
Gegenschein	22 Jan 74 0130	BV 29	SL4-162-5479	Vis 1.2	360	8 ^h 10 ^m	+22.0
Gegenschein	22 Jan 74 0137	BV 29	SL4-162-5480	Vis 1.2	480	8 ^h 10 ^m	+22.0
Gegenschein	22 Jan 74 0145	BV 29	SL4-162-5481	Vis 1.2	360	8 ^h 10 ^m	+22.0
Gegenschein	22 Jan 74 1527	BV 29	SL4-162-5484	UV 2.0	120	8 ^h 00 ^m	+20.0
Gegenschein	22 Jan 74 1529	BV 29	SL4-162-5485	UV 2.0	840	8 ^h 00 ^m	+20.0
Gegenschein	22 Jan 74 1544	BV 29	SL4-162-5486	UV 2.0	480	8 ^h 00 ^m	+20.0
Gegenschein	23 Jan 74 1311	BV 49	SL4-167-5600	Vis 1.2	120	8 ^h 10 ^m	+20.0
Gegenschein	23 Jan 74 1313	BV 49	SL4-167-5601	Vis 1.2	300	8 ^h 10 ^m	+20.0
Gegenschein	23 Jan 74 1319	BV 49	SL4-167-5602	Vis 1.2	480	8 ^h 10 ^m	+20.0
Gegenschein	23 Jan 74 1327	BV 49	SL4-167-5603	Vis 1.2	360	8 ^h 10 ^m	+20.0
Gegenschein	23 Jan 74 2057	BV 49	SL4-167-5617	Vis 1.2	300	8 ^h 10 ^m	+20.0
Gegenschein	23 Jan 74 2102	BV 49	SL4-167-5618	Vis 1.2	420	8 ^h 10 ^m	+20.0
Gegenschein	23 Jan 74 2111	BV 49	SL4-167-5619	Vis 1.2	540	8 ^h 10 ^m	+20.0
Gegenschein	23 Jan 74 2119	BV 49	SL4-167-5620	Vis 1.2	300	8 ^h 10 ^m	+20.0
Zodiacal Light East E1	19 Jan 74 2213	BV 29	SL4-162-5461	UV 2.0	360	13 ^h 50 ^m	-10.0
Zodiacal Light East E1	30 Jan 74 1910	BV 42	SL4-168-5645	Vis 1.2	480		
Zodiacal Light East E1	30 Jan 74 1919	BV 42	SL4-168-5646	Vis 1.2	420		
Zodiacal Light East E1	30 Jan 74 1927	BV 42	SL4-168-5647	Vis 1.2	420		
Zodiacal Light East E1	30 Jan 74 2054	BV 42	SL4-168-5650	UV 2.0	480		
Zodiacal Light East E1	30 Jan 74 2103	BV 42	SL4-168-5651	UV 2.0	420		
Zodiacal Light East E1	30 Jan 74 2111	BV 42	SL4-168-5652	UV 2.0	420		
Zodiacal Light West E1	22 Dec 73 0241	BV 43	SL4-164-5522	Vis 1.2	300		
Zodiacal Light West E1	27 Dec 73 1921	BV 48	SL4-166-5581	UV 2.0	360	12 ^h 25 ^m	- 0.5
Zodiacal Light West E1	27 Dec 73 1928	BV 48	SL4-166-5582	UV 2.0	300	12 ^h 25 ^m	+ 3.0
Zodiacal Light West E1	28 Dec 73 0000	BV 48	SL4-166-5588	Vis 2.0	360	12 ^h 25 ^m	- 1.0
Zodiacal Light West E1	28 Dec 73 0007	BV 48	SL4-166-5589	Vis 2.0	300	12 ^h 30 ^m	+ 3.0
North Ecliptic Pole	30 Jan 74 1936	BV 42	SL4-168-5648	Vis 1.2	480	18 ^h 00 ^m	+66.5
South Ecliptic Pole	19 Jan 74 2221	BV 29	SL4-162-5462	UV 2.0	360	6 ^h 00 ^m	-66.5
Kohoutek Comet Plane	10 Dec 73 0121	BV 44	SL4-165-5541	Vis 1.2	360	10 ^h 45 ^m	- 7.0
Kohoutek Comet Plane	10 Dec 73 0127	BV 44	SL4-165-5542	Vis 1.2	540	10 ^h 45 ^m	- 7.0
Kohoutek Comet Plane	10 Dec 73 0137	BV 44	SL4-165-5543	Vis 1.2	120	10 ^h 45 ^m	- 7.0
Kohoutek Comet Plane	22 Dec 73 0227	BV 43	SL4-164-5520	Vis 1.2	360	10 ^h 45 ^m	- 7.4
Lunar Libration L4	10 Dec 73 0113	BV 44	SL4-165-5540	Vis 1.2	360	9 ^h 05 ^m	+11.5
Lunar Libration L4	27 Dec 73 1859	BV 48	SL4-166-5578	UV 2.0	360	0 ^h 29 ^m	+ 7.8
Lunar Libration L4	27 Dec 73 2338	BV 48	SL4-166-5585	Vis 2.0	360	0 ^h 40 ^m	+ 9.0
Lunar Libration L4	28 Dec 73 1355	BV 48	SL4-166-5592	Vis 1.2	360	1 ^h 04 ^m	+11.2
Lunar Libration L4	28 Jan 74 1248	BV 40	SL4-163-5487	Vis 1.2	480	3 ^h 55 ^m	+23.5
Lunar Libration L4	28 Jan 74 1257	BV 40	SL4-163-5488	Vis 1.2	360	4 ^h 05 ^m	+23.0
Lunar Libration L4	28 Jan 74 1304	BV 40	SL4-163-5489	Vis 1.2	420	4 ^h 05 ^m	+26.0
Lunar Libration L5	10 Dec 73 0106	BV 44	SL4-165-5539	Vis 1.2	360	00 ^h 57 ^m	+11.5
Lunar Libration L5	22 Dec 73 0234	BV 43	SL4-164-5521	Vis 1.2	360	12 ^h 03 ^m	- 5.0
Lunar Libration L5	20 Jan 74 0119	BV 29	SL4-162-5465	UV 2.0	120	13 ^h 10 ^m	-14.5
Lunar Libration L5	20 Jan 74 0121	BV 29	SL4-162-5466	UV 2.0	480	13 ^h 10 ^m	-14.5
Lunar Libration L5	20 Jan 74 0129	BV 29	SL4-162-5467	UV 2.0	360	13 ^h 10 ^m	-14.5

Table 2

EXPERIMENT S073 ASTRONOMICAL PHOTOGRAPHY ON SKYLAB 4 BY SUBJECT

Subject	Date & Time (GMT)	Magaz Desig	NASA Frame Number	Lens Type & f/No	Expos Time (Sec)	Cntr Frm Loc	
						Rt Asc (Hr:Mn)	Dec (Deg)
Galaxy NGC 224	22 Dec 73 0213	BV 43	SL4-164-5518	Vis 1.2	300	00 ^h 40 ^m	+40.0
Galaxy NGC 224	22 Dec 73 0218	BV 43	SL4-164-5519	Vis 1.2	480	00 ^h 40 ^m	+40.0
Galaxy NGC 224	27 Dec 73 1906	BV 48	SL4-166-5579	UV 2.0	480	00 ^h 40 ^m	+41.0
Galaxy NGC 224	27 Dec 73 1914	BV 48	SL4-166-5580	UV 2.0	360	00 ^h 40 ^m	+41.0
Galaxy NGC 224	27 Dec 73 2345	BV 48	SL4-166-5586	Vis 2.0	480	00 ^h 40 ^m	+41.0
Galaxy NGC 224	27 Dec 73 2353	BV 48	SL4-166-5587	Vis 2.0	360	00 ^h 40 ^m	+41.0
Galaxy NGC 4472	28 Dec 73 1402	BV 48	SL4-166-5593	Vis 1.2	480	12 ^h 28 ^m	+10.3
Galaxy NGC 4472	28 Dec 73 1410	BV 48	SL4-166-5594	Vis 1.2	120	12 ^h 28 ^m	+10.3
Galaxy NGC 4472	1 Jan 74 1713	BV 26	SL4-161-5414	UV 2.0	480	12 ^h 28 ^m	+10.0
Galaxy NGC 4472	1 Jan 74 2158	BV 26	SL4-161-5416	Vis 1.2	480	12 ^h 28 ^m	+10.0
Coma Cluster Galaxies	1 Jan 74 1704	BV 26	SL4-161-5413	UV 2.0	360	12 ^h 57 ^m	+28.0
Coma Cluster Galaxies	1 Jan 74 2151	BV 26	SL4-161-5415	Vis 1.2	360	12 ^h 50 ^m	+27.0
Galaxy NGC 5128	28 Jan 74 1313	BV 40	SL4-163-5490	Vis 1.2	480	13 ^h 20 ^m	-40.0
Galaxy NGC 5128	30 Jan 74 2044	BV 42	SL4-168-5649	UV 2.0	480	13 ^h 23 ^m	-39.8

Table 2 (Concluded)

EXPERIMENT SO73 CONTAMINATION PHOTOGRAPHY ON SKYLAB 4

Background Subject	S/C Sset or Srise	Date & Time (GMT)	Magaz Desig	NASA Frame Number	Lens Type & f/No	Expos Time (Sec)	Cntr Frm Loc		
							Rt Asc (Hr:Mn)	Dec (Deg)	
Gegenschein	Sunset	20 Jan 74 1343	BV 29	SL4-162-5470	Vis 1.2	10	8 ^h 10 ^m	+20.5	
Gegenschein	Sunrise	20 Jan 74 1403	BV 29	SL4-162-5474	Vis 1.2	240	8 ^h 10 ^m	+20.5	
Gegenschein	Sunset	22 Jan 74 0124	BV 29	SL4-162-5476	Vis 1.2	10	8 ^h 10 ^m	+22.0	
Gegenschein	Sunset	22 Jan 74 0125	BV 29	SL4-162-5477	Vis 1.2	120	8 ^h 10 ^m	+22.0	
Gegenschein	Sunset	22 Jan 74 1522	BV 29	SL4-162-5482	UV 2.0	10	7 ^h 50 ^m	+20.0	
Gegenschein	Sunset	22 Jan 74 1523	BV 29	SL4-162-5483	UV 2.0	120	7 ^h 50 ^m	+20.0	
Gegenschein	Sunrise	22 Jan 74 1552	BV 29		UV 2.0	10	8 ^h 00 ^m	+20.0	
Gegenschein	Sunset	23 Jan 74 1307	BV 49	SL4-167-5598	Vis 1.2	10	8 ^h 10 ^m	+20.0	
Gegenschein	Sunset	23 Jan 74 1307	BV 49	SL4-167-5599	Vis 1.2	120	8 ^h 10 ^m	+20.0	
Gegenschein	Sunset	23 Jan 74 2053	BV 49	SL4-167-5615	Vis 1.2	10	8 ^h 10 ^m	+20.0	
Gegenschein	Sunset	23 Jan 74 2054	BV 49	SL4-167-5616	Vis 1.2	120	8 ^h 10 ^m	+20.0	
Zodiacal Lt.	Sunset	19 Jan 74 2209	BV 29	SL4-162-5459	UV 2.0	10	13 ^h 50 ^m	-10.0	
Zodiacal Lt.	Sunset	19 Jan 74 2210	BV 29	SL4-162-5460	UV 2.0	120	13 ^h 50 ^m	-10.0	
Zodiacal Lt.	Sunrise	22 Dec 73 0247	BV 43	SL4-164-5523	Vis 1.2	120	12 ^h 30 ^m	- 6.0	
Zodiacal Lt.	Sunrise	22 Dec 73 0249	BV 43	SL4-164-5524	Vis 1.2	10	12 ^h 30 ^m	- 6.0	
Zodiacal Lt.	Sunrise	28 Dec 73 0014	BV 48	SL4-166-5590	Vis 2.0	120	12 ^h 30 ^m	+ 3.0	
Zodiacal Lt.	Sunrise	28 Dec 73 0016	BV 48	SL4-166-5591	Vis 2.0	10	12 ^h 25 ^m	- 0.5	
Comet Tail	Sunrise	10 Dec 73 0140	BV 44	SL4-165-5544	Vis 1.2	117	10 ^h 45 ^m	- 7.0	
Comet Tail	Sunrise	10 Dec 73 0142	BV 44	SL4-165-5545	Vis 1.2	10	10 ^h 45 ^m	- 7.0	
Libration L4	Sunset	27 Dec 73 1855	BV 48	SL4-166-5576	UV 2.0	10	00 ^h 29 ^m	+ 7.8	
Libration L4	Sunset	27 Dec 73 1856	BV 48	SL4-166-5577	UV 2.0	120	00 ^h 29 ^m	+ 7.8	
Libration L4	Sunset	27 Dec 73 2334	BV 48	SL4-166-5583	Vis 2.0	10	00 ^h 38 ^m	+ 8.7	
Libration L4	Sunset	27 Dec 73 2334	BV 48	SL4-166-5584	Vis 2.0	120	00 ^h 38 ^m	+ 8.7	
Libration L5	Sunset	10 Dec 73 0102	BV 44	SL4-165-5537	Vis 1.2	5	00 ^h 57 ^m	+11.5	
Libration L5	Sunset	10 Dec 73 0103	BV 44	SL4-165-5538	Vis 1.2	120	00 ^h 57 ^m	+11.5	
Libration L5	Sunset	20 Jan 74 0115	BV 29	SL4-162-5463	UV 2.0	10	13 ^h 10 ^m	-14.5	
Libration L5	Sunset	20 Jan 74 0116	BV 29	SL4-162-5464	UV 2.0	120	13 ^h 10 ^m	-14.5	
Libration L5	Sunrise	20 Jan 74 0137	BV 29	SL4-162-5468	UV 2.0	120	13 ^h 10 ^m	-14.5	
Libration L5	Sunrise	20 Jan 74 0139	BV 29	SL4-162-5469	UV 2.0	10	13 ^h 10 ^m	-14.5	
NGC 224	Sunset	22 Dec 73 0209	BV 43	SL4-164-5515	Vis 1.2	10	00 ^h 40 ^m	+40.0	
NGC 224	Sunset	22 Dec 73 0210	BV 43	SL4-164-5516	Vis 1.2	120	00 ^h 40 ^m	+40.0	
NGC 4472	Sunrise	28 Dec 73 1413	BV 48	SL4-166-5595	Vis 1.2	120	12 ^h 28 ^m	+10.3	
NGC 4472	Sunrise	28 Dec 73 1415	BV 48	SL4-166-5596	Vis 1.2	10	12 ^h 28 ^m	+10.3	
Coma Cluster	Sunset	1 Jan 74 1659	BV 26	SL4-161-5411	UV 2.0	10	12 ^h 57 ^m	+28.0	
Coma Cluster	Sunset	1 Jan 74 1700	BV 26	SL4-161-5412	UV 2.0	120	12 ^h 57 ^m	+28.0	

Table 3

ORIGINAL PAGE IS
OF POOR QUALITY

APPLY PREFLIGHT CALIBRATIONS ON FLIGHT AND BACKUP FILM

COLLECT SCIENTIFIC DATA ON FLIGHT FILM

RETURN BACKUP & UNUSED FILM STOCK FOR STUDIES
OF FLIGHT VS. BACKUP BASE FOG + RADIATION

RECOVER AND RETURN ORIGINAL FLIGHT FILM

APPLY POSTFLIGHT CALIBRATIONS
TO FLIGHT AND BACKUP FILM

APPLY CALIBRATIONS TO UNUSED FLIGHT FILM
STOCK FOR LENS VIGNETTING TESTS

PROCESS FLIGHT AND BACKUP FILM

USE FLIGHT-LIKE LENS, CAMERA, EXP. TO25
CAN. AND EXP. SO19 AMS FOR VIGN. TESTS

DUPLICATE, PRINT
AND PROCESS COPIES
OF FLIGHT FILM

STORE
ORIGINAL
FLIGHT
FILM

PERFORM CAMERA-LENS-EXP. EQUIPMENT VIGN.
TEST PHOTOGRAPHY USING FLIGHT FILM STOCK

DEVELOP VIGN. TEST & RELATED CAL. FILM

DISTRIBUTE
DUPLICATE
FILM

DIST. REAL-TIME
POINTING, TIMING
& TRAJ./ATT. DATA

DIST. CREW A/G
TRANS., LOGS &
DEBRIEFINGS

LOAN ORIG.
FLIGHT FILM
TO PI

RELEASE ORIG.
BACKUP FILM
TO PI

NASA RESPONSIBILITY

PI TEAM RESPONSIBILITY

COMPILE
QUICK-LOOK
ID LISTS

PRODUCE
WORKING
PRINTS

RETURN ORIG.
FLIGHT FILM

PHOTODIGITIZE FLIGHT DATA, FLIGHT
CALCS., BACKUP CALCS., VIGN. DATA &
VIGN. CALCS. ON USDA EQUIPMENT

MEASURE, ANALYZE
AND INTERPRET
DATA

COPY MAG. TAPES OF PHOTODIGITIZED DATA &
CONVERT DATA TO VICAR COMPATIBLE FORMATS

PROCESS THROUGH
VICAR PROGRAM

EVALUATE, ANALYZE
& INTERPRET DATA

REMOVE STARS

PRODUCE ISOPHOTE MAPS

MAKE NUMERICAL COMPUTATIONS

PRODUCE FIGURES FOR PUBLICATION

PRODUCE SLIDES FOR PRESENTATIONS

MAKE FINAL ANALYSES, INTERPRETATIONS & EXPLANATIONS OF SIGNIFICANCE

PREPARE PAPERS & PUBLICATIONS

PREPARE LECTURES & PRESENTATIONS

PROVIDE DATA TO NATIONAL
SPACE SCIENCE DATA CENTER

REPORT DATA TO NASA
SCI. & TECH. GROUPS

REPORT DATA TO ASTRON.
& SCI. COMMUNITY

Figure 4

Data Processing, cont'd

calibration frames have already been digitized and converted to VICAR format. They will undergo further image manipulations shortly using VICAR processors. Eventually, absolute measurements of surface brightnesses versus position within the frame should indicate the shape and extent of the gegenschein. These data in white light can then be compared to the color brightness data obtained with the photometer on SL-2 and SL-3.

In order to prepare for VICAR processing, the flow chart indicates that vignetting tests of the camera lens must be performed and the resulting photographs photodigitized along with the flight film and their calibrations. Vignetting tests and photodigitizations take place in parallel with the work on quick-look identifications, production of working prints and analysis of these data to determine, among other things, the best order for processing images through the VICAR Program. The vignetting tests will be discussed in detail later, but a short description of the photodigitization operation will be presented here.

The details of the photodigitization process are quite simple in principle. A square aperture, 80 microns on a side, of collimated, white light is allowed to pass perpendicularly through the original negative of a selected photographic frame. This beam then impinges upon the photocathode of a calibrated photomultiplier tube with the emulsion grain in focus. The output voltage of this photomultiplier is recorded in terms of density, that is, in terms of the logarithm, base 10, of transmitted beam intensity. The beam is scanned horizontally across the frame in the "x-direction" and parallel to a side of the square aperture while readings of intensity are digitized and stored at every 80 microns of travel. The scanning is accomplished by mechanically moving the stage, to which the film is attached, using computer controlled servomotors. At the end of this line scan, the stage is stepped vertically downward in the "y-direction" by 80 microns and scanned back in the "negative x-direction". Individual readings and information on position are temporarily stored by the control computer, then written onto a magnetic tape as a string of values following the frame identification character group loaded by the operator. One 35mm frame scanned side-to-side produces 458 readings per line, and from the bottom part of the upper sprocket holes to the top part of the lower sprocket holes requires 332 scan lines to produce 152,056 "pixels".

The photodigitizer used belongs to the US Department of Agriculture and is located in Washington, D.C. Arrangements for its use in SL-4 data processing is the direct, follow-on result of similar arrangements established for the Apollo Lunar photographic data processing. In addition, computer studies of the Apollo images indicated that the aperture size required could be as large as 80 microns instead of the 36 and 40 micron sizes originally used. The grain size in the very high-speed 2485 type emulsion is on the order of ten microns; so, the 80 micron square aperture provides some smoothing in the grain noise with little

Data Processing, cont'd

sacrifice in signal-following capability. The error introduced is estimated at a few percent and certainly below the error from conversion of density into VICAR-formatted absolute intensity; this conversion error is about ten percent. Determination of the optimum aperture is important from the standpoint of economics. By using an aperture twice as large as the one originally used, the number of readings is reduced four times. Considering the magnetic tape, disk file and main memory computer storage space required and the input/output and computer computation time to process a frame or combine two frames, the savings become significant. For instance, the photo-digitizer scanning time for a full data frame from SL-4 was about nine minutes compared to 35 minutes for the Apollo lunar data.

The VICAR image processing program is resident in the IEM360/75 computer at GSFC. It was originally developed at JPL for processing videoscans from the Ranger and Surveyor lunar missions; in fact, it has been named for that application -- the Video Image Communication And Retrieval Program. However, it can deal with any image that is expressed as a series of discrete brightness, intensity or density readings whose positions in the image are known and recorded in an ordered array. Capabilities exist to geometrically expand, reduce or reshape the image, to stretch, shrink or convert scales over its range of brightnesses, and to perform many other sophisticated processing operations such as removing constant level background densities, clipping brightness spikes of stars, smoothing noise, producing isophote maps and tracing values of brightness over straight or curved paths. A series of such computer processing operations requires many iterations resulting in the generation of many intermediate digital images and readings. Each image array must be returned to pictorial form by special equipment that can generate photographic negatives from magnetic tape files of the computed digital images, or, in the case of brightness signal traces through portions of an image, to graphic form by automatic plotters. Visual analyses of pictorial results and associated histograms of their density distributions indicate to what extent and through which VICAR processors the data should be processed in the following step.

Postflight Activities

Postflight activities accomplished or now in progress fall into seven major areas of work. Some of these tasks are self-explanatory or their techniques have been described above; others will need elaboration. The seven tasks are:

1. Postflight calibration of flight and backup film.
2. Support at PTD during photoprocessing of flight film, backup film, and prior film calibrations.

Postflight Activities, cont'd

3. Collection of real-time Mission Control data, crew logs and transcribed voice tapes.
4. Quick-Look Identification List preparation, production of working prints and identification of anomalies and unexpected sources of light on data frames.
5. Performance of the Visual and UV 55mm Nikon lens/T025/S019 AMS vignetting test photography.
6. Digitization of flight data, vignetting test data and their associated calibration frames.
7. Computer conversion of digitized data to VICAR-formatted data for further digital processing and the associated familiarization with the GSFC IBM 360/75 and peripheral systems specifically required for VICAR operations.

The postflight calibrations were required to cover exposure times up to fourteen minutes duration. One such exposure of the gegenschein had been scheduled in real time using the UV, f/2.0 lens. Because of its lower f-stop, it was almost three times slower than the Visible, f/1.2 lens. This photograph was as much exploratory as it was scientific; nevertheless, its final usefulness would have been compromised if there were no calibration frame of matching exposure. To carry out this calibration, Mercer obtained the flight calibration cassette, BV45, after its return from the spacecraft as well as the backup calibration film and one calibrated control strip from PTD for calibrations at the High Altitude Observatory in Boulder. These exposures were added in space reserved for just such possible use during the postflight calibration activities. The films were returned to JSC within two days to be ready for development processing along with one data film.

Collection of real-time Mission Control data was greatly simplified, because Co-I Kessler was a corollary experiment controller and had ready access to all pertinent computation records and dump voice tape transcripts. Mercer was able to xerox crew logs while supporting the PTD photoprocessing activities. The Quick Look Identification Lists preparation, star field determinations (which are quite difficult when out of focus) and extensive review of supporting data to explain anomalies in the data have been carried out almost exclusively by Senior Research Assistant K.L. Jacobs. Tables 2 and 3 and Appendices A through D are heavily based on her work.

Perhaps the largest postflight task was the testing of the Visible and UV lenses in the same equipment configuration as used on-board Skylab. Lens vignetting measurements from the prior Apollo work had shown that there was little difference in vignetting patterns between the same lens types. The Apollo 15 and 17 Visible, f/1.2 lens patterns had been photo-

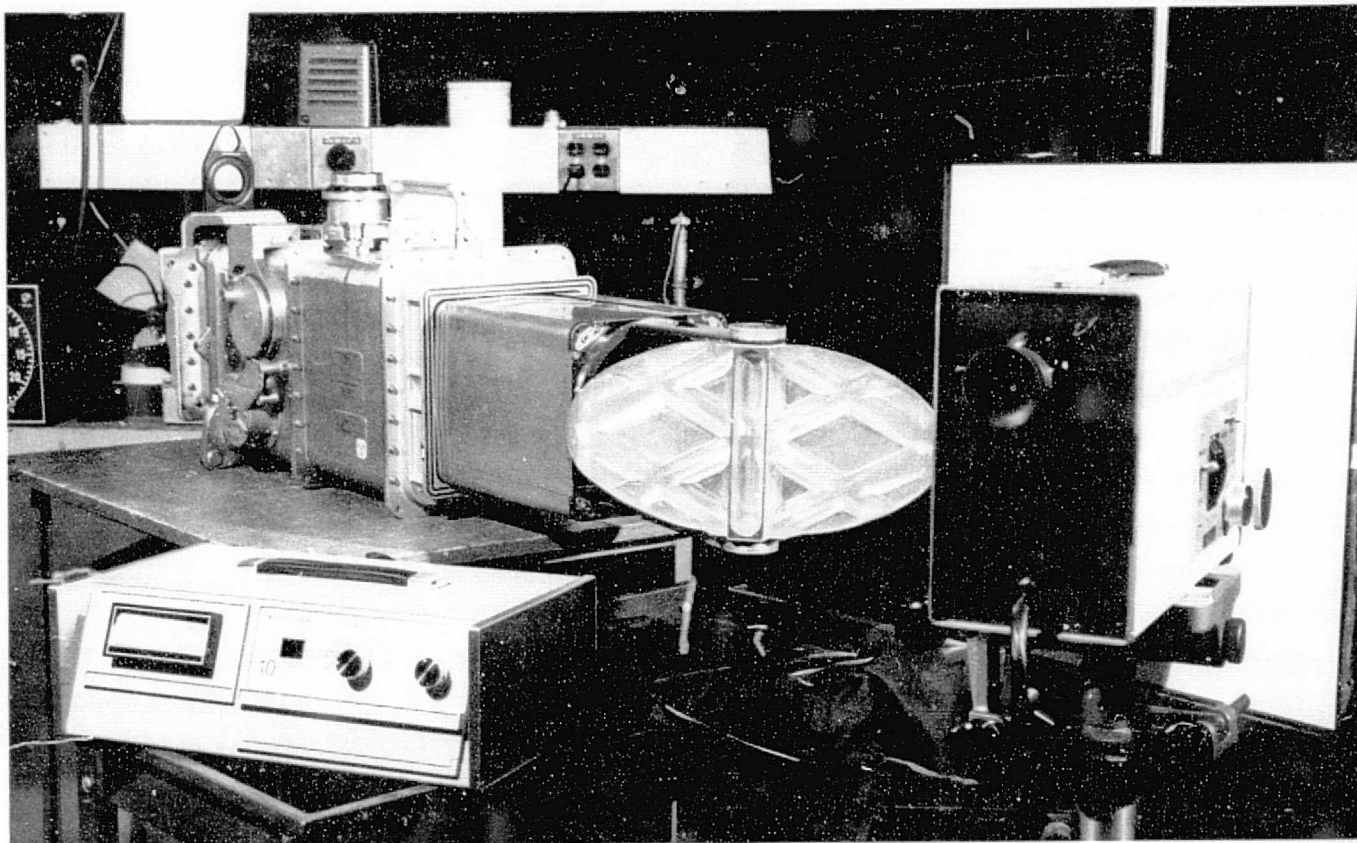
Postflight Activities, cont'd

digitized and differenced by the VICAR program. The increase in the standard deviation for this difference image was not greatly changed from the deviation when each lens vignetting function was subtracted from itself; therefore, this source of error proved to be very small. This is fortunate for the SL-4 data, because the photography had been added after launch of the equipment, and there was no possibility for directly measuring vignetting functions for the flight lenses. However, it was possible to obtain lenses of the same type for testing with the T025 cannister and S019 AMS and with the T025 cannister alone. The cannister contained a light baffle designed to the T025 experiment needs, and this was expected to have a much greater effect on vignetting than any difference between lenses. Arrangements were made to have the training equipments for the experiments sent to GSFC where they could be set up in proper configuration to photograph a diffusely reflecting white screen illuminated as evenly as possible. Figure 5, Experiment S073 Vignetting Test Arrangement with S019 and T025 Equipment, shows one set up in which both the Visible and UV lenses were tested using a series of focal lengths to duplicate the flight conditions and problem. Figure 6, Experiment S073 Vignetting Test Arrangement with T025 Equipment shows the other set up, and Figure 7, Light Source Used to Illuminate Vignetting Test Screen, shows the large aperture, diffuser box and illuminant required to produce an even lighting across the screen. To verify the constancy of field within an acceptable error level, light reflected from the screen was measured with a precision photometer. The readings and overview of test equipment arrangement are shown in Figure 8, Vignetting Test Screen Measurements. In spite of great care, the screen readings do show a slight specularity to the right and slightly below center, although it is not serious. The photographs were recorded on type 2485 film, emulsion number 107-2 and developed along with calibrations performed at the High Altitude Observatory on strips of that same emulsion. These tests, as well as all of the photodigitizations for SL-4, were carried out in March by Jacobs, Kessler, Mercer and Zook. Details are shown in Appendices C and D.

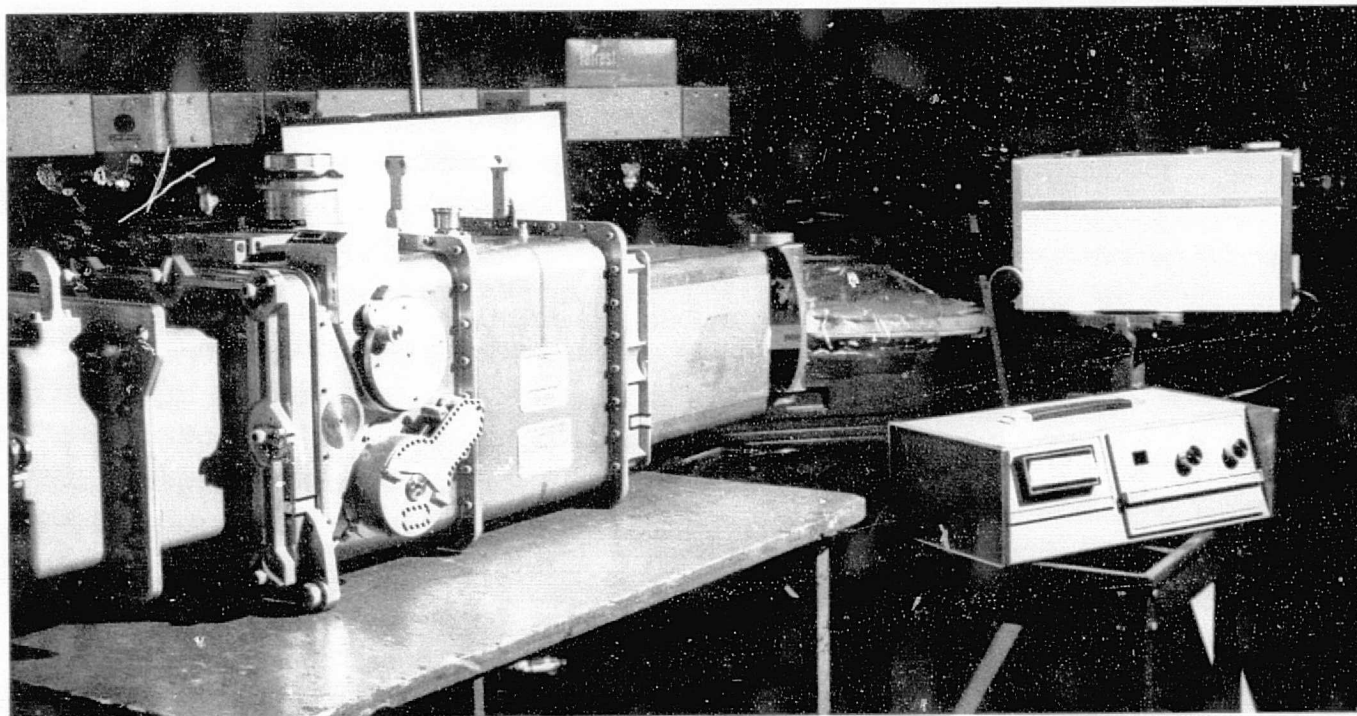
Preliminary Data Analysis

The out-of-focus problem is the weak point in these data. The scientific value of this experiment will depend primarily on the ability of the investigators to overcome its effect in the data processing. This will not be simple, and at present it appears that only the gegenschein data may produce useful results. Even here the out-of-focus problem has caused the star images off axis to assume quite different shapes (see lower left in Figure 3). Sophisticated fourier integral transform techniques would be required to completely remedy such problems, but only simple versions are now available and checked out as VICAR processors. Simpler ideas may work, but it is still too early to promise such results.

EXPERIMENT S073 VIGNETTING TEST ARRANGEMENT WITH S019 AMS AND T025 EQUIPMENT

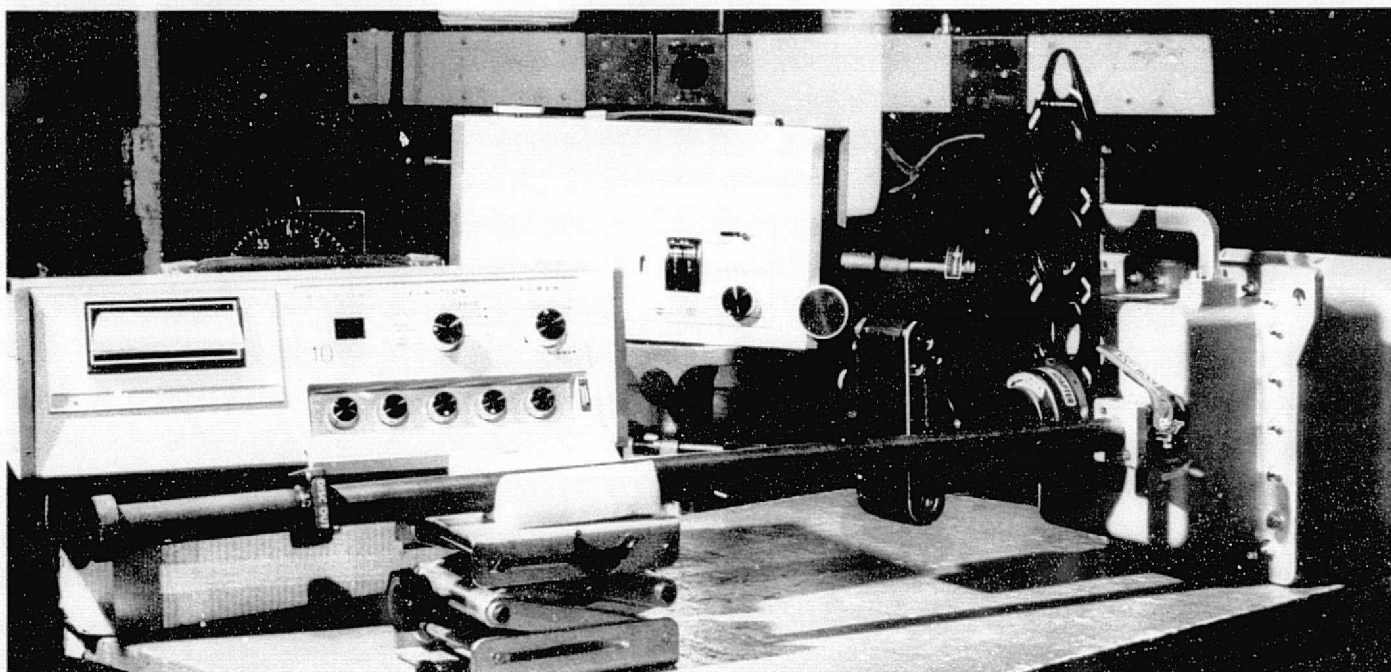


Flight-like training equipment is assembled and arranged to photograph a diffusely reflecting, white screen providing constant illumination across the field-of-view. Equipment includes S019 Articulated Mirror System, T025 cannister and Nikon camera at far end. Pritchard Photometer in foreground used to measure light from screen.



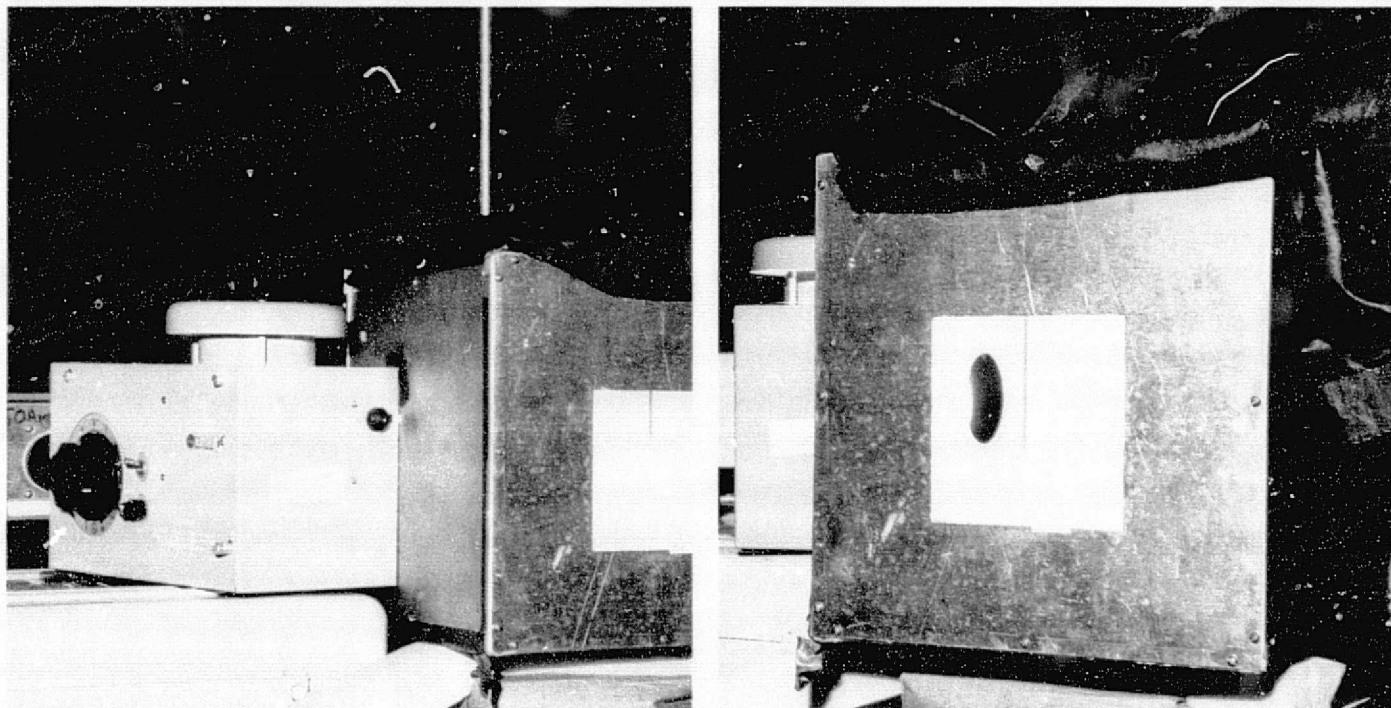
Second view of vignetting test arrangement showing more of T025 cannister at far left. Tests were performed in a light tunnel at NASA Goddard Space Flight Center with light source 156 feet from screen producing an illumination level of 2.9×10^{-4} foot-lamberts for exposures from 15 to 480 seconds. (GSFC Photographs G-74-05544 and G-74-05545)

EXPERIMENT S073 VIGNETTING TEST ARRANGEMENT WITH T025 EQUIPMENT



Nikon 35mm Camera with UV, f/2.0 lens attached to quartz window port at rear of T025 cannister to obtain photographs for assessing system vignetting. Diffusely reflecting screen providing constant illumination over the test field is out of view to the right. Pritchard Photometer used to measure field illumination. (GSFC Photograph G-74-05542)

LIGHT SOURCE USED TO ILLUMINATE VIGNETTING TEST SCREEN

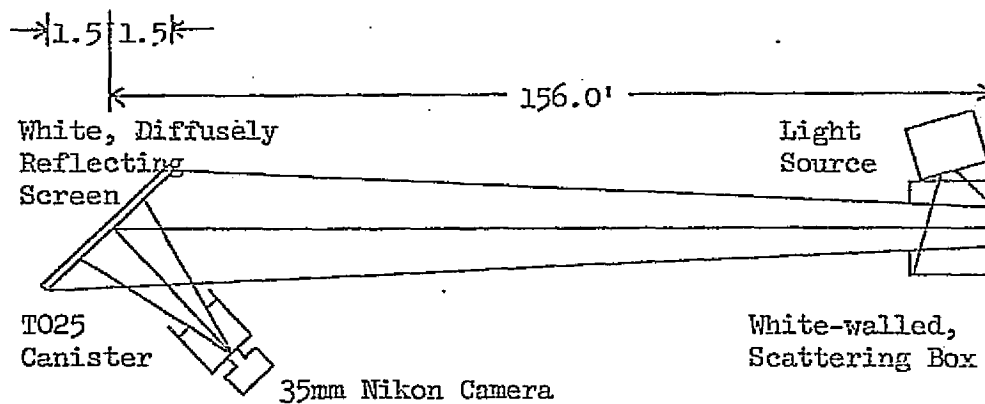


Views from left and right of light source for illuminating vignetting test screen a distance of 156 feet away. Light from Cary lamp illuminated white painted inner surface of metal box from side. Illumination source was diffuse reflection from back wall through aperture of about 3 inches square. (GSFC Photographs G-74-005543 and G-74-05541)

VIGNETTING TEST SCREEN MEASUREMENTS

2.77 2.84	2.77 2.86	2.81 2.88	2.85 2.93	2.90 3.00
2.77 2.83	2.82 2.88	2.84 2.93	2.89 2.96	2.93 3.00
2.80 2.87	2.82 2.88	2.85 2.92	2.89 2.96	2.94 3.00
2.81 2.86	2.83 2.88	2.86 2.91	2.90 2.96	2.96 3.00
2.81 2.83	2.82 2.84	2.85 2.88	2.89 2.90	2.94 2.94

Front view diagram of vignetting test screen showing array of reflectance readings using Pritchard Photometer. All readings are in 10^{-4} foot-lamberts. Each sector was read once beginning at upper left, always moving left to right, progressing to next lower row and finishing at lower right; this procedure was repeated to produce second set of readings. Screen had very weak specular characteristics which produced brightening towards right side near center as angle of reflectance approached angle of incidence from source.



Top view diagram showing arrangement of illuminating source, diffusely reflecting screen and TO25 training equipment in test position for the collection of vignetting data. Area of screen used provided white light field uniform to approximately $\pm 2\%$.

Figure 8

Preliminary Data Analysis, cont'd

It appears that the low transmission characteristics of the UV lens combined with its slower speed lost more of the available light than could be made up by the extended spectral range. Sunlight scattered from particles, which is the source of the phenomena studied in this investigation, has a fast dropoff in the UV anyway. The UV lens contains many quartz elements, a material which will pass UV light. Unfortunately, the lens designer is limited in the range of refractive indices available for this glass; thus, it is not possible to deviate the light to a short focus within a few lens elements. Remarkable as the $f/2.0$ value is for such a small lens, the price paid in terms of thickness of glass appears to be too much for this subject matter. One can state that future studies in the UV of these phenomena should probably employ reflecting optics, at least to achieve the low f -number.

Following his review of working prints for photographs of galaxies, H.C. Arp wrote, in part: "It is particularly tantalizing and frustrating to inspect them because they are almost usable. The longer exposures show the sky well and begin to hint at the large dimensions of the nebulae (at least in the case of M31). They would have been spectacular and important pictures if only the camera had been a little more in focus." The photograph he specifically refers to is shown at the lower right in Figure 3.

Finally, the ability of the type 2485 emulsion to provide a low threshold of detectability, even in the presence of high radiation background, is well demonstrated by the data presented in Appendix E. The ground backup to the flight calibration film shows a base plus fog level density of 0.155 while that for the flight calibration film, BV45, is 1.295. If a horizontal line were drawn on the ground film at the 1.295 density level, then it would appear that no usable signal could be detected below a log exposure value of about 1.4. However, the "toe" of the H&D curve can be seen to form well to the left of this log exposure value on BV45. In fact, usable data is detectable at a log exposure value of 0.9 or less, and this value holds for other SL-4 cassettes shown in Appendix E. For BV15, the only SL-3 cassette measured, with a base plus fog density of 1.075, data is indicated at 0.7 log exposure, which is quite good even when compared to the non-flight emulsion. Some investigators argue that the signal-to-noise is greatly reduced, even if the toe of the H&D curve does not shift appreciably to the right. That depends, of course, on a good definition of noise. One could say that the change in density from 0.155 to 1.295 is almost an order of magnitude increase in noise, but this would be an improper interpretation. Most of that change is constant greying of the background over the entire film, and this DC component can be subtracted with no effect on either noise or data. The true noise is the RMS variation on top of this background. Signal levels become unrecognizable only when they fall close to this amplitude. Hence, the true change in signal-to-noise is the signal level above average background divided by grain noise amplitude. While this ratio was decreased by the radiation, the result was by no means as catastrophic as

Preliminary Data Analysis, cont'd

some had predicted.

Data processing and analysis will continue with emphasis now shifting strongly to the VICAR computer runs. In addition to the SL-4 data, four frames of BV15 on SL-3 have also been digitized. The scenes are in good focus and should produce some very useful information on gegenschein. However, no equivalent calibrations were carried on-board for comparisons to photography of an absolute light source. This will diminish the accuracy of the absolute brightness measurements, although the SL-4 calibrations will be of some help in setting levels. However, the relative brightness falloff, showing the shape and extent of the phenomenon, should be excellent.

Film Type EK 2485-112-1Film Size 35mm

Quick Look Fr No	NASA Frame No.	Subject	Time of Exposure		Exp. Time (sec)	Cntr Frm Loc		Top Frm Loc		Remarks
			Date	GMT		Rt Asc	Dec	Rt Asc	Dec	
1		OWS Interior Half Frame								
2	5410	OWS Interior Half Frame								
3	5411	S073 Contamination	1 Jan 74	1659	10	12 ^h 57 ^m	+28.0			UV Lens, f/2.0
4	5412	S073 Contamination	1 Jan 74	1700	120	12 ^h 57 ^m	+28.0			UV Lens, f/2.0
5	5413	S073 Coma Cluster	1 Jan 74	1704	360	12 ^h 57 ^m	+28.0			UV Lens, f/2.0
6	5414	S073 NGC 4472	1 Jan 74	1713	480	12 ^h 28 ^m	+10.0			UV Lens, f/2.0
7	5415	S073 Coma Cluster	1 Jan 74	2151	360	(12 ^h 50 ^m	+27.0	12 ^h 50 ^m	+30.0	Vis Lens, f/1.2
8	5416	S073 NGC 4472	1 Jan 74	2158	480	(12 ^h 25 ^m	+10.5	12 ^h 25 ^m	+15.0	Vis Lens, f/1.2
9	5417	S063 With Airglow	2 Jan 74							
10	5418	S063 With Glare	2 Jan 74							
11	5419	S063 With Airglow & Obstr.	2 Jan 74							
12	5420	S063 With Airglow & Obstr.	2 Jan 74							
13	5421	S063 With Airglow & Obstr.	2 Jan 74							
14	5422	S063 With Airglow & Glare	2 Jan 74							
15	5423	S063 With Airglow	2 Jan 74							
16	5424	S063	2 Jan 74							
17	5425	S063 With Airglow	2 Jan 74							
18	5426	S063 With Clouds	3 Jan 74							
19	5427	S063	3 Jan 74							
20	5428	S063 With Clouds	3 Jan 74							
21	5429	S063 With Clouds	3 Jan 74							
22	5430	S063 With Clouds	3 Jan 74							
23	5431	S063 With Clouds	3 Jan 74							
24	5432	S063	3 Jan 74							
25	5433	S063	3 Jan 74							

NASA Magazine No SL4-161Magazine Flight Designator BV26Film Type EK 2485-112-1Film Size 35mm

Quick Look Fr No	NASA Frame No.	Subject	Time of Exposure		Exp. Time (sec)	Cntr Frm Loc		TOP Frm Loc		Remarks
			Date	GMT		Rt Asc	Dec	Rt Asc	Dec	
26	5434	S063	3 Jan 74							
27	5435	S063 With Clouds	3 Jan 74							
28	5436	S063 With Clouds	3 Jan 74							
29	5437	S063 With Clouds	3 Jan 74							
30	5438	S063 With Clouds	3 Jan 74							
31	5439	S063 With Clouds	3 Jan 74							
32	5440	S063 With Clouds	3 Jan 74							
33	5441	S063 With Clouds	3 Jan 74							
34	5442	S063 With Clouds	3 Jan 74							
35	5443	S063 With Clouds	3 Jan 74							
36	5444	S063 With Clouds	3 Jan 74							
37	5445	S063 With Clouds	3 Jan 74							
38	5446	S063 With Clouds	3 Jan 74							
39	5447	S063 With Clouds	3 Jan 74							
40	5448	S063 With Clouds	3 Jan 74							
41	5449	S063 With Clouds	3 Jan 74							
42	5450	S063 With Clouds	3 Jan 74							
43	5451	S063 With Clouds	3 Jan 74							
44	5452	S063 With Clouds	3 Jan 74							
45	5453	S063 With Clouds	3 Jan 74							

Film Type EK 2485-112-1Film Size 35mm

Quick Look Fr No	NASA Frame No.	Subject	Time of Exposure		Exp. Time (sec)	Cntr Frm Loc		Top Frm Loc		Remarks
			Date	GMT		Rt Asc	Dec	Rt Asc	Dec	
1		Unused Frame								
2		Unused Frame								
3		Unused Frame								
4		Unused Frame								
5		Unused Frame								
6		Unused Frame								
7		Unused Frame								
8	5454	Unused Frame								
9	5455	Unused Frame								
10	5456	Unused Frame								
11	5457	Unused Frame								
12	5458	Unused Frame								
13	5459	S073 Contamination	19 Jan 74	2209	10	13 ^h 50 ^m	-10.0			UV Lens, f/2.0
14	5460	S073 Contamination	19 Jan 74	2210	120	13 ^h 50 ^m	-10.0			UV Lens, f/2.0, Spica
15	5461	S073 Zodiacal Light	19 Jan 74	2213	360	13 ^h 50 ^m	-10.0			UV Lens, f/2.0, Spica
16	5462	S073 South Ecliptic Pole	19 Jan 74	2221	360	6 ^h 00 ^m	-66.5			UV Lens, f/2.0
17	5463	S073 Contamination	20 Jan 74	0115	10	13 ^h 10 ^m	-14.5			UV Lens, f/2.0
18	5464	S073 Contamination	20 Jan 74	0116	120	13 ^h 10 ^m	-14.5			UV Lens, f/2.0
19	5465	S073 Libration Region L ₅	20 Jan 74	0119	120	13 ^h 10 ^m	-14.5			UV Lens, f/2.0
20	5466	S073 Libration Region L ₅	20 Jan 74	0121	480	13 ^h 10 ^m	-14.5			UV Lens, f/2.0
21	5467	S073 Libration Region L ₅	20 Jan 74	0129	360	13 ^h 10 ^m	-14.5			UV Lens, f/2.0
22	5468	S073 Contamination	20 Jan 74	0137	120	13 ^h 10 ^m	-14.5			UV Lens, f/2.0
23	5469	S073 Contamination	20 Jan 74	0139	10	13 ^h 10 ^m	-14.5			UV Lens, f/2.0 -
24	5470	S073 Contamination	20 Jan 74	1343	10	8 ^h 10 ^m	+20.5	7 ^h 20 ^m	+19.0	Vis Lens, f/1.2
25	5471	S073 Gegendeschein	20 Jan 74	1344	360	8 ^h 10 ^m	+20.5	7 ^h 20 ^m	+19.0	Vis Lens, f/1.2, Pollux

Film Type EK 2485-112-1Film Size 35mm

Quick Look Fr No	NASA Frame No.	Subject	Time of Exposure		Exp. Time (sec)	Cntr Frm Loc		Top Frm Loc		Remarks
			Date	GMT		Rt Asc	Dec	Rt Asc	Dec	
26	5472	S073 Gegenschein	20 Jan 74	1350	480	8 ^h 10 ^m	+20.5	7 ^h 20 ^m	+19.0	Vis Lens, f/1.2, Pollux
27	5473	S073 Gegenschein	20 Jan 74	1359	240	8 ^h 10 ^m	+20.5	7 ^h 20 ^m	+19.0	Vis Lens, f/1.2, Pollux
28	5474	S073 Contamination	20 Jan 74	1403	240	8 ^h 10 ^m	+20.5	7 ^h 20 ^m	+19.0	Vis Lens, f/1.2, Pollux
29	5475	Film Cassette Removal								
30	5476	S073 Contamination	22 Jan 74	0124	10	8 ^h 10 ^m	+22.0	7 ^h 40 ^m	+10.0	Vis Lens, f/1.2, Pollux
31	5477	S073 Contamination	22 Jan 74	0125	120	8 ^h 10 ^m	+22.0	7 ^h 40 ^m	+10.0	Vis Lens, f/1.2, Pollux
32	5478	S073 Gegenschein	22 Jan 74	0128	120	8 ^h 10 ^m	+22.0	7 ^h 40 ^m	+10.0	Vis Lens, f/1.2, Pollux
33	5479	S073 Gegenschein	22 Jan 74	0130	360	8 ^h 10 ^m	+22.0	7 ^h 40 ^m	+10.0	Vis Lens, f/1.2, Pollux
34	5480	S073 Gegenschein	22 Jan 74	0137	480	8 ^h 10 ^m	+22.0	7 ^h 40 ^m	+10.0	Vis Lens, f/1.2, Pollux
35	5481	S073 Gegenschein	22 Jan 74	0145	360	8 ^h 10 ^m	+22.0	7 ^h 40 ^m	+10.0	Vis Lens, f/1.2, Pollux
36	5482	S073 Contamination	22 Jan 74	1522	10	7 ^h 50 ^m	+20.0	7 ^h 10 ^m	+20.0	UV Lens, f/2.0
37	5483	S073 Contamination	22 Jan 74	1523	120	7 ^h 50 ^m	+20.0	7 ^h 10 ^m	+20.0	UV Lens, f/2.0
38	5484	S073 Gegenschein	22 Jan 74	1527	120	8 ^h 00 ^m	+20.0	7 ^h 20 ^m	+20.0	UV Lens, f/2.0
39	5485	S073 Gegenschein	22 Jan 74	1529	840	8 ^h 00 ^m	+20.0	7 ^h 20 ^m	+20.0	UV Lens, f/2.0
40	5486	S073 Gegenschein	22 Jan 74	1544	480	8 ^h 00 ^m	+20.0	7 ^h 20 ^m	+20.0	UV Lens, f/2.0
41		S073 Contamination	22 Jan 74	1552	10	8 ^h 00 ^m	+20.0	7 ^h 20 ^m	+20.0	UV Lens, f/2.0

NASA Magazine No SL4-163Magazine Flight Designator BV40Film Type EK 2485-112-1Film Size 35mm

Quick Look Fr No	NASA Frame No.	Subject	Time of Exposure		Exp. Time (sec)	Cntr Frm Loc		Top Frm Loc		Remarks
			Date	GMT		Rt Asc	Dec	Rt Asc	Dec	
1	5487	S073 Libration Region L ₄	28 Jan 74	1248	480	3 ^h 55 ^m	+23.5	4 ^h 20 ^m	+23.0	Vis Lens, f/1.2, Pleides
2	5488	S073 Libration Region L ₄	28 Jan 74	1257	360	4 ^h 05 ^m	+23.0	4 ^h 20 ^m	+22.0	Vis Lens, f/1.2, Pleides
3	5489	S073 Libration Region L ₄	28 Jan 74	1304	420	4 ^h 05 ^m	+26.0	4 ^h 20 ^m	+23.5	Vis Lens, f/1.2, Pleides
4	5490	S073 NGC 5128	28 Jan 74	1313	480	13 ^h 20 ^m	-40.0	13 ^h 20 ^m	-43.5	Vis Lens, f/1.2
5	5491	Unused Frame								
6	5492	Unused Frame								
7	5493	Unused Frame								
8	5494	Unused Frame								
9	5495	Unused Frame								
10	5496	Unused Frame								
11	5497	Unused Frame								
12	5498	Interior								
13	5499	Interior								
14	5500	Unknown Subject Matter								
15	5501	Unknown Subject Matter								
16	5502	Unknown Subject Matter								
17	5503	Unknown Subject Matter								
18	5504	Unknown Subject Matter								
19	5505	Unknown Subject Matter								
20	5506	Unknown Subject Matter								
21	5507	Unknown Subject Matter								
22	5508	Unknown Subject Matter								
23	5509	Unknown Subject Matter								
24	5510	Film Cassette Removal								
25	5511									
26	5512									

NASA Magazine No SL4-164Magazine Flight Designator BV43Film Type EK 2485-112-1Film Size 35mm

Quick Look Fr No	NASA Frame No.	Subject	Time of Exposure		Exp. Time (sec)	Cntr Frm Loc		Top Frm Loc		Remarks
			Date	GMT		Rt Asc	Dec	Rt Asc	Dec	
1	5513	S063 Cloud Cover								
2	5514	S063 Cloud Cover								
3		Unused Frame								
4		Unused Frame								
5		Unused Frame								
6		Unused Frame								
7		Unused Frame								
8		Unused Frame								
9		Unused Frame								
10		Unused Frame								
11		Unused Frame								
12		Unused Frame								
13		Unused Frame								
14		Unused Frame								
15		Unused Frame								
16		Unused Frame								
17		Unused Frame								
18		Unused Frame								
19		Unused Frame								
20		Unused Frame								
21		Unused Frame								
22		Unused Frame								
23		Unused Frame								
24		Unused Frame								
25		Unused Frame								

NASA Magazine No SL4-164Magazine Flight Designator BV43Film Type EK 2485-112-1Film Size 35mm

Quick Look Fr No	NASA Frame No.	Subject	Time of Exposure		Exp. Time (sec)	Cntr Frm Loc		Top Frm Loc		Remarks
			Date	GMT		Rt Asc	Dec	Rt Asc	Dec	
26		Unused Frame								
27		Unused Frame								
28		Unused Frame								
29		Unused Frame								
30		Unused Frame								
31	5515	S073 Contamination	22 Dec 73	0209	10	00 ^h 40 ^m	+40.0			Vis Lens, f/1.2
32	5516	S073 Contamination	22 Dec 73	0210	120	00 ^h 40 ^m	+40.0			Vis Lens, f/1.2
33	5517	Blank	22 Dec 73							Vis Lens, f/1.2
34	5513	S073 NGC 224	22 Dec 73	0213	300	00 ^h 40 ^m	+40.0	00 ^h 45 ^m	+44.0	Vis Lens, f/1.2
35	5519	S073 NGC 224	22 Dec 73	0218	480	00 ^h 40 ^m	+40.0	00 ^h 45 ^m	+44.0	Vis Lens, f/1.2
36	5520	S073 Comet Tail	22 Dec 73	0227	360	10 ^h 45 ^m	- 7.3			Vis Lens, f/1.2
37	5521	S073 Libration Region L5	22 Dec 73	0234	360	12 ^h 03 ^m	- 5.0			Vis Lens, f/1.2
38	5522	S073 Zodiacal Light	22 Dec 73	0241	300					Vis Lens, f/1.2
39	5523	S073 Contamination	22 Dec 73	0247	120					Vis Lens, f/1.2
40	5524	S073 Contamination	22 Dec 73	0249	10					Vis Lens, f/1.2
41	5525	Unused Frame								
42	5526	Unused Frame								
43	5527	Unused Frame								
44	5528	Unused Frame								
45	5529	Unused Frame								
46	5530	Unused Frame								
47	5531	S063 with Airglow								
48		Unused Frame								
49		Unused Frame								
50		Unused Frame								

NASA Magazine No SL4-165Magazine Flight Designator BV44Film Type EK 2485-112-1Film Size 35mm

Quick Look Fr No	NASA Frame No.	Subject	Time of Exposure		Exp. Time (sec)	Cntr Frm Loc		Top Frm Loc		Remarks
			Date	GMT		Rt Asc	Dec	Rt Asc	Dec	
1	5532	S063 Cloud Cover	10 Dec 73							
2	5533	Unused Frame	10 Dec 73							
3	5534	Extra Data Frame	10 Dec 73							
4	5535	Extra Data Frame	10 Dec 73							
5	5536	S073 Contamination	10 Dec 73	0102	5	00 ^h 57 ^m	+41.5			Vis Lens, f/1.2
6	5537	S073 Contamination	10 Dec 73	0103	120	00 ^h 57 ^m	+41.5			Vis Lens, f/1.2
7	5538	S073 Libration Region L5	10 Dec 73	0106	360	00 ^h 57 ^m	+41.5			Vis Lens, f/1.2
8	5539	Blank	10 Dec 73							Vis Lens, f/1.2
9	5540	S073 Libration Region L4	10 Dec 73	0113	360	(9 ^h 05 ^m	+11.5	9 ^h 15 ^m	+15.5)	Vis Lens, f/1.2
10	5541	S073 Comet Tail	10 Dec 73	0121	360	10 ^h 45 ^m	- 7.0			Vis Lens, f/1.2
11	5542	S073 Comet Tail	10 Dec 73	0127	540	10 ^h 45 ^m	- 7.0			Vis Lens, f/1.2
12	5543	S073 Comet Tail	10 Dec 73	0137	120	10 ^h 45 ^m	- 7.0			Vis Lens, f/1.2
13	5544	S073 Contamination	10 Dec 73	0140	117	10 ^h 45 ^m	- 7:0			Vis Lens, f/1.2
14	5545	S073 Contamination	10 Dec 73	0142	10	10 ^h 45 ^m	- 7.0			Vis Lens, f/1.2
15	5546	Possible Unused Film								
16	5547	Possible Unused Film								
17	5548	Possible Unused Film								
18	5549	Possible Unused Film								
19	5550	Possible Unused Film								
20	5551	Possible Unused Film								
21	5552	Possible Unused Film								
22	5553	Possible Unused Film								
23	5554	Possible Unused Film								
24	5555	Possible Unused Film								
25	5556	Possible Unused Film								

NASA Magazine No SI4-165Magazine Flight Designator BV44Film Type EK 2485-112-1Film Size 35mm

Quick Look Fr No	NASA Frame No.	Subject	Time of Exposure		Exp. Time (sec)	Cntr Frm Loc		Top Frm Loc		Remarks
			Date	GMT		Rt Asc	Dec	Rt Asc	Dec	
26	5557	Possible Unused Frame								
27	5558	S063								
28	5559	Possible Unused Frame								
29	5560	Possible Unused Frame								
30	5561	S063								
31	5562	Possible Unused Frame								
32	5563	Possible Unused Frame								
33	5564	Possible Unused Frame								
34	5565	Possible Unused Frame								
35	5566	Possible Unused Frame								
36	5567	Possible Unused Frame								
37	5568	S063 Cloud Cover								
38	5569	S063 Cloud Cover								
39	5570	S063 Cloud Cover								
40	5571	Possible Unused Frame								
41	5572	Possible Unused Frame								
42	5573	S063								
43	5574	Unused Frame								

Film Type EK 2485-112-1Film Size 35mm

Quick Look Fr No	NASA Frame No.	Subject	Time of Exposure		Exp. Time (sec)	Cntr Frm Loc		Top Frm Loc		Remarks
			Date	GMT		Rt Asc	Dec	Rt Asc	Dec	
1	5575	Protect Frame								
2	5576	S073 Contamination	27 Dec 73	1855	10	0 ^h 29 ^m	+ 7.7			UV Lens, f/2.0
3	5577	S073 Contamination	27 Dec 73	1856	120	0 ^h 29 ^m	+ 7.7			UV Lens, f/2.0
4	5578	S073 Libration Region L4	27 Dec 73	1859	360	0 ^h 29 ^m	+ 7.7			UV Lens, f/2.0
5	5579	S073 NGC 224	27 Dec 73	1906	480	0 ^h 40 ^m	+41.0	0 ^h 35 ^m	+45.5	UV Lens, f/2.0
6	5580	S073 NGC 224	27 Dec 73	1914	360	0 ^h 40 ^m	+41.0	0 ^h 35 ^m	+45.5	UV Lens, f/2.0
7	5581	S073 Zodiacal Light	27 Dec 73	1921	360	12 ^h 25 ^m	- 0.5	12 ^h 35 ^m	+ 3.5	UV Lens, f/2.0
8	5582	S073 Zodiacal Light	27 Dec 73	1928	300	12 ^h 25 ^m	+ 3.0	12 ^h 35 ^m	+ 7.0	UV Lens, f/2.0
9	5583	S073 Contamination	27 Dec 73	2334	10	0 ^h 38 ^m	+ 8.6			Vis Lens, f/2.0
10	5584	S073 Contamination	27 Dec 73	2334	120	0 ^h 38 ^m	+ 8.6			Vis Lens, f/2.0
11	5585	S073 Libration Region L4	27 Dec 73	2338	360	0 ^h 40 ^m	+ 9.0	0 ^h 40 ^m	+14.0	Vis Lens, f/2.0
12	5586	S073 NGC 224	27 Dec 73	2345	480	0 ^h 40 ^m	+41.0	0 ^h 45 ^m	+46.0	Vis Lens, f/2.0
13	5587	S073 NGC 224	27 Dec 73	2353	360	0 ^h 40 ^m	+41.0	0 ^h 45 ^m	+46.0	Vis Lens, f/2.0
14	5588	S073 Zodiacal Light	28 Dec 73	0000	360	12 ^h 25 ^m	- 1.0	12 ^h 40 ^m	+ 4.0	Vis Lens, f/2.0
15	5589	S073 Zodiacal Light	28 Dec 73	0007	300	12 ^h 30 ^m	+ 3.0	12 ^h 40 ^m	+ 7.0	Vis Lens, f/2.0
16	5590	S073 Contamination	28 Dec 73	0014	120	12 ^h 30 ^m	+ 3.0	12 ^h 40 ^m	+ 7.0	Vis Lens, f/2.0
17	5591	S073 Contamination	28 Dec 73	0016	10	12 ^h 25 ^m	- 0.5			Vis Lens, f/2.0
18	5592	S073 Libration Region L4	28 Dec 73	1355	360	1 ^h 04 ^m	+11.1			Vis Lens, f/1.2
19	5593	S073 NGC 4472	28 Dec 73	1402	480	(12 ^h 45 ^m	+10.0	13 ^h 00 ^m	+ 7.0	Vis Lens, f/1.2
20	5594	S073 NGC 4472	28 Dec 73	1410	120	(12 ^h 45 ^m	+10.0	13 ^h 00 ^m	+ 7.0	Vis Lens, f/1.2
21	5595	S073 Contamination	28 Dec 73	1413	120	12 ^h 45 ^m	+10.0			Vis Lens, f/1.2
22	5596	S073 Contamination	28 Dec 73	1415	10	12 ^h 45 ^m	+10.0			Vis Lens, f/1.2
23		Unused Frame								
24		Unused Frame								
25		Unused Frame								
26		Unused Frame								

Film Type EK 2485-112-1Film Size 35mm

Quick Look Fr No	NASA Frame No.	Subject	Time of Exposure		Exp. Time (sec)	Cntr Frm Loc		Top Frm Loc		Remarks
			Date	GMT		Rt Asc	Dec	Rt Asc	Dec	
0	5597									
1	5598	S073 Contamination	23 Jan 74	1307	10	8h 10 ^m	+20.0	7h 15 ^m	+23.5	Vis Lens, f/1.2
2	5599	S073 Contamination	23 Jan 74	1307	120	8h 10 ^m	+20.0	7h 15 ^m	+23.5	Vis Lens, f/1.2
3	5600	S073 Gegendchein	23 Jan 74	1311	120	8h 10 ^m	+20.0	7h 15 ^m	+23.5	Vis Lens, f/1.2
4	5601	S073 Gegendchein	23 Jan 74	1313	300	8h 10 ^m	+20.0	7h 15 ^m	+23.5	Vis Lens, f/1.2
5	5602	S073 Gegendchein	23 Jan 74	1319	480	8h 10 ^m	+20.0	7h 15 ^m	+23.5	Vis Lens, f/1.2
6	5603	S073 Gegendchein	23 Jan 74	1327	360	8h 10 ^m	+20.0	7h 15 ^m	+23.5	Vis Lens, f/1.2
7	5604	Unused Frame								
8	5605	Unused Frame								
9	5606	Unused Frame								
10	5607	Unused Frame								
11	5608	Unused Frame								
12	5609	Unused Frame								
13	5610	Unused Frame								
14	5611	Unused Frame								
15	5612	Unused Frame								
16	5613	Unused Frame								
17	5614	Unused Frame								
18		Unused Frame								
19	5615	S073 Contamination	23 Jan 74	2053	10	8h 10 ^m	+20.0	8h 00 ^m	+9.5	Vis Lens, f/1.2
20	5616	S073 Contamination	23 Jan 74	2054	120	8h 10 ^m	+20.0	8h 00 ^m	+9.5	Vis Lens, f/1.2
21	5617	S073 Gegendchein	23 Jan 74	2057	300	8h 10 ^m	+20.0	8h 00 ^m	+9.5	Vis Lens, f/1.2
22	5618	S073 Gegendchein	23 Jan 74	2102	420	8h 10 ^m	+20.0	8h 00 ^m	+9.5	Vis Lens, f/1.2
23	5619	S073 Gegendchein	23 Jan 74	2110	540	8h 10 ^m	+20.0	8h 00 ^m	+9.5	Vis Lens, f/1.2
24	5620	S073 Gegendchein	23 Jan 74	2119	300	8h 10 ^m	+20.0	8h 00 ^m	+9.5	Vis Lens, f/1.2
25	5621	S063 Cloud Cover								

NASA Magazine No SL4-167Magazine Flight Designator BV49Film Type EK 2485-112-1Film Size 35mm

Quick Look Fr No	NASA Frame No.	Subject	Time of Exposure		Exp. Time (sec)	Cntr Frm Loc		Top Frm Loc		Remarks
			Date	GMT		Rt Asc	Dec	Rt Asc	Dec	
26	5622	S063 Cloud Cover								
27	5623	S063 Cloud Cover								
28	5624	S063 Cloud Cover								
29	5625	S063 Cloud Cover								
30	5626	S063 Cloud Cover								
31	5627	S063 Cloud Cover								
32	5628	S063 Cloud Cover								
33	5629	S063 Cloud Cover								
34	5630	S063 Cloud Cover								
35	5631	S063 Cloud Cover								
36	5632	S063 Cloud Cover								
37	5633	S063 Cloud Cover								
38	5634	S063 Cloud Cover								
39	5635	S063 Cloud Cover								
40	5636	S063 Cloud Cover								
41	5637	S063 Cloud Cover								
42	5638	S063 Cloud Cover								
43	5639	S063 Cloud Cover								
44	5640	S063 Cloud Cover								
45	5641	S063 Cloud Cover								
46	5642	S063 Cloud Cover								

NASA Magazine No SL4-168Magazine Flight Designator BV42Film Type EK 2485-112-1Film Size 35mm

Quick Look Fr No	NASA Frame No.	Subject	Time of Exposure		Exp. Time (sec)	Cntr Frm Loc		Top Frm Loc		Remarks
			Date	GMT		Rt Asc	Dec	Rt Asc	Dec	
1	5643	Exposed Frame								
2	5644	Exposed Frame								
3	5645	S073 Zodiacal Light	30 Jan 74	1910	480					Vis Lens, f/1.2
4	5646	S073 Zodiacal Light	30 Jan 74	1919	420					Vis Lens, f/1.2
5	5647	S073 Zodiacal Light	30 Jan 74	1927	420					Vis Lens, f/1.2
6	5648	S073 North Ecliptic Pole	30 Jan 74	1936	480	18 ^h 00 ^m	+66.5			Vis Lens, f/1.2
7	5649	S073 NGC 5128	30 Jan 74	2044	480	13 ^h 30 ^m	-38.0			UV Lens, f/2.0
8	5650	S073 Zodiacal Light	30 Jan 74	2054	480					UV Lens, f/2.0
9	5651	S073 Zodiacal Light	30 Jan 74	2103	420					UV Lens, f/2.0
10	5652	S073 Zodiacal Light	30 Jan 74	2111	420					UV Lens, f/2.0
11	5653	Unused Frame								
12	5654	Unused Frame								
13	5655	Unused Frame								
14	5656	Unused Frame								
15	5657	Unused Frame								
16	5658	Unused Frame								
17	5659	Unused Frame								
18	5660	Unused Frame								
19	5661	Unused Frame								
20	5662	Unused Frame								
21	5663	Unused Frame								
22	5664	Unused Frame								
23	5665	Unused Frame								
24	5666	Unused Frame								
25	5667	Unused Frame								

FLIGHT DATA CALIBRATION PHOTOGRAPHY

Film Type EK 2485-112-1Calibration Unit HAO Sensitometer Box No. 1Film Size 35 mmCalibrated By R. D. Mercer (Boulder, Colo.)

Quick Look Fr No	Date of Photography	Exposure Time (Sec)	Neutral Density Filt No	Calibration Unit Bulb Manufacturer	Frame Digitization		Remarks
					Date	Mag Tape	
1	12 Feb 74	420	3.0	Sylvania	19 Mar 74	D-721	
2	12 Feb 74	480	3.0	Sylvania	19 Mar 74	D-721	
3	12 Feb 74	540	3.0	Sylvania	19 Mar 74	D-721	
4	12 Feb 74	600	3.0	Sylvania			
5	12 Feb 74	840	3.0	Sylvania			
6	12 Feb 74	720	3.0	Sylvania			
7	12 Feb 74	540	4.0	Sylvania	19 Mar 74	D-721	
8	12 Feb 74	600	4.0	Sylvania			
9	12 Feb 74	720	4.0	Sylvania			
10	12 Feb 74	840	4.0	Sylvania			
11							
12							
13							
14							
15	23 Oct 74	540	3.0	General Electric	19 Mar 74	D-721	
16	23 Oct 74	480	3.0	General Electric	19 Mar 74	D-721	
17	23 Oct 74	420	3.0	General Electric	19 Mar 74	D-721	
18	23 Oct 74	360	3.0	General Electric	19 Mar 74	D-721	
19	23 Oct 74	330	3.0	General Electric			
20	23 Oct 74	300	3.0	General Electric	19 Mar 74	D-721	
21	23 Oct 74	270	3.0	General Electric			
22	23 Oct 74	240	3.0	General Electric	19 Mar 74	D-721	
23	23 Oct 74	60	2.0	General Electric			
24	23 Oct 74	90	2.0	General Electric			
25	23 Oct 74	120	2.0	General Electric	19 Mar 74	D-721	
26	23 Oct 74	150	2.0	General Electric			
27	23 Oct 74	180	2.0	General Electric			
28	23 Oct 74	210	2.0	General Electric			
29	23 Oct 74	240	2.0	General Electric	19 Mar 74	D-721	
30	23 Oct 74	270	2.0	General Electric			
31	23 Oct 74	90	1.0	General Electric			
32	23 Oct 74	60	1.0	General Electric			
33	23 Oct 74	45	1.0	General Electric			
34	23 Oct 74	30	1.0	General Electric			
35	23 Oct 74	20	1.0	General Electric			
36	23 Oct 74	10	1.0	General Electric			
37	23 Oct 74	6	1.0	General Electric			
38	23 Oct 74	4	1.0	General Electric			
39	23 Oct 74	1/8	None	General Electric			
40	23 Oct 74	1/4	None	General Electric			
41	23 Oct 74	1/2	None	General Electric			
42	23 Oct 74	1	None	General Electric			
43	23 Oct 74	2	None	General Electric			
44	23 Oct 74	4	None	General Electric			
45	23 Oct 74	6	None	General Electric			
46	23 Oct 74	10	None	General Electric			

VIGNETTING DATA IDENTIFICATION LIST

Film Type EK 2485-107-2Test Location NASA GSFC, Bldg. 6 Light TunnelFilm Size 35mmPerformed By Jacobs, Kessler, Mercer & Zook

Quick Look Fr No	Date of Photography	Exposure Time (Sec)	Photographic Equipment Information				Frame Digitization	
			Auxiliary Equip	Lens Type	Aperture	Focus	Date	Mag Tape
A-01								
A-02								
A-03	26 Mar 74	15	T025	Visual	f/1.2	Inf		
A-04	26 Mar 74	30	T025	Visual	f/1.2	Inf	28 Mar 74	D-724
A-05	26 Mar 74	60	T025	Visual	f/1.2	Inf	28 Mar 74	D-724
A-06	26 Mar 74	120	T025	Visual	f/1.2	Inf	28 Mar 74	D-724
A-07	26 Mar 74	240	T025	Visual	f/1.2	Inf	28 Mar 74	D-724
A-08								
A-09								
A-10								
A-11								
A-12								
A-13	26 Mar 74	15	T025 + S019 AMS	Visual	f/1.2	Inf		
A-14	26 Mar 74	30	T025 + S019 AMS	Visual	f/1.2	Inf	28 Mar 74	D-724
A-15	26 Mar 74	60	T025 + S019 AMS	Visual	f/1.2	Inf	28 Mar 74	D-724
A-16	26 Mar 74	120	T025 + S019 AMS	Visual	f/1.2	Inf	28 Mar 74	D-724
A-17	26 Mar 74	240	T025 + S019 AMS	Visual	f/1.2	Inf	28 Mar 74	D-724
A-18								
A-19	26 Mar 74	15	T025 + S019 AMS	Visual	f/1.2	10'		
A-20	26 Mar 74	30	T025 + S019 AMS	Visual	f/1.2	10'	28 Mar 74	D-724
A-21	26 Mar 74	60	T025 + S019 AMS	Visual	f/1.2	10'	28 Mar 74	D-724
A-22	26 Mar 74	120	T025 + S019 AMS	Visual	f/1.2	10'	28 Mar 74	D-724
A-23	26 Mar 74	240	T025 + S019 AMS	Visual	f/1.2	10'	28 Mar 74	D-724
A-24								
A-25	26 Mar 74	15	T025 + S019 AMS	Visual	f/1.2	7'		
A-26	26 Mar 74	30	T025 + S019 AMS	Visual	f/1.2	7'	28 Mar 74	D-724
A-27	26 Mar 74	60	T025 + S019 AMS	Visual	f/1.2	7'	28 Mar 74	D-724
A-28	26 Mar 74	120	T025 + S019 AMS	Visual	f/1.2	7'	28 Mar 74	D-724
A-29	26 Mar 74	240	T025 + S019 AMS	Visual	f/1.2	7'	28 Mar 74	D-724
A-30								
A-31	26 Mar 74	15	T025 + S019 AMS	Visual	f/1.2	5'		
A-32	26 Mar 74	30	T025 + S019 AMS	Visual	f/1.2	5'	28 Mar 74	D-724
A-33	26 Mar 74	60	T025 + S019 AMS	Visual	f/1.2	5'	28 Mar 74	D-724

VIGNETTING DATA IDENTIFICATION LIST

Film Type EK 2485-107-2Test Location NASA GSFC, Bldg. 6 Light TunnelFilm Size 35mmPerformed By Jacobs, Kessler, Mercer & Zook

Quick Look Fr No	Date of Photography	Exposure Time (Sec)	Photographic Equipment Information				Frame Digitization	
			Auxiliary Equip	Lens Type	Aperture	Focus	Date	Mag Tape
B-00	27 Mar 74	15	T025 + S019 AMS	Visual	f/1.2	5'		
B-01	27 Mar 74	30	T025 + S019 AMS	Visual	f/1.2	5'	28 Mar 74	D-724
B-02	27 Mar 74	60	T025 + S019 AMS	Visual	f/1.2	5'	28 Mar 74	D-724
B-03	27 Mar 74	120	T025 + S019 AMS	Visual	f/1.2	5'	28 Mar 74	D-724
B-04	27 Mar 74	240	T025 + S019 AMS	Visual	f/1.2	5'	28 Mar 74	D-724
B-05								
B-06	27 Mar 74	15	T025 + S019 AMS	Visual	f/1.2	4'		
B-07	27 Mar 74	30	T025 + S019 AMS	Visual	f/1.2	4'	29 Mar 74	D-724
B-08	27 Mar 74	60	T025 + S019 AMS	Visual	f/1.2	4'	29 Mar 74	D-724
B-09	27 Mar 74	120	T025 + S019 AMS	Visual	f/1.2	4'	29 Mar 74	D-724
B-10	27 Mar 74	240	T025 + S019 AMS	Visual	f/1.2	4'	29 Mar 74	D-724
B-11								
B-12								
B-13	27 Mar 74	15	T025 + S019 AMS	Ultraviolet	f/2.0	Inf		
B-14	27 Mar 74	30	T025 + S019 AMS	Ultraviolet	f/2.0	Inf		
B-15	27 Mar 74	60	T025 + S019 AMS	Ultraviolet	f/2.0	Inf	29 Mar 74	D-724
B-16	27 Mar 74	120	T025 + S019 AMS	Ultraviolet	f/2.0	Inf	29 Mar 74	D-724
B-17	27 Mar 74	240	T025 + S019 AMS	Ultraviolet	f/2.0	Inf	29 Mar 74	D-724
B-18	27 Mar 74	480	T025 + S019 AMS	Ultraviolet	f/2.0	Inf	29 Mar 74	D-724
B-19								
B-20		15	T025	Ultraviolet	f/2.0	Inf		
B-21		30	T025	Ultraviolet	f/2.0	Inf		
B-22		60	T025	Ultraviolet	f/2.0	Inf		
B-23	27 Mar 74	120	T025	Ultraviolet	f/2.0	Inf	29 Mar 74	D-724
B-24	27 Mar 74	240	T025	Ultraviolet	f/2.0	Inf	29 Mar 74	D-724
B-25								
B-26	27 Mar 74	480	T025	Ultraviolet	f/2.0	Inf	29 Mar 74	D-724
B-27								
B-28								
B-29	27 Mar 74	15	T025	Visual	f/1.2	5'		
B-30	27 Mar 74	30	T025	Visual	f/1.2	5'	29 Mar 74	D-724
B-31	27 Mar 74	60	T025	Visual	f/1.2	5'	29 Mar 74	D-724
B-32	27 Mar 74	120	T025	Visual	f/1.2	5'	29 Mar 74	D-724
B-33	27 Mar 74	240	T025	Visual	f/1.2	5'	29 Mar 74	D-724
B-34								
B-35	27 Mar 74	240	T025	Visual	f/1.2	4'	29 Mar 74	D-724
B-36	27 Mar 74	240	T025	Visual	f/1.2	7'	29 Mar 74	D-724

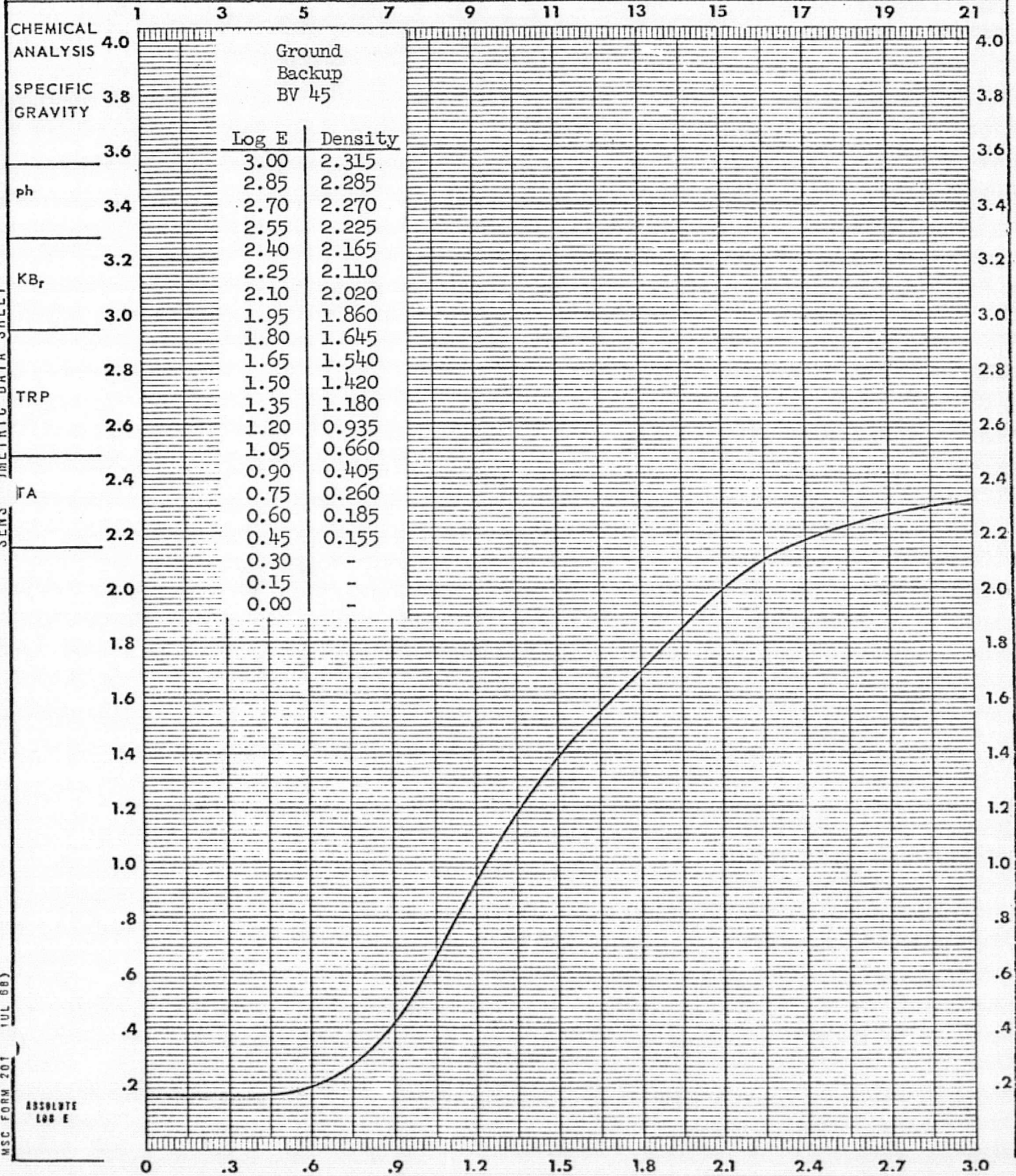
VIGNETTING DATA CALIBRATION PHOTOGRAPHY

Film Type EK 2485-107-2Calibration Unit HAO Sensitometer Box No. 1Film Size 35 mmCalibrated By R. D. Mercer (Boulder, Colo.)

Quick Look Fr No	Date of Photography	Exposure Time (Sec)	Neutral Density Filt No	Calibration Unit Bulb Manufacturer	Frame Digitization		Remarks
					Date	Mag Tape	
1	25 Oct 73						
2	25 Oct 73						
3	25 Oct 73						
4	25 Oct 73						
5	25 Oct 73	40	2.0	Sylvania	28 Mar 74	D-724	
6	25 Oct 73	80	2.0	Sylvania			
7	25 Oct 73	20	2.0	Sylvania	28 Mar 74	D-724	
8	25 Oct 73	90	2.0	Sylvania			
9	25 Oct 73	60	2.0	Sylvania	28 Mar 74	D-724	
10	25 Oct 73	30	2.0	Sylvania	28 Mar 74	D-724	
11	25 Oct 73	15	2.0	Sylvania	28 Mar 74	D-724	
12	25 Oct 73	30	1.0	Sylvania	28 Mar 74	D-724	
13	25 Oct 73	15	1.0	Sylvania	28 Mar 74	D-724	
14	25 Oct 73	5	1.0	Sylvania			
15	25 Oct 73	2	1.0	Sylvania			
16	25 Oct 73	5	None	Sylvania			
17	25 Oct 73	2	None	Sylvania			
18	25 Oct 73	1	None	Sylvania			
19	25 Oct 73						
20	25 Oct 73						
21	25 Oct 73						
22	25 Oct 73	40	2.0	General Electric	28 Mar 74	D-724	
23	25 Oct 73	80	2.0	General Electric			
24	25 Oct 73	20	2.0	General Electric	28 Mar 74	D-724	
25	25 Oct 73	90	2.0	General Electric			
26	25 Oct 73	60	2.0	General Electric	28 Mar 74	D-724	
27	25 Oct 73	30	2.0	General Electric	28 Mar 74	D-724	
28	25 Oct 73	15	2.0	General Electric	28 Mar 74	D-724	
29	25 Oct 73	30	1.0	General Electric			
30	25 Oct 73	15	1.0	General Electric	28 Mar 74	D-724	
31	25 Oct 73	5	1.0	General Electric			
32	25 Oct 73	2	1.0	General Electric			
33	25 Oct 73	5	None	General Electric			
34	25 Oct 73	2	None	General Electric			
35	25 Oct 73	1	None	General Electric			
36	25 Oct 73						
37	25 Oct 73						

DATE 22 Oct 73	CONTROL NUMBER Ground Backup BV45	TASK S073	PREPARED BY R.D. Mercer
FILM EK 2485	EMULSION NUMBER 112-1	MFG. ISSR, Inc.	EXPIRATION DATE 31 May 74
EXPOSURE DATA		DENSITOMETRY	
SENSITOMETER I-B	PROCESSOR Hi-Speed	INSTRUMENT Macbeth	SPEED ()
ILLUMINANT 2850°F	CHEMISTRY D-19	TYPE Quantalog TD-102	
TIME 1/100 Sec.	TIME 30 feet/minute	APERTURE SIZE 2mm	GAMMA 1.82
FILTER 5500°K + 1.0 ND	TEMP. OF 85°F	FILTER Visual	BASE FOG 0.155

SENSITOMETRIC DATA SHEET

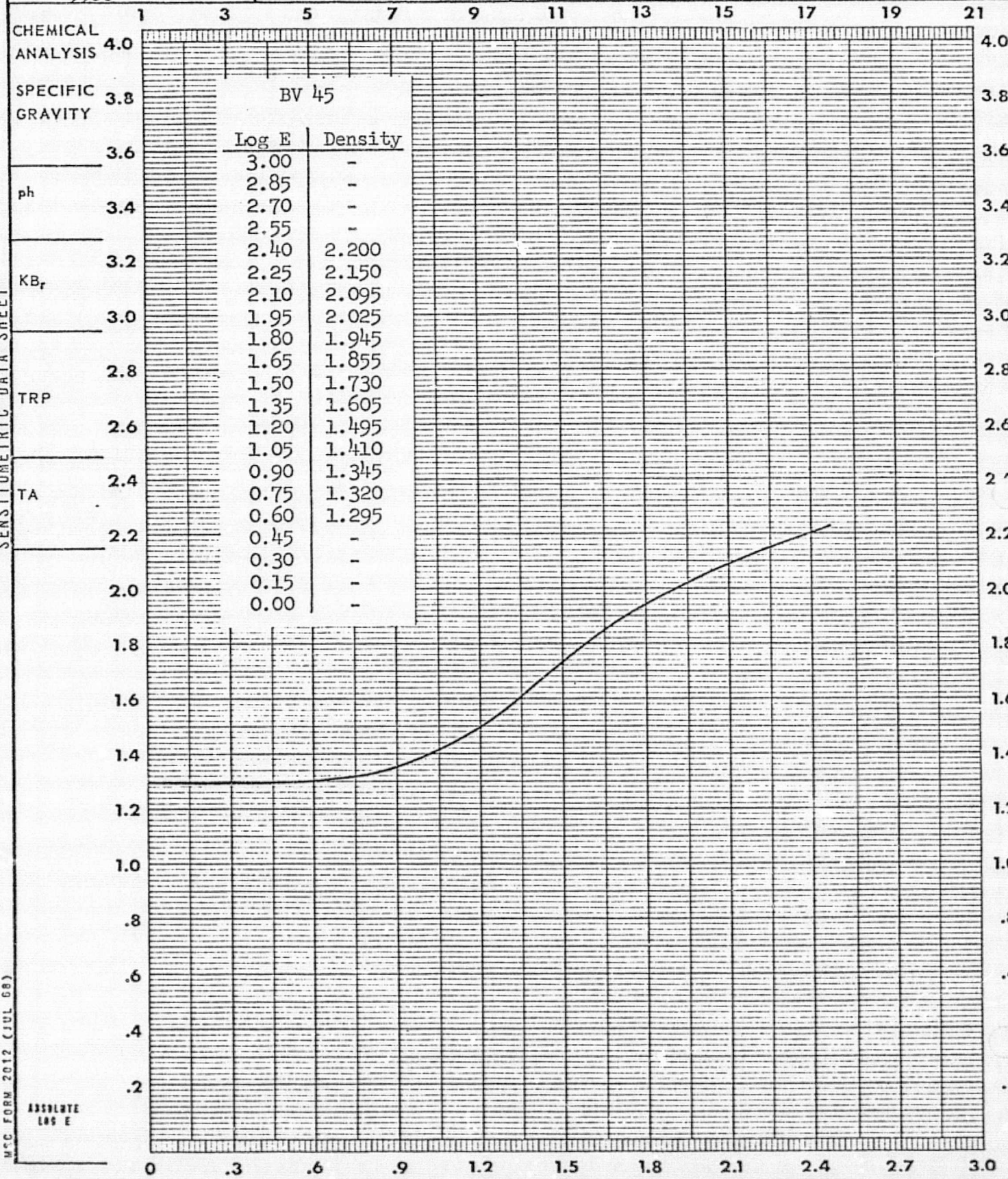


MSC FORM 201 (JUL 68)

ABSOLUTE LOG E

DATE 22 Oct 73	CONTROL NUMBER BV45	TASK S073	PREPARED BY R.D. Mercer
FILM EK 2485	EMULSION NUMBER 112-1	MFG. ISSR, Inc.	EXPIRATION DATE 31 May 74
EXPOSURE DATA		PROCESSING DATA	DENSITOMETRY
SENSITOMETER I-B	PROCESSOR Hi-Speed	INSTRUMENT Macbeth	SPEED ()
ILLUMINANT 2850°F	CHEMISTRY D-19	TYPE Quantalog TD-102	
TIME 1/100 Sec.	TIME 30 feet/minute	APERTURE SIZE 2mm	GAMMA 0.89
FILTER 5500°K + 1.0 ND	TEMP. OF 85°F	FILTER Visual	BASE FOG 1.295

SENSITOMETRIC DATA SHEET

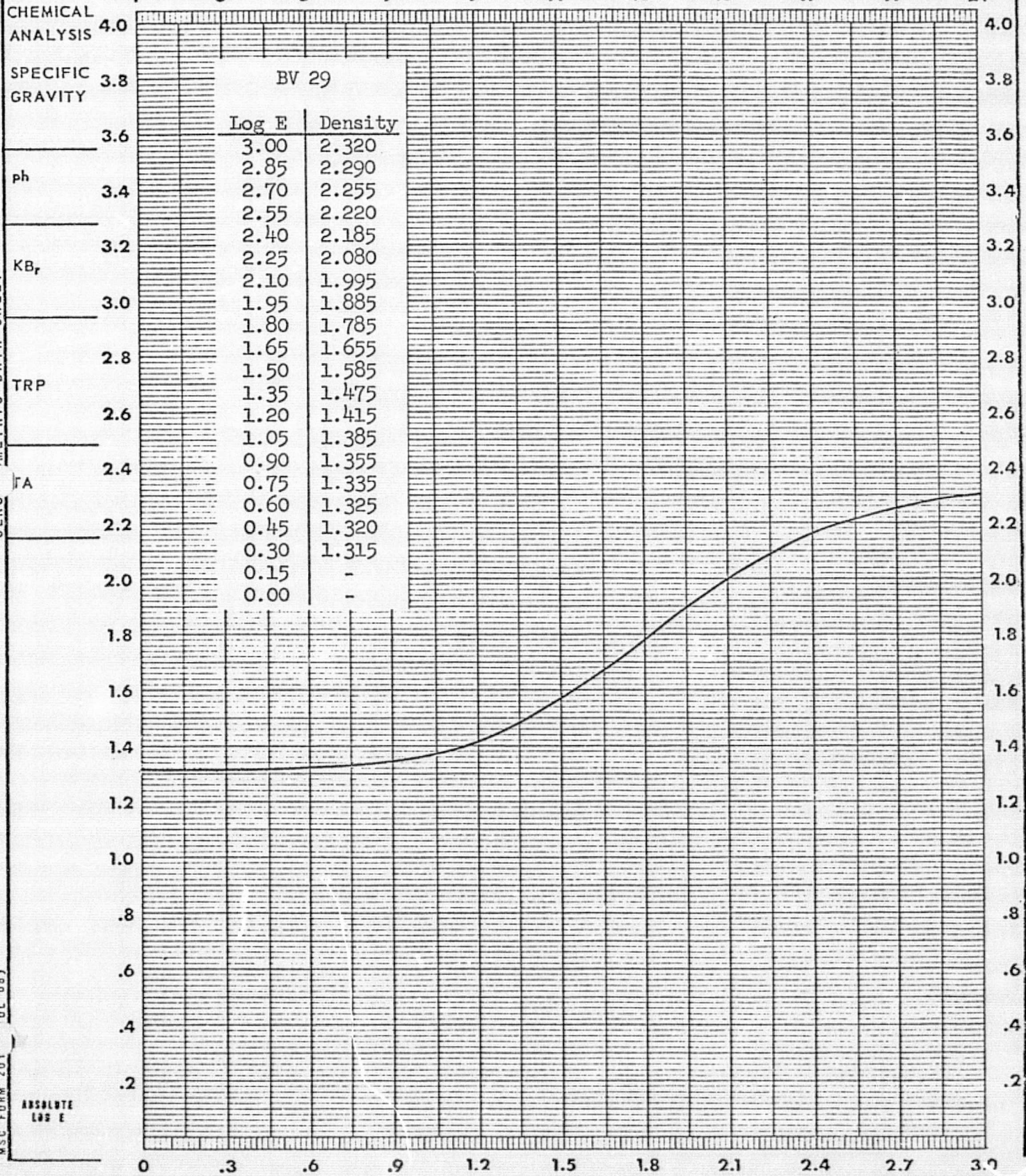


M.S.C. FORM 2012 (JUL 68)

ABSOLUTE LOG E

DATE 22 Oct 73	CONTROL NUMBER BV29	TASK S073	PREPARED BY R.D. Mercer
FILM EK 2485	EMULSION NUMBER 112-1	MFG. ISSR, Inc.	EXPIRATION DATE 31 May 74
EXPOSURE DATA		DENSITOMETRY	
SENSITOMETER I-B	PROCESSOR Hi-Speed	INSTRUMENT Macbeth	SPEED ()
ILLUMINANT 2850°	CHEMISTRY D-19	TYPE Quantalog TD-102	
TIME 1/100 Sec.	TIME 30 feet/minute	APERTURE SIZE 2mm	GAMMA 0.77
FILTER 5500°K + 1.0 ND	TEMP. OF 85°F	FILTER Visual	BASE FOG 1.315

SENSITOMETRIC DATA SHEET

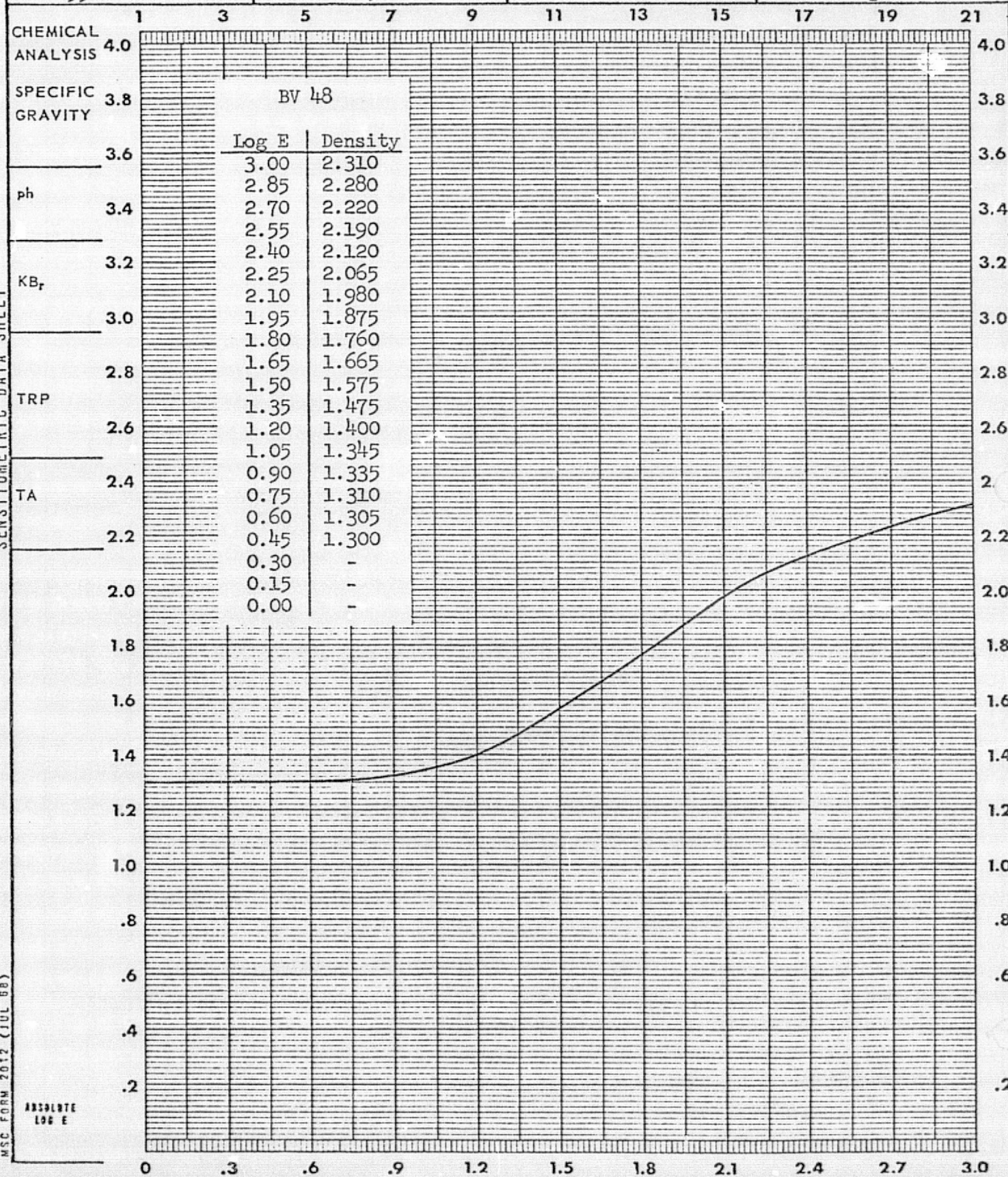


MSC FORM 201 (UL 68)

ABSOLUTE LOG E

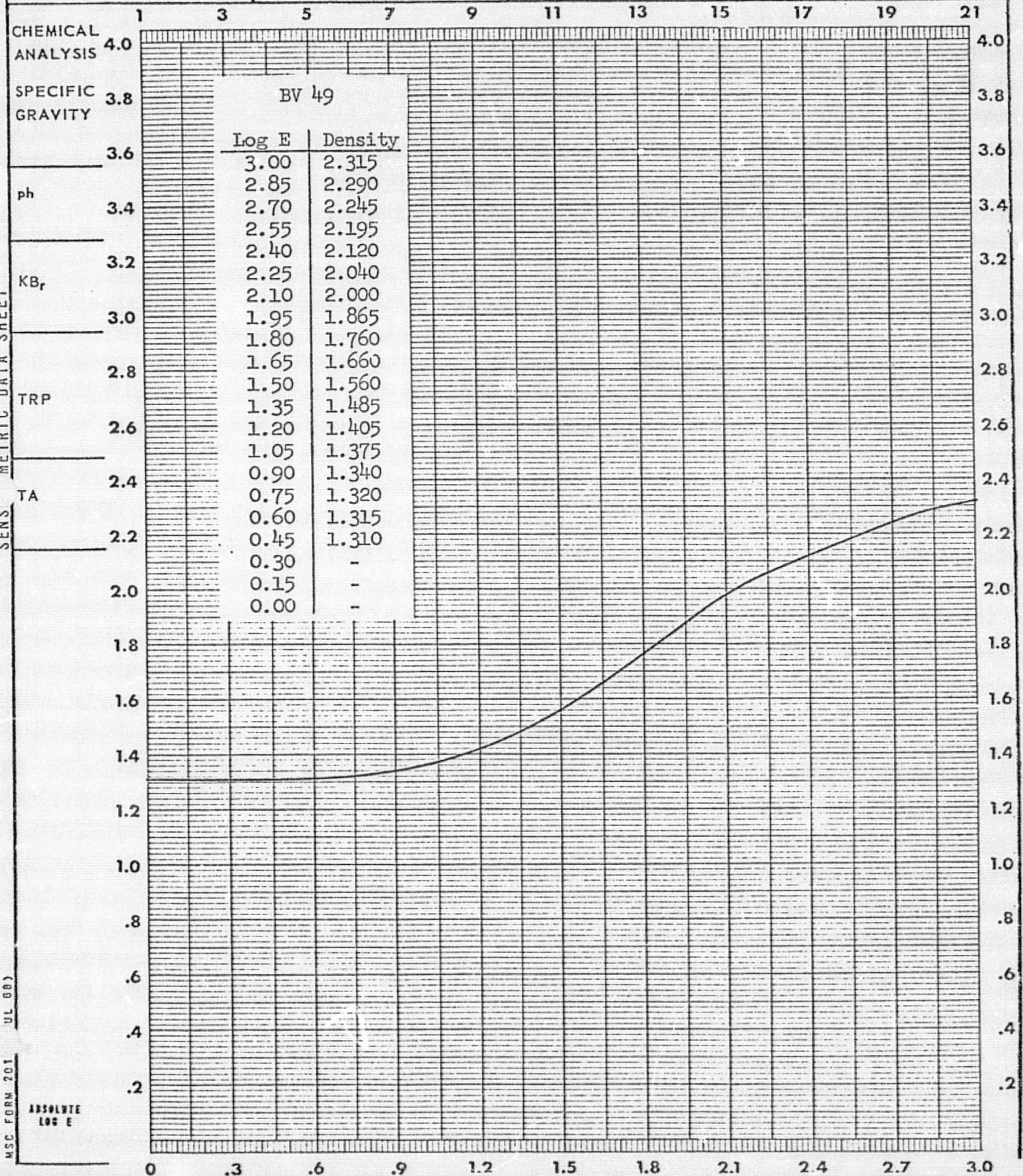
DATE 22 Oct 73	CONTROL NUMBER BV48	TASK S073	PREPARED BY R.D. Mercer
FILM EK 2485	EMULSION NUMBER 112-1	MFG. ISSR, Inc.	EXPIRATION DATE 31 May 74
EXPOSURE DATA		DENSITOMETRY	
SENSITOMETER I-B	PROCESSOR Hi-Speed	INSTRUMENT Macbeth	SPEED ()
ILLUMINANT 2850°F	CHEMISTRY D-19	TYPE Quantalog TD-102	
TIME 1/100 Sec.	TIME 30 feet/minute	APERTURE SIZE 2mm	GAMMA 0.68
FILTER 5500°K + 1.0 ND	TEMP. °F 85°F	FILTER Visual	BASE FOG 1.300

SENSITOMETRIC DATA SHEET



DATE 22 Oct 73	CONTROL NUMBER BV49	TASK S073	PREPARED BY R.D. Mercer
FILM EK 2485	EMULSION NUMBER 112-1	MFG. ISSR, Inc.	EXPIRATION DATE 31 May 74
EXPOSURE DATA		PROCESSING DATA	
SENSITOMETER I-B	PROCESSOR Hi-Speed	INSTRUMENT Macbeth	SPEED ()
LUMINANT 2850°F	CHEMISTRY D-19	TYPE Quantalog TD-102	
TIME 1/100 Sec.	TIME 30 feet/minute	APERTURE SIZE 2mm	GAMMA 0.73
FILTER 5500°K + 1.0 ND	TEMP. OF 85°F	FILTER Visual	BASE FOG 1.310

SENS. METRIC DATA SHEET

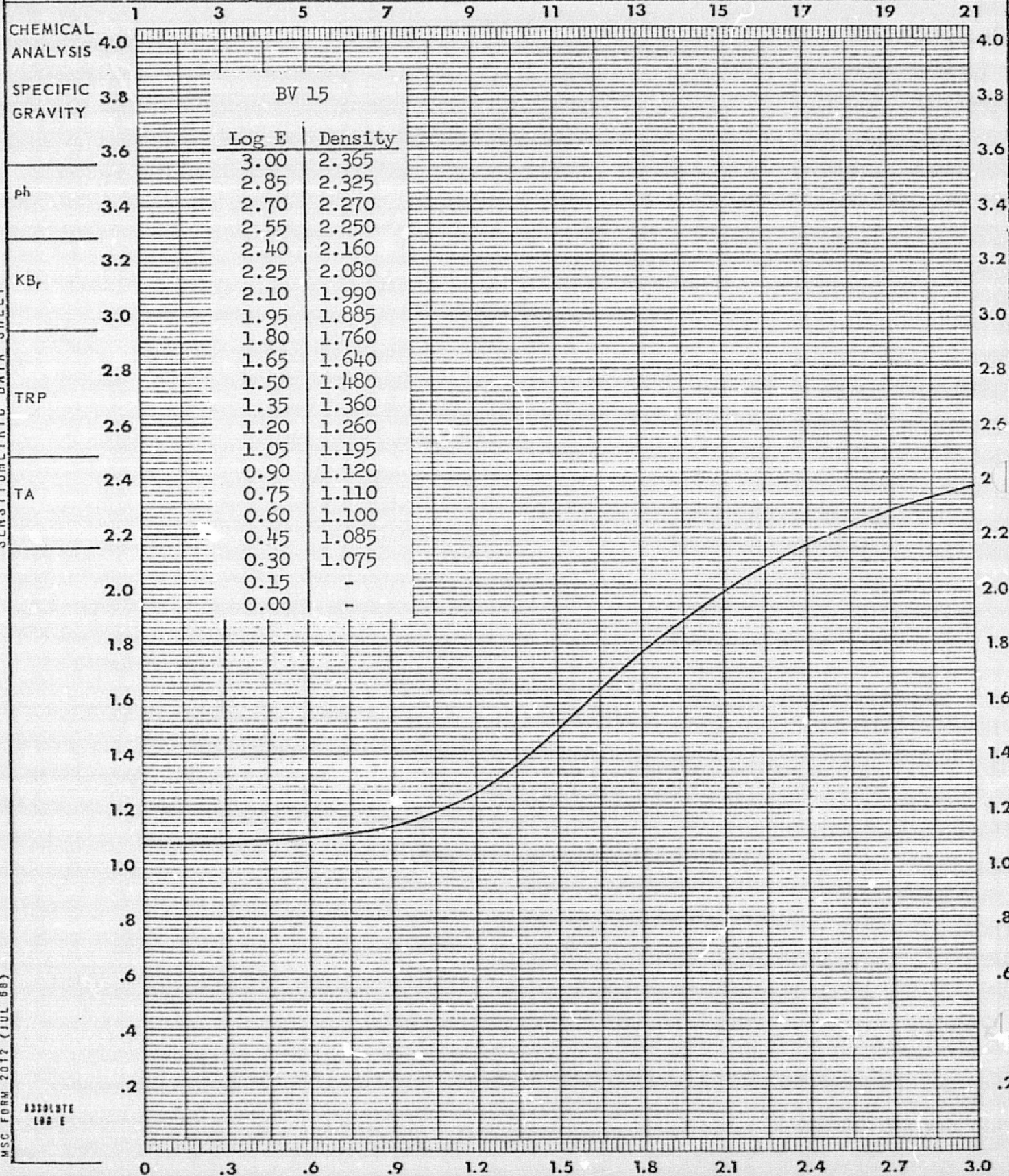


MSC FORM 201 (UL 68)

ABSOLUTE LOG E

DATE Approx 10 Jul 73	CONTROL NUMBER BV15 (SL3)	TASK S073	PREPARED BY R.D. Mercer
FILM EK 2485	EMULSION NUMBER 112-1	MFG. ISSR, Inc.	EXPIRATION DATE 31 May 74
EXPOSURE DATA		PROCESSING DATA	
SENSITOMETER I-B	PROCESSOR Hi-Speed	INSTRUMENT Macbeth	SPEED ()
ILLUMINANT 2850°F	CHEMISTRY D-19	TYPE Quantalog TD-102	
TIME 1/100 Sec.	TIME 30 feet/minute	APERTURE SIZE 2mm	GAMMA 0.98
FILTER 5500°K + 1.0 ND	TEMP. OF 85°F	FILTER Visual	BASE FOG 1.075

SENSITOMETRIC DATA SHEET



MSC FORM 2012 (JUL 68)

ABSOLUTE
LOG E

MEMORANDUM ON LOW LIGHT LEVEL PHOTOGRAPHY FOR SL-4

The Goddard Space Flight Center (GSFC) document X-614-73-147 of May 1973 entitled, "Manual for Hand-Held Photography from Skylab", presents low light level photographic information including checklists for optional use by the crew. The goals of this photography for SL-4 have just been reviewed and compared to the proposed new S073 Functional Objectives (FO's) 1 through 5. These FO's are consistent with pages DC-1 through DC-5 of the GSFC document. Therefore, the S073 film budget of eight (8) 35 mm film cassettes of VHBW (Eastman Kodak Type 2485 emulsion) for data and two (2) additional cassettes for preflight and postflight calibrations need not be duplicated for these GSFC suggested astronomical tasks.

However, the S073 FO's do not address the earthward looking photography contained in pages DA-1 through DB-3. While such photography is also a crew option task using the ward room window, it can also utilize the T025 cannister and the Articulated Mirror System (AMS) of S019 as S073 proposes. This arrangement of equipment would greatly enhance opportunities for viewing earthward at nighttime from the Antisolar Scientific Airlock, particularly as the magnitude of the orbital-plane-to-sun (beta) angle becomes greater than 20° . The nighttime earth photography will require four (4) more film cassettes for data; no (0) calibration cassettes may be required, because the exposure durations appropriate to this remaining crew option photography can be included on the S073 calibration cassettes requested above. The specific uses and film budget for the earthward photography would be as follows:

1. Photography of cities at night, divided more or less evenly between cities of eastern and western cultures (60 frames).
2. Photography of very dark regions where astronomical observatories now exist or are under consideration as future observatory sites. These regions might include Western Texas, Southern Andes, Northern Baha Penninsula, mountains east of the California coast from San Diego to San Francisco, all of Arizona, Utah, New Mexico and Colorado, and the mountains eastward from Mexico City to the Isthmus of Tehauntepec (30 frames).
3. Photography of forest fires, extensive lightning and active volcanoes (30 frames).
4. Photography of crew selected targets of opportunity (40 frames).

L. Dunkelman
R. D. Mercer

Albany, New York
14 October 1973